Estimating Geodesic Barycentres Using Conformal Geometric Algebra, With Application to Human Movement

by

Bernie C. Till
M.Sc., Simon Fraser University, 1990

A Dissertation Submitted in Partial Fulfillment
of the Requirements for the Degree of

DOCTOR OF PHILOSOPHY

in the Department of Electrical and Computer Engineering

University of Victoria

Supervisory Committee

Estimating Geodesic Barycentres
Using Conformal Geometric Algebra,
With Application to Human Movement

by

Bernie C. Till
M.Sc., Simon Fraser University, 1990

Supervisory Committee

Dr. Peter F. Driessen, Department of Electrical and Computer Engineering
Supervisor

Dr. T. Aaron Gulliver, Department of Electrical and Computer Engineering
Departmental Member

Dr. Daniel N. Bub, Department of Psychology
Outside Member

Abstract

Supervisory Committee
Dr. Peter F. Driessen, Department of Electrical and Computer Engineering
Supervisor
Dr. T. Aaron Gulliver, Department of Electrical and Computer Engineering
Departmental Member
Dr. Daniel N. Bub, Department of Psychology
Outside Member

Statistical analysis of 3-dimensional motions of humans, animals or objects is instrumental to establish how these motions differ, depending on various influences or parameters. When such motions involve no stretching or tearing, they may be described by the elements of a Lie group called the Special Euclidean Group, denoted SE(3). Statistical analysis of trajectories lying in SE(3) is complicated by the basic properties of the group, such as non-commutativity, non-compactness and lack of a bi-invariant metric. This necessitates the generalization of the ideas of "mean" and "variance" to apply in this setting.

We describe how to exploit the unique properties of a formalism called Conformal Geometric Algebra to express these generalizations and carry out such statistical analyses efficiently; we introduce a practical method of visualizing trajectories lying in the 6-dimensional group manifold of SE(3); and we show how this methodology can be applied, for example, in testing theoretical claims about the influence of an attended object on a competing action applied to a different object.

The two prevailing views of such movements differ as to whether mental action-representations evoked by an object held in working memory should perturb only the early stages of subsequently reaching to grasp another object, or whether the perturbation should persist over the entire movement. Our method yields "difference trajectories" in SE(3), representing the continuous effect of a variable of interest on an action, revealing statistical effects on the forward progress of the hand as well as a corresponding effect on the hand's rotation.

Table of Contents

List of Figures

Acknowledgments

Firstly, I would like to thank Dr. Peter Driessen for his keen foresight, unwavering support, and very practical advice. Without him, this dissertation would never have been written. Secondly, I would like to thank Dr. Daniel Bub for his endless patience, kind encouragement, and steadfast refusal to take no for an answer. Without him, this dissertation would have been very different. And last but certainly not least, I would like to thank Dr. Mike Masson for his light-handed guidance, conscientious attention to detail, and steady focus on the big picture. I am particularly grateful to Daniel and Mike for inviting me along on a journey of scientific discovery that turned out to be most fruitful and rewarding.

Introduction

Many 3D movements of interest in science and engineering can be modelled as the motion of an articulated rigid body, consisting of a set of articulations connected together by joints. Subject to constraints imposed by the joints, each articulation undergoes rigid body motion, which is any 3D motion that does not involve stretching or tearing. Such movements entail *rotation* about a point as well as *translation* of that point through space; we refer to this combination as *displacement*. The set of all such displacements forms a transformation group which is also a continuous manifold (that is, a Lie group), called the Special Euclidean group of rigid body motions in 3-dimensional space and denoted $\mathbb{SE}(3)$. The statistical analysis of such motions plays a very important role in a wide range of applications.

In particular, any human movement – for example, reaching toward and grasping an object – can be modelled in this way. The statistical analysis of rigid body motion is thus crucial for determining how actions vary in response to a given set of experimental parameters. Consider a group of individual subjects who carry out the same action over a large number of trials under two or more conditions. The critical question is whether the average trajectories generated in the various conditions differ from one another, and if so, in what way. Current approaches to this problem are almost universally restricted to the analysis of 1 or 2 (effective) dimensions, and even those analyses that purport to study spatial trajectories are usually limited to projections of these trajectories onto the coordinate planes [Bicchi, Gabiccini, & Santello 2011; Chapman, Gallivan, Wood,

Milne, Culham, & Goodale 2010a; Ramsay & Silverman 2005]. Consequently, there is a tendency to extract less information from the measured data than they actually contain. What is badly needed is an efficient methodological approach that provides statistical tests of entire trajectories, including all six degrees of freedom: three for translation and three for rotation.

In a great many cases, the problem can be reduced to estimating the "means" and "covariances" of coeval sets of time-dependent 3D rigid body motions, and exploiting the "covariances" to discriminate between the "means." We enclose these terms in quotes because their usual definitions do not carry over literally to the case of a group like $\mathbb{SE}(3)$, which is non-commutative and whose group manifold is curved, non-compact, and non-Riemannian. We must therefore modify the definitions of our terms to be consistent with these properties of $\mathbb{SE}(3)$, while retaining the core concepts: the *effective location* of a set of samples and the *dispersion* of the samples about that location. In this context, the essence of the idea of a mean or effective location is perhaps best captured by defining it as the *barycentre* (centre of mass) of a set of weighted points: the point about which the dispersion of the given points is minimized and, equivalently, about which the sum of the moments vanishes.

Each observation of a moving rigid body yields a displacement from its original position and orientation – that is, an element of $\mathbb{SE}(3)$, corresponding to a point in the 6-dimensional manifold of the group. Over time, this results in a sequence of such elements, which traces a curve or trajectory in that manifold. Thus the time evolution of

the kinematic state of the rigid body moving through 3D space is represented by a point moving along the curve in $\mathbb{SE}(3)$. Given a collection of repetitions of the movement sampled at discrete intervals, each repetition contributes one point to a cloud of points for each sampling interval, and we take the curve passing through the barycentres of these clouds to be the effective trajectory of the cloud as a whole. In order to perform time-dependent statistical comparisons of 3D rigid body motions, then, we need ways of calculating barycentres and measuring dispersions of clouds of points in the 6D group manifold of $\mathbb{SE}(3)$. This paper presents an efficient way of doing this using Conformal Geometric Algebra.

We begin with some background material and a survey of related work. Then we motivate the formalism of Geometric Algebra and illustrate how expressively it unifies fundamental geometric constructs, including the conformal model of 3D Euclidean geometry and the elements of the Special Euclidean group. Next, we outline some of some of the basic ideas which characterize mathematical statistics in a group-theoretical setting. This leads into a description of the algorithm we have developed for statistical analysis of trajectories lying in $\mathbb{SE}(3)$, and the data visualization techniques we have found most useful for interpreting the results. Finally, we provide an example of how these statistical procedures can be used to provide crucial evidence on how control of a reach-and-grasp action is modulated by higher-level cognitive influences.

Background and Related Work

The Geometry of Lie-Group Statistics

In a Riemannian manifold, we have a natural measure of distance, determined by the metric tensor, so the natural measure of dispersion is the weighted sum of squared distances from the barycentre. In this case, we define a geodesic between any two points to be the minimum-length curve joining them; conversely, we define the distance between any two points as the length of the geodesic joining them.

Using these concepts, we obtain the well-known Fréchet, or Karcher, mean [Fréchet 1948; Karcher 1977] of elements of a commutative group whose manifold is Riemannian. For a non-commutative group, the metric must additionally be bi-invariant (invariant under both left- and right actions of the group elements). When such a metric exists, it is always possible to use it in conjunction with the group operation to define a barycentre [Moakher 2002], and a closed-form solution has been given recently [Fiori 2010] for matrix representations of $\mathbb{SO}(3)$, the group of 3D rotations.

For any group endowed with a bi-invariant Riemannian metric, bi-invariance of the barycentre defined using that metric is automatic. However, many important Lie groups, including $\mathbb{SE}(3)$, do not possess such a metric. One effective expedient in such cases is to calculate the average in the tangent space [Govindu 2004], which, being a vector space, is naturally endowed with a Euclidean metric. Under certain conditions, this yields an acceptable approximation of the group mean. See Sharf et al. [2010] for a recent survey. Buchholz & Sommer [2005] use geometric algebra to do this in $\mathbb{SO}(3)$ and Gebken &

Sommer [2008] extend the approach to $\mathbb{SE}(3)$. It must be emphasised, however, that this approach yields usable results only when the dispersion is small.

In the non-Riemannian, non-commutative case, we have no metric, but the idea of dispersion remains meaningful because we can still define bi-invariant geodesics. We do this using an affine connection (in particular, the unique torsion-free connection given by Cartan and Schouten [1926]), which determines how the tangent space transforms when transported along any curve in the manifold. We thus define the geodesic between two points to be the unique curve joining them, along which transverse acceleration (more precisely, the covariant derivative of the curve's tangent vector) vanishes. Such curves turn out to be one-parameter subgroups, so we can use the group logarithm and exponential map to pass back and forth between the Lie group and its Lie algebra. The Lie algebra is just a flat vector space, tangent to the group manifold at the group's identity element. Being a vector space, it does have a metric, by means of which we may induce an affine parameter (analogous to arc length) along any given geodesic in the group manifold. This does not constitute a metric in the group manifold, however, because it fails to satisfy the triangle inequality. Nonetheless, it does suffice to define *moments about a common point of intersection* of a set of geodesics, yielding a measure of dispersion which permits a barycentre to be defined in a consistent way.

In the case of $\mathbb{SE}(3)$, we can always parameterize the resulting geodesics as scalar multiples of *screw displacements* (rotations about an axis coupled with translation along that axis), because of a long-known result called Chasles' Theorem [Mozzi 1763; Chasles

1830], according to which every rigid body displacement can be expressed as a screw displacement. Thus we have a rigorous theoretical foundation upon which to ground the statistical analysis of 3D kinematic data, as described by trajectories lying in the 6D group manifold of $\mathbb{SE}(3)$.

The Path to Conformal Geometric Algebra

A fair amount of work has been done on the statistical analysis of planar trajectories [Maroulas 2012; Brillinger 2010], but the methods commonly used do not generalize well to the case of 3D rigid body motions. Analyses which rightly belong in $\mathbb{SE}(3)$ typically either retreat to one of the subgroups, $\mathbb{R}^3$ [Chapman et al., 2010a; Faraway, Reed, & Wang, 2007] or $\mathbb{SO}(3)$ [Choe, 2006], in order to simplify the calculations, or resort to the unnecessary intricacies of differential geometry and matrix group representations [Pennec & Arsigny, 2013].

Our work overcomes these limitations by employing an invariant, coordinate-free formalism which defines an associative and invertible product on geometric objects, called the *geometric product*. This formalism, called Geometric Algebra [Dorst, Fontijne & Mann 2009; Doran & Lasenby 2007], represents points, lines, planes, volumes, and so on, by *multivectors* – linear combinations of monomials formed by geometric products of vectors. All of these constructs have a *declarative* interpretation, according to which they represent geometric *entities*, and also have a *procedural* interpretation, according to which they represent geometric *transformations*. Thus the representation of geometric

objects is unified with the representation of elements of the transformation groups acting on them.

This is in contradistinction to the bulk of the work in the area of statistical analysis of 3D kinematic data [e.g. Chirikjian 2012, 2010; Chirikjian & Kyatkin 2001], which uses 4D homogeneous vectors to model Euclidean geometry and 4×4 homogeneous matrices represent the Euclidean motion group. This formulation adjoins an *explicit representation of the origin*, lying outside the 3D vector space being modeled, and has been in common use long enough that its advantages are widely appreciated, though its drawbacks [Blinn 2002; Goldman 2003] are less well known.

We circumvent these drawbacks by adopting a 5D conformal model of Euclidean geometry, well known in the 18th century, which fell into obscurity before recently experiencing something of a renaissance [Hestenes 2001; Sobczyk 2013]. This model extends the homogeneous model by adjoining an *explicit representation of the point at infinity*. The very significant benefits of doing this are outlined in the next section. In consequence, we are led to work in a branch of geometric algebra particularly well suited to this model, called Conformal Geometric Algebra [Hestenes 2010, 2001; Lasenby et al. 2004; Dorst & Mann 2002; Mann & Dorst 2002].

The application of conformal geometric algebra to analysis of articulated rigid bodies [McCarthy & Soh 2011; Selig & Bayro-Corrochano 2009] and problems related to 3D motion capture [Aristidou 2010; Chavarria-Fabila 2009; Zhao et al. 2006] is gaining acceptance, and it has been used to solve problems in 3D computer vision, like the

perspective n-point problem [Buchholz & Sommer 2005; Dorst 2005; Gebken & Sommer 2008]. Valkenburg & Dorst [2011] discuss the estimation of elements of $\mathbb{SE}(3)$ using conformal geometric algebra, but they proceed by maximizing a particular class of similarity measures applied to the transformed objects and are thus unable to provide a measure of dispersion in the group manifold of the transformations themselves. The use of conformal geometric algebra for time-dependent hypothesis testing based on statistical comparison of trajectories in the group manifold of $\mathbb{SE}(3)$, however, has not previously been described in the literature. This is the problem which our work solves.

The Algebra of Geometry

Drawbacks of Conventional Vector Algebra

Analytic geometry is usually done by assigning coordinates to points and deducing the properties of geometric objects from (arithmetic) operations on these coordinates. This leads to a very specific mindset: we think of vectors as tuples of numbers which behave differently if we arrange them in rows or columns, we represent operations on vectors (elements of transformation groups) by matrices, and we introduce the imaginary unit as an abstract quantity, which mysteriously squares to –1, by fiat.

Necessary though this may ultimately be for purposes of calculation, doing so from the outset has many shortcomings – not least of which being lack of homogeneity and manifest covariance, i.e., it makes the origin seem special, and forces us to prove that our results are not merely fortuitous consequences of our choice of coordinates. Of course, there is nothing special about the origin, and the relationships between geometric objects

cannot possibly depend on how we choose coordinates. Yet there is no general way to exploit these powerful facts in conventional vector algebra and tensor analysis.

Calculations in vector algebra are greatly hampered by the fact that it rests on two very different vector products – the inner (dot) product and the outer (cross) product – neither of which is invertible. Not only does this result in an artificial proliferation of special cases which exist only to compensate for the poverty of the notation, it complicates calculations, e.g., by forcing the adoption of iterative techniques, all dictated by the tricks needed in different contexts to avoid the need to "divide by" geometric constructs like vectors. Even worse, the cross product is defined only in 3D and the vectors it produces transform differently under reflection than those produced in other ways, leading to yet another mystery, the distinction between axial and polar vectors. This appears already in elementary mechanics, and as we proceed to study more advanced subjects, we are forced to introduce more exotic constructs – differential forms, quaternions, spinors, twistors and so on – whose physical and geometric interpretations become increasingly conflated.

The most important consequence of the ability to divide by a vector this is that it makes it possible to differentiate with respect to a vector directly, rather than cobble vector differentiation together out of differentiation with respect to the individual components. This is what permits the coordinate-free formulation to extend beyond algebra and give rise to a geometric calculus.

Advantages of Geometric Algebra

Geometric algebra is an alternative formulation of the familiar geometric constructs, whose incisive clarity and broad generality have only relatively recently begun to be fully appreciated [Hestenes 1988, Hestenes 1991; Hestenes & Sobczyk 1987], and which follows very simply and naturally from the unification of the inner and outer products into the geometric product, which is invertible and associative, but not commutative. Formally, geometric algebra is Clifford algebra [Clifford 1878] augmented by a specific geometric interpretation, refined from the one given by Hermann Grassmann [1844; 1877]. This elegant and powerful formalism has languished at the periphery of mathematics and physics, of interest primarily to a small cadre of specialists, for well over a century. Only in the last decade have reference works appeared which are aimed at a wider audience of physicists, engineers and computer scientists [Doran & Lasenby 2007; Dorst et al. 2009].

By working in geometric algebra, we can dispense entirely with the unwieldy machinery of coordinates, index manipulation, and matrix representations, because the properties of the underlying geometric objects are reflected directly in the elements of the algebra. Coordinates need not be introduced until the final stages of calculating results. Thus geometric algebra permits exceptionally clear and concise problem representations, enhancing geometric insight and conceptual transparency while improving computational efficiency. Not only does geometric algebra provide a single unified framework containing all of the above mentioned formalisms, it unifies metric, affine, projective and conformal geometry with complex numbers, quaternions, octonions – indeed, all the

composition algebras – and thereby endows imaginary units with a very real geometric interpretation while revealing axial vectors to be nothing more than an artifact of overloading a single algebraic entity with multiple geometric interpretations (representing a plane by its normal vector is a trick that only works in three dimensions).

Being coordinate free, expressions in geometric algebra are inherently covariant, and transformation groups do not require matrix representations, so they cannot exhibit coordinate singularities (e.g. the "gimbal lock" which plagues rotation matrices) or artifactual redundancies (e.g. Euler angles lead to 12 different representations of the same rotation matrix). When coordinates are finally introduced at some convenient stage of a calculation, representations in geometric algebra are considerably more compact and efficient than conventional ones. Of particular interest to us, $\mathbb{SE}(3)$ has 6 parameters, but the corresponding 4×4 homogeneous matrices have 16 elements, leaving 10 highly nonlinear constraints, which are artifacts of the representation and completely extraneous to the group itself. The equivalent objects in geometric algebra have only 8 elements and 2 quadratic (unit magnitude) constraints. This advantage of geometric algebra only increases with the dimensionality of the group manifold.

Another benefit, which we exploit repeatedly below, is that all the objects of interest belong to a single graded algebra, which makes transitions between a Lie group and its Lie algebra seamless. Many awkward postures one is compelled to adopt in standard Lie theory (viz, the split personality of the word, adjoint) simply become moot. In geometric algebra, one simply has multivectors acting on multivectors by conjugation, qvq^{-1}, and

the group product pq is no different than any other instance of the geometric product in a nested conjugation $pqvq^{-1}p^{-1}$; it is simply a matter of emphasis: $(pq)v(q^{-1}p^{-1})$ vs. $p(q(v)q^{-1})p^{-1}$.

In standard representations, the group of translations acts additively, while the group of rotations acts multiplicatively. For groups like $\mathbb{SE}(3)$, this complicates calculations immensely: repeated applications of group elements result in unwieldy, non-invertible polynomials, and the group exponential and logarithm are cumbersome to work with. In order to circumvent this, we must adopt a model of Euclidean geometry that permits a multiplicative formulation of the group of translations.

The homogeneous model represents points in 3D space by rays through the origin in 4D space. Thus the representation is projective and the origin is removed from the object space. When we extend this model by adjoining the point at infinity, the representation becomes conformal and the object space is represented by a *horosphere* – a uniformly curved 3D manifold of rays lying in the 4D null cone of a 5D space – which has a geometry that is nonetheless Euclidean. This results in numerous very significant benefits, which are not widely known. Fontijne & Dorst [2003] give a detailed comparison of the various 3D, 4D and 5D formalisms as they concern computer graphics, and the thrust of their argument is equally valid the present context.

In the homogeneous model, the rotations are compact but the translations are not, and this forces us to treat rotations and translations very differently. In the conformal model, rectilinear objects (called *flats:* lines, planes, etc.) are unified with uniformly curved

objects (called *rounds:* circles, spheres, etc.). A line (plane) is just a circle (sphere) passing through the point at infinity – an obvious property which cannot be exploited in the homogeneous model because there is no way to express it, but in conformal geometric algebra it becomes trivial [Hestenes 2001; Lasenby et al. 2004]. The importance of this cannot be overstated, because it removes the formal distinction between rotations and translations and thereby compactifies the group manifold. In consequence, *rigid body displacements reduce to orthogonal transformations*.

A Guided Tour of Geometric Algebra

We sketch very briefly the aspects of geometric algebra required to underpin the main result, and give additional detail, including proofs and figures, in the appendices, but we must refer the reader to the literature for a thorough treatment. Our main purpose here is to show how the basic elements of geometry, and the transformations acting on them, can be represented by a unified algebra and its operations.

Beginning with the basic notion of a zero-dimensional *point*, we construct higher-level entities by *extension*. Thus we form a *vector* by extending a point towards another point to create an oriented line segment. Similarly, we extend the vector to form a *bivector* by sweeping it along a second vector to create an oriented area. For two independent vectors $\boldsymbol{a}$ and $\boldsymbol{b}$, we represent this operation by a product, called the *outer product* or *wedge product*, $\boldsymbol{a}\wedge\boldsymbol{b}$. This is the oriented area of the parallelogram formed when $\boldsymbol{b}$ is swept along $\boldsymbol{a}$. The orientation is given by the order of the factors:

$$\boldsymbol{a}\wedge\boldsymbol{b} = -\boldsymbol{b}\wedge\boldsymbol{a} \qquad\qquad |\boldsymbol{a}\wedge\boldsymbol{b}| = |\boldsymbol{a}||\boldsymbol{b}|\sin\theta \tag{1}$$

where $|\boldsymbol{x}|$ is the magnitude of $\boldsymbol{x}$ and θ is the angle from $\boldsymbol{a}$ to $\boldsymbol{b}$. A bivector of this simple form is called a 2-*blade* and a general bivector may consist of a linear combination of 2-blades.

A *trivector* is then formed by sweeping a bivector along a third vector to form a directed parallelepiped, and so on. The wedge product of n independent vectors is called an n-blade, and we refer to n as its *grade*. The general term *multivector* refers to a linear combination in which the blades need not all be of the same grade.

While the operation of extension is grade-increasing, the operation of *contraction* is grade-decreasing. We represent this operation by another product, called the *inner product*, or *dot product*, $\boldsymbol{a}\cdot\boldsymbol{b}$, formed by projecting one vector onto another and multiplying the resulting lengths:

$$\boldsymbol{a}\cdot\boldsymbol{b}=\boldsymbol{b}\cdot\boldsymbol{a} \qquad |\boldsymbol{a}\cdot\boldsymbol{b}|=|\boldsymbol{a}||\boldsymbol{b}|\cos\theta \tag{2}$$

Now, the dot product depends on the parallel parts its factors, and the wedge product depends on their perpendicular parts. Thus we can define a new, more general product, the *geometric product*, which depends on both:

$$\boldsymbol{ab}=\boldsymbol{a}\cdot\boldsymbol{b}+\boldsymbol{a}\wedge\boldsymbol{b} \qquad |\boldsymbol{ab}|=|\boldsymbol{a}||\boldsymbol{b}| \tag{3}$$

However, the viewpoint of underlying geometric algebra is to reverse this logic, so we consider the geometric product to be fundamental and derive the other two products from its symmetric and anti-symmetric parts:

$$\boldsymbol{a}\cdot\boldsymbol{b}=\frac{1}{2}(\boldsymbol{ab}+\boldsymbol{ba}) \qquad \boldsymbol{a}\wedge\boldsymbol{b}=\frac{1}{2}(\boldsymbol{ab}-\boldsymbol{ba}) \tag{4}$$

From this starting point, it is very easy to show that every vector squares to a scalar, and this allows us to define the inverse of a vector, and indeed the inverses of arbitrary blades:

$$a^2\in R \quad\Rightarrow\quad a^{-1}=\frac{1}{a^2}a \qquad (ab)^{-1}=b^{-1}a^{-1}=\frac{b}{b^2}\frac{a}{a^2}=\frac{ba}{a^2b^2}=\frac{\overleftarrow{ab}}{a^2b^2} \tag{5}$$

where $a^2=|a|^2$ is a scalar and we have introduced the operation of *reversion* by the notation $\overleftarrow{ab}=ba$, meaning that we take the geometric products in reverse order, so the reverse of ab is just ba. General multivectors do not necessarily have inverses, though

blades always do. An invertible multivector of unit magnitude is called a *versor*, and in such case we have $x\bar{x}=1$ or just $x^{-1}=\bar{x}$.

We employ the following notation. Scalars: $a,b,c\ldots$ Vectors: $\boldsymbol{a},\boldsymbol{b},\boldsymbol{c}\ldots$ Bivectors: $\boldsymbol{a},\boldsymbol{b},\boldsymbol{c}\ldots$ General multivectors: $a,b,c\ldots$ We call the basis vectors of a space *etalons*, and denote them by $e_1,e_2,e_3\ldots$ Geometric products of etalons are denoted by multiple subscripts, so $e_{12}=e_1e_2=e_1\wedge e_2$, $e_{123}=e_1e_2e_3=e_1\wedge e_2\wedge e_3$ etc. Etalons may square to +1, –1, or 0. A space having p etalons squaring to +1, q etalons squaring to –1, and r etalons squaring to 0 is said to have *signature* (p,q,r), and *dimension* $n=p+q+r$. The geometric algebra of this space is denoted $\mathcal{G}_{p,q,r}$. By convention, trailing zeros are dropped, so $\mathcal{G}_{p,q}$ means $\mathcal{G}_{p,q,0}$ and so on. The geometric algebra of an n-dimensional space contains elements of every grade from 0 to n, with the real number 1 acting as the etalon of grade 0.

Consider now the Euclidean plane spanned by the etalons $\{e_1,e_2\}$, both squaring to 1. The geometric algebra of the plane, $\mathcal{G}_2$, is spanned by the elements $\{1,e_1,e_2,e_{12}\}$. Just as every scalar is linearly dependent on the unit scalar 1, every bivector in the e_{12}-plane is linearly dependent on the unit bivector e_{12}. Further, $e_{12}^2=-1$, which follows immediately from our definitions: $e_{12}^2=e_1e_2e_1e_2=-e_1e_2e_2e_1=-e_1e_1=-1$. Therefore e_{12} is a very real geometric object which behaves exactly like the imaginary scalar $i=\sqrt{-1}$. Hence we call it the *pseudoscalar* of the plane.

The significance of this fact cannot be overstated; it hinges on the fact that $\mathcal{G}_2^+$, the even subalgebra of $\mathcal{G}_2$ spanned by the even-grade elements $\{1,e_{12}\}$, is isomorphic to the

complex numbers, with the operation of reversion standing in for complex conjugation. Indeed, any element z of $\mathcal{G}_2^+$ with $z\tilde{z}=1$ can be put in the form $z=\cos\theta-\sin\theta e_{12}$. If $\boldsymbol{v}=xe_1+ye_2$ is any vector in the plane, then

$$\begin{aligned} z\boldsymbol{v}\tilde{z} &= (\cos\theta-\sin\theta e_{12})(xe_1+ye_2)(\cos\theta+\sin\theta e_{12}) \\ &= (x\cos 2\theta - y\sin 2\theta)e_1 + (y\cos 2\theta + x\sin 2\theta)e_2 \end{aligned} \tag{6}$$

but this is just the result of rotating $\boldsymbol{v}$ by an angle of 2θ. In addition, for any two versors we have $ab=(\cos\alpha-\sin\alpha e_{12})(\cos\beta-\sin\beta e_{12})=\cos(\alpha+\beta)-\sin(\alpha+\beta)e_{12}$. Thus the versors act on each other by simple multiplication, yielding composition, and act on the vectors in the plane by conjugation, producing a rotation.

Further, we can define the exponential of a bivector using the standard power-series definition of the exponential function, $\exp(x)=\sum x^n/n!$. Substituting the bivector $-\theta e_{12}$ for x, we have

$$\begin{aligned} \exp(-\theta e_{12}) &= \sum_{n=0}^{\vdots}\frac{(-\theta e_{12})x^n}{n!} = \underbrace{\sum_{n=0}^{\vdots}\frac{(-1)^n(\theta)^{2n}}{(2n)!}}_{\cos\theta} - e_{12}\underbrace{\sum_{n=0}^{\vdots}\frac{(-1)^n(\theta)^{2n+1}}{(2n+1)!}}_{\sin\theta} \\ &= \cos\theta-\sin\theta e_{12} \end{aligned} \tag{7}$$

so that every versor is the exponential of a bivector and, conversely, every bivector is the logarithm of a versor. Versors of this kind are called rotation versors, or simply *rotors*, independent of the dimensionality of the space in which they are embedded.

Taken together, these results create a most remarkable situation. The geometric algebra $\mathcal{G}_2$ contains a unified representation of, firstly, the Euclidean plane (the vector space spanned by the elements of odd grade $\{e_1,e_2\}$), secondly, the Lie group $\mathbb{SO}(2)$ of

rotations in the plane (in the guise of its double cover, Spin(2), consisting of the rotors belonging to the even subalgebra $\mathcal{G}_2^+$, spanned by the elements of even grade $\{1, e_{12}\}$), and thirdly, its Lie algebra (consisting of the bivectors, spanned by e_{12} alone). In Appendix C, we demonstrate that vectors generate reflections by conjugation, and therefore bivectors generate rotations by conjugation because every rotation is the result of two successive reflections. Standard Lie theory arrives at the equivalent conclusion by a rather involved differential-geometric argument, but for us it is an elementary consequence of the algebraic encoding of the underlying geometry.

In Appendix A, we generalize this to $\mathcal{G}_3$, the geometric algebra of 3D Euclidean space. The space is spanned by the etalons $\{e_1, e_2, e_3\}$, so its geometric algebra is spanned by the elements $\{1, e_1, e_2, e_3, e_{23}, e_{31}, e_{12}, e_{123}\}$. Its even subalgebra $\mathcal{G}_3^+$ is spanned by the even-grade elements $\{1, e_{23}, e_{31}, e_{12}\}$, and its unit trivector $e_{123} = e_1 e_2 e_3 = e_1 \wedge e_2 \wedge e_3$, with $e_{123}^2 = -1$, is the pseudoscalar of 3D space. In this case, the pseudoscalars of the coordinate planes, $e_{23}^2 = e_{31}^2 = e_{12}^2 = -1$, correspond to (a right-handed version of) the quaternion basis $\{i, j, k\}$, so the even subalgebra is isomorphic to the quaternions and the rotors $r = \cos\theta - \sin\theta \boldsymbol{r}$, with $\boldsymbol{r} = x e_{23} + y e_{31} + z e_{12}$, $x^2 + y^2 + z^2 = 1$, so $\boldsymbol{r}^2 = -1$ and $r\tilde{r} = 1$, are isomorphic to the unit quaternions, forming a faithful representation of Spin(3), the double cover of the Lie group $\mathbb{SO}(3)$ of rotations in space, with the vector space spanned by the bivectors $\{e_{23}, e_{31}, e_{12}\}$ forming its Lie algebra.

In the models of Euclidean geometry considered above, the group of translations acts additively. We, however, require a multiplicative representation, so we adopt a richer

model. We do this by embedding our representation of 3D Euclidean space in a 5D space of Minkowski signature. Thus, we have the etalons $\{e_1, e_2, e_3, e_+, e_-\}$, with $e_1^2 = e_2^2 = e_3^2 = e_+^2 = +1$ and $e_-^2 = -1$. This leads to the geometric algebra $\mathcal{G}_{4,1}$, but the real benefit comes from shifting to another geometric algebra for the same space, $\mathcal{G}_{3,0,2}$. This is accomplished by a simple change of basis: $e_o = \frac{1}{2}(e_- - e_+)$, $e_\infty = (e_- + e_+)$. It is easily verified that $e_o^2 = e_\infty^2 = 0$, so e_o and e_∞ are null vectors. However, orthonormal null vectors behave differently from orthonormal vectors which are not null. Indeed, $e_\infty \cdot e_0 = -1$ and $e_\infty \wedge e_0 = e_{+-}$, the pseudoscalar of the plane spanned by $\{e_+, e_-\}$, with $e_{+-}^2 = 1$.

Appendix B explains why we call e_o the origin and e_∞ the point at infinity. Briefly, we stereographically project the 3D Euclidean space spanned by $\{e_1, e_2, e_3\}$ onto the surface of the 3-sphere in the 4D Euclidean space spanned by $\{e_1, e_2, e_3, e_+\}$, then we project the result onto the 4D null "cone" of the full 5D Minkowski space, forming a curved 3D submanifold, called the horosphere. For any 3D point $\boldsymbol{x}$, this leads to the canonical representation

$$p(\boldsymbol{x}) = \boldsymbol{x} + \tfrac{1}{2}\boldsymbol{x}^2 e_\infty + e_0 \tag{8}$$

This is the conformal model of Euclidean geometry. Remarkably, the resulting curved manifold of null vectors is isomorphic to 3D Euclidean space, with metric defined as usual, by the inner product: $p(\boldsymbol{x}) \cdot p(\boldsymbol{y}) = (\boldsymbol{x} - \boldsymbol{y})^2$. Not only that, but the rotors preserve their function in this seemingly unlikely setting: $rp(\boldsymbol{x})\tilde{r} = p(r\boldsymbol{x}\tilde{r})$.

Most importantly, working in the conformal model allows us to define translation versors, or *translators*. If $\boldsymbol{t} = xe_1 + ye_2 + ze_3$ is any 3D vector, then the null bivector $\boldsymbol{t}e_\infty = xe_{1\infty} + ye_{2\infty} + ze_{3\infty}$ is a generator of translations. Intuitively, we may picture it as the arc length swept out by an infinitesimal rotation with an infinite radius; the limit, as $r \Rightarrow \infty$ and $\theta \Rightarrow 0$ while $r\theta$ remains constant. However, this is only an aid to understanding. To show that the versor $t = \exp(\boldsymbol{t}e_\infty)$ is a translator by purely algebraic means, without resorting to limits or approximations, we use the familiar power-series expansion of the exponential

$$\begin{aligned} t = \exp(-\boldsymbol{t}e_\infty) &= \sum_{n=0}^{\infty} \frac{(-\boldsymbol{t}e_\infty)^n}{n!} = 1 - \boldsymbol{t}e_\infty + \boldsymbol{t}^2 \cancel{e_\infty^2} \sum_{n=2}^{\infty} \frac{(-1)^n (\boldsymbol{t}e_\infty)^n}{n!} \\ &= 1 - \boldsymbol{t}e_\infty \end{aligned} \tag{9}$$

and verify that $tp(\boldsymbol{x})\overleftarrow{t} = (1 - \boldsymbol{t}e_\infty)p(\boldsymbol{x})(1 + \boldsymbol{t}e_\infty) = p(\boldsymbol{x} + 2\boldsymbol{t})$, which is just the result of translating $\boldsymbol{x}$ by $2\boldsymbol{t}$. Further, $t\overleftarrow{t} = 1$, and $st = (1 - \boldsymbol{s}e_\infty)(1 - \boldsymbol{t}e_\infty) = 1 - (\boldsymbol{s} + \boldsymbol{t})e_\infty$. Thus the translators are indeed versors which act on each other by simple multiplication, yielding composition, and act on the vectors in the horosphere by conjugation, producing a translation. The conformal model of Euclidean space is crucial for this argument, because it is easily verified that $tp(\boldsymbol{x})\overleftarrow{t} \neq p(t\boldsymbol{x}\overleftarrow{t})$. Indeed, $t\boldsymbol{x}\overleftarrow{t} = \boldsymbol{x}$, so every translator reduces to the identity transformation when acting on Euclidean space directly.

We are now in a position to introduce the general element of $\mathbb{SE}(3)$ as the product of a translator and a rotor, which we shall refer to as a *motor*. Let the vector $\boldsymbol{t} = d\boldsymbol{a}$, $\boldsymbol{a}^2 = 1$, so the translator $t = \exp(-\frac{1}{2} d\boldsymbol{a}e_\infty) = 1 - \frac{1}{2} d\boldsymbol{a}e_\infty$ translates by distance d along $\boldsymbol{a}$. And

let the vectors $\boldsymbol{b}$ and $\boldsymbol{c}$ define a bivector $\boldsymbol{r} = \boldsymbol{bc}$, $\boldsymbol{r}\tilde{\boldsymbol{r}} = 1$, so the rotor $r = \exp(-\frac{1}{2}\alpha\boldsymbol{bc}) = \cos\frac{1}{2}\alpha - \sin\frac{1}{2}\alpha\,\boldsymbol{bc}$ rotates by angle α in the $\boldsymbol{bc}$ plane. Then their product is the motor

$$\begin{aligned} m = tr &= \exp(-\tfrac{1}{2}d\boldsymbol{a}e_\infty)\exp(-\tfrac{1}{2}\alpha\boldsymbol{bc}) = (1-\tfrac{1}{2}d\boldsymbol{a}e_\infty)(\cos\tfrac{1}{2}\alpha - \sin\tfrac{1}{2}\alpha\,\boldsymbol{bc}) \\ &= \underbrace{\cos\tfrac{1}{2}\alpha}_{\text{scalar}} - \underbrace{(\sin\tfrac{1}{2}\alpha\,\boldsymbol{bc} + \tfrac{1}{2}d\cos\tfrac{1}{2}\alpha\,\boldsymbol{a}e_\infty)}_{\text{bivector}} + \underbrace{\tfrac{1}{2}d\sin\tfrac{1}{2}\alpha\,\boldsymbol{abc}e_\infty}_{\text{quadvector}} \end{aligned} \tag{10}$$

which acts on the horosphere by performing the indicated rotation followed by the indicated translation. That is, $mp(\boldsymbol{x})\tilde{m} = trp(\boldsymbol{x})\tilde{r}\tilde{t} = tp(r\boldsymbol{x}\tilde{r})\tilde{t} = p(r\boldsymbol{x}\tilde{r} + \boldsymbol{t})$, so motors represent general rigid body motions when working in the conformal model of Euclidean geometry. We have $m\tilde{m} = tr\tilde{t}\tilde{r} = tr\tilde{r}\tilde{t} = t\tilde{t} = 1$, so motors are versors, meaning that $m^{-1} = \tilde{m}$.

We have thus found a geometric algebra which contains a model of 3D Euclidean space (represented by the horosphere), a unitary representation of the Lie group of rigid body motions (the motors), and a representation of its Lie algebra (spanned by the unit bivectors $\{e_{23}, e_{31}, e_{12}\}$ and the null bivectors $\{e_{1\infty}, e_{2\infty}, e_{3\infty}\}$). All of this is completely consistent with standard Lie theory – just simpler. We have used only elementary algebraic operations, and this greatly simplifies the calculations we are about to undertake.

In standard Lie theory, the elements of the Lie algebra are constructed by taking the derivative of the group action at the identity. Thus they are conceived as "tangent vectors" in the abstract sense, meaning that they satisfy the axioms of a flat vector space

which is tangent to the group manifold at the identity. In geometric algebra, we represent these as bivectors, but these also form an abstract vector space. Thus we sometimes refer to bivectors as "tangent vectors" below, both to make contact with standard Lie theory and to emphasise their role in the formal differential geometry of the group manifold.

We close this section with two facts that are very easy to establish using our representation of $\mathbb{SE}(3)$ and its Lie algebra, but require much more intricate constructions and very careful argumentation in the standard Lie theory. Firstly, any curve of the form $\varphi(s) = \exp(s\boldsymbol{x})$ passes through the identity element, where we have $\partial_s \varphi = \boldsymbol{x}$. It is immediate that $\varphi(s+t) = \varphi(s)\varphi(t)$, so curves of this kind are one-parameter subgroups. In standard Lie theory, we say that such a curve passes through the identity with tangent vector $\boldsymbol{x}$. Secondly, for every bivector $\boldsymbol{x}$ and for all versors g and h, we have $g(\exp \boldsymbol{x})g^{-1} = \exp(g\boldsymbol{x}g^{-1})$ and $\log(ghg^{-1}) = g(\log h)g^{-1}$, again by simple algebra. In standard Lie theory, these two equalities follow from the fact that the exponential map commutes with the adjoint action. Not only these facts themselves, but the ease with which such facts are obtained using conformal geometric algebra, are pivotal to the development of our argument in the next section.

Statistical Analysis in $\mathbb{SE}(3)$

In general terms, our problem may be stated as follows. Given a set of points $\{x_k\}_{k=1}^N$ lying in the manifold of a Lie group, and a set of real-valued weights $\{\omega_k\}_{k=1}^N$ which sum to 1, we define the barycentre as $x_0 = \arg\min_{x\in\mathbb{G}} \sigma^2(x)$, where $\sigma^2(x)$ is the function we use to measure dispersion of the x_k about x and $\mathbb{G}$ is the group to which the x_k belong. In the simplest case, each point represents a member of the additive group of Euclidean translations. The natural definition of dispersion in this case us just the weighted sum of squared distances from the barycentre, which we find by setting the derivative of the dispersion to zero. Thus

$$\sigma^2(x) = \sum_{k=1}^{N} \omega_k (x_k - x)^2 \qquad \partial_x \sigma^2 = -2\sum_{k=1}^{N} \omega_k (x_k - x) \tag{11a}$$

$$\partial_x \sigma^2 |_{x_0} = 0 \Rightarrow x_0 = \frac{1}{N}\sum_{k=1}^{N} \omega_k x_k \tag{11b}$$

yields the arithmetic mean and variance familiar from basic statistics. Similarly,

$$\sigma^2(x) = \sum_{k=1}^{N} \omega_k (\log x_k - \log x_0)^2 \qquad \partial_x \sigma^2 = -\frac{2}{x}\sum_{k=1}^{N} \omega_k (\log x_k - \log x_0) \tag{12a}$$

$$\partial_x \sigma^2 |_{x_0} = 0 \Rightarrow x_0 = \exp\left(\frac{1}{N}\sum_{k=1}^{N} \omega_k \log x_k\right) = \left(\prod_{k=1}^{N} x_k{}^{\omega_k}\right)^{1/N} \tag{12b}$$

yields the geometric mean, and so on. In these expressions, exp and log are the ordinary exponential and logarithmic functions. But the positive real numbers under multiplication are a Lie group, and the real numbers under addition are its Lie algebra.

Thus we can view exp and log as mappings back and forth between a Lie group and its Lie algebra. We adopt this viewpoint because it lends itself to the generalizations we need for the problem at hand. Indeed, it is crucial to our approach. Because Euclidean space under addition is its own Lie algebra, the first example also fits this pattern, though the group is additive, so we use multiplication and addition on the right hand side of eq. 11b in place of the exponentiation and multiplication in eq. 12b.

Of course, we want the barycentre to depend only on properties intrinsic to the elements, and not on the arbitrary conventions we use to describe them, so bi-invariance is an essential property which we want it to have. This is guaranteed in the above examples, because the group manifolds possess bi-invariant Riemannian metrics. Now, a Riemannian metric is a positive-definite bi-linear form defined on a manifold, and it is well known [Zefran et al. 1999] that there are exactly two bi-invariant bi-linear forms on $\mathbb{SE}(3)$, neither of which is positive-definite: the Killing form, which is degenerate (it vanishes identically), and the Klein form, which is indefinite (it can be positive, negative or zero). Consequently, there is no bi-invariant Riemannian metric on $\mathbb{SE}(3)$.

Remarkably, this does not prevent us from defining a bi-invariant mean on $\mathbb{SE}(3)$, because we can still define geodesics joining the points x_k to the barycentre x_0. We do this by giving up the idea of finding a minimum-length curve between two points, and rely on the more general definition of a geodesic as a curve along which the acceleration relative to the manifold vanishes at each point. Even in the absence of a metric, we can parameterize a curve by an *affine* parameter which permits us to carry out the necessary

calculations, even though it fails to satisfy the triangle inequality, and therefore does not qualify as a metric.

We are free to do this because the group structure of the manifold is essentially topological, and does not uniquely determine its geometry. It is the *connection* which specifies the geometry by specifying how the tangent space transforms as its point of tangency to the manifold moves along a curve that lies in the manifold. In general, a change in any vector lying in the tangent space will be composed of a *intrinsic part*, which is entirely contained in the tangent space, and an *extrinsic part*, which lies entirely outside it. The intrinsic part is called the *covariant derivative*, and if it is zero, then the vector remains constant, relative to the tangent space at each point – and therefore, relative to the manifold – as it is transported along the curve. Such transport is called *parallel transport*.

How the change in the vector is decomposed into intrinsic and extrinsic parts is determined by the connection, which specifies the transformation of the tangent space brought about by moving the point of tangency along the curve. Under parallel transport, the vector and the tangent space transform together in lock step, so the relative transformation between them (the covariant derivative) vanishes. Thus a point moving along the curve undergoes no acceleration, relative to the manifold, when the curve parallel-transports its own tangent vector. Such a curve is called a geodesic.

There are infinitely many connections, which differ in the curvature and torsion they assign to the manifold at each point. In keeping with generally-familiar notation, we

write the covariant derivative of a vector field $\boldsymbol{y}$ along a curve with tangent vector $\boldsymbol{x}$ as $\nabla_{\boldsymbol{x}}\boldsymbol{y}$ without losing sight of the fact that $\boldsymbol{x}$ and $\boldsymbol{y}$ are elements of the Lie algebra, which we represent as bivectors. A rigorous definition of multivector derivative may be found in Hestenes & Sobczyk [1987] or Doran & Lasenby [2007]; for a standard treatment of the differential geometry of Lie groups, see Nomizu [1956]. For given $\boldsymbol{x}$ and $\boldsymbol{y}$, which depend on the position a in the group manifold, we refer to $\nabla_{\boldsymbol{x}}\boldsymbol{y}$ as the action of the connection relative to the group's tangent space at a. Using this notation, the torsion is just

$$T(\boldsymbol{x},\boldsymbol{y}) = \nabla_{\boldsymbol{x}}\boldsymbol{y} - \nabla_{\boldsymbol{y}}\boldsymbol{x} - [\boldsymbol{x},\boldsymbol{y}] \tag{13}$$

and the curvature is

$$R(\boldsymbol{x},\boldsymbol{y})\boldsymbol{z} = \nabla_{\boldsymbol{x}}(\nabla_{\boldsymbol{y}}\boldsymbol{z}) - \nabla_{\boldsymbol{y}}(\nabla_{\boldsymbol{x}}\boldsymbol{z}) - \nabla_{[\boldsymbol{x},\boldsymbol{y}]}\boldsymbol{z} \tag{14}$$

When a bi-invariant metric g_{ij} exists, it fixes both curvature and torsion at every point in the manifold, so there is a unique connection, called the Levi-Civita connection, which is compatible with the metric. In this case the connection coefficients, or Christoffel symbols Γ^{m}_{ij}, are defined by the relation $\nabla_{\partial_i}\partial_j \cdot \partial_k = g_{mk}\Gamma^{m}_{ij}$. When there is no such metric, we can still write $\nabla_{\partial_i}\partial_j = \Gamma^{k}_{ij}\partial_k$ and derive the transformation connecting tangent spaces at neighbouring points from the Maurer-Cartan form, which maps the tangent space at any point of the manifold to the tangent space at the identity; that is, from the tangent space at any element of the group to the Lie algebra. Affine connections of this type are uniquely determined by their action at the identity, $\nabla_{\boldsymbol{x}}\boldsymbol{y}|_1$, in which writing the

identity as 1 is not a mere notational convention; in geometric algebra, the real number 1 actually does serve as the identity element of the group.

Of these, the family known as Cartan-Schouten connections [Cartan & Schouten 1926; Nomizu 1954] satisfy $\nabla_{\boldsymbol{x}} \boldsymbol{x}|_1 = 0$ for every vector x in the tangent space at the identity; that is, for every element of the Lie algebra. Now, the Cartan-Schouten connections which are bi-invariant are of the form $\nabla_{\boldsymbol{x}} \boldsymbol{y}|_1 = a[\boldsymbol{x}, \boldsymbol{y}]$, for some real constant a, as shown by Laquer [1992]. Of these, two have zero curvature and constant torsion, and one has constant curvature and zero torsion:

The (+)-connection is defined by	$\nabla_{\boldsymbol{x}} \boldsymbol{y}\|_1 = [\boldsymbol{x}, \boldsymbol{y}]$	$R = 0$	$T = +[\boldsymbol{x}, \boldsymbol{y}]$
The (0)-connection is defined by	$\nabla_{\boldsymbol{x}} \boldsymbol{y}\|_1 = \frac{1}{2}[\boldsymbol{x}, \boldsymbol{y}]$	$R = -\frac{1}{4}[[\boldsymbol{x}, \boldsymbol{y}], \boldsymbol{z}]$	$T = 0$
The (–)-connection is defined by	$\nabla_{\boldsymbol{x}} \boldsymbol{y}\|_1 = 0$	$R = 0$	$T = -[\boldsymbol{x}, \boldsymbol{y}]$

This table follows by direct substitution of the action $\nabla_{\boldsymbol{x}} \boldsymbol{y}|_1$ into eq. 13 and 14, together with the Jacobi identity.

Clearly, the vanishing of the torsion makes the antisymmetric part of the covariant derivative equal to the Lie derivative: $\nabla_{\boldsymbol{x}} \boldsymbol{y} - \nabla_{\boldsymbol{y}} \boldsymbol{x} = [\boldsymbol{x}, \boldsymbol{y}]$. This has the consequence, crucial for our purposes, that the curves which parallel-transport their own tangent vectors under the action of the connection are also the integral curves of their tangent vectors under the group action. The unique, torsion-free, bi-invariant Cartan-Schouten 0-connection satisfies exactly this requirement. Hence, every geodesic is a one-parameter subgroup; that is, a curve of the form $\varphi(s) = \exp(s\boldsymbol{x})$. This is why it is essential to work

in a compact representation of the group, because it is then guaranteed that every element of the group lies on a geodesic through the identity.

The bi-invariance of the Cartan-Schouten 0-connection fixes the geometry in such a way that the geodesic $\varphi(s)$ passing from x_0 to x_k remains invariant when the curve is transformed to pass from the identity to $x_0^{-1}x_k$. But this is just the one-parameter subgroup $\varphi(s) = \exp(s \log(x_0^{-1}x_k))$, and for this curve, the affine measure increases monotonically from $s = 0$ at the identity to $s = |\log(x_0^{-1}x_k)|$ at $x_0^{-1}x_k$. Hence, we may define the dispersion of our weighted set of points as

$$\sigma^2(x) = \sum_{k=1}^{N} \omega_k \, |\log(x_0^{-1}x_k)|^2 \tag{15}$$

This formula is very reminiscent of eq. 12a, but we are now dealing with the group logarithm of a noncommutative group, so the computation of derivatives is not so straight-forward. In view of these results, Pennec & Arsigny [2013] suggested a fixed-point algorithm, as follows:

Set the initial estimate of x_0 to $x_{0,0} = 1$

Repeat $x_{0,n+1} = x_{0,n} \exp\left(\sum_{k=1}^{N} \omega_k \log(x_{0,n}^{-1} x_k) \right)$ until $|\log x_{0,n+1}^{-1} x_{0,n}|^2 \le \varepsilon \sigma^2(x_{0,n})$

Essentially, this algorithm performs gradient descent, and terminates when the change in the solution between successive iterations is smaller than some fixed fraction ε of the dispersion. Gebken & Sommer [2008] apparently use a similar algorithm on $\mathbb{SE}(3)$, but give very little detail. Buss & Fillmore [2001] give a derivation and a proof of

uniqueness in the context of $\mathbb{SO}(3)$, but the result carries over to $\mathbb{SE}(3)$, and indeed to any group for which the one-parameter subgroups are geodesics of the Cartan-Schouten (0)-connection.

When this algorithm converges, we have $x_{0,n+1} = x_{0,n} = x_0$, so we must have

$$\exp\left(\sum_{k=1}^{N} \omega_k \log(x_0^{-1} x_k)\right) = 1 \quad \text{or just} \quad \sum_{k=1}^{N} \omega_k \log(x_0^{-1} x_k) = 0 \tag{16}$$

Thus the dispersion is minimized when the affine displacements along the geodesics sum to zero. In Appendix E, we show that the point x_0 which satisfies this equation is invariant under left-displacements, right-displacements, and inversion. Therefore it is the unique bi-invariant barycentre of the points $\{x_k\}_{k=1}^{N}$ with weights $\{\omega_k\}_{k=1}^{N}$.

This algorithm, implemented in terms of matrix representations of $\mathbb{SE}(3)$, incurs heavy computational penalties. Firstly, because the matrix exponential and logarithm must be calculated by cumbersome series expansions [Cardoso & Leite 2010]. Secondly, because the Baker-Campbell-Hausdorff (BCH) formula makes an infinite series of commutations out of the logarithm of a product of general group elements, recent improvements in efficiency [Weyrauch & Scholz 2009] notwithstanding.

In addition, even though a measure of dispersion is defined, corresponding roughly to the idea of variance, the existing work on geodesic barycentres provides no practical means of calculating any anisotropy in the dispersion, analogous to covariance. Therefore it is unable to provide a reliable means of performing statistical comparisons between geodesic barycentres, let along curves passing through such barycentres. In the

following sections, we show how to use conformal geometric algebra to solve these problems.

Logarithms Using Conformal Geometric Algebra

As before, we write the general element of $\mathbb{SE}(3)$ as a motor m, composed of a translation versor $t = \exp(-\frac{1}{2}\boldsymbol{t}e_\infty) = 1 - \frac{1}{2}\boldsymbol{t}e_\infty$ and rotation versor $r = \exp(-\frac{1}{2}\theta\boldsymbol{r})$ $= \cos\frac{1}{2}\theta - \sin\frac{1}{2}\theta\boldsymbol{r}$ so that

$$m = tr = \exp(-\tfrac{1}{2}\boldsymbol{t}e_\infty)\exp(-\tfrac{1}{2}\theta\boldsymbol{r}) = (1-\tfrac{1}{2}\boldsymbol{t}e_\infty)(\cos\tfrac{1}{2}\theta - \sin\tfrac{1}{2}\theta\boldsymbol{r}) \quad (17)$$

where $\boldsymbol{t}$ is the translation vector and θ is the angle of rotation in the plane of the unit bivector $\boldsymbol{r}$. The logarithm of the motor expressed in this form is given by the Baker-Campbell-Hausdorff (BCH) formula:

$$\log m = \log(\exp(-\tfrac{1}{2}\boldsymbol{t}e_\infty)\exp(-\tfrac{1}{2}\theta\boldsymbol{r})) = -\tfrac{1}{2}\boldsymbol{t}e_\infty - \tfrac{1}{2}\theta\boldsymbol{r} + \tfrac{1}{8}\theta[\boldsymbol{t}e_\infty, \boldsymbol{r}] + \ldots \quad (18)$$

where $[\boldsymbol{t}e_\infty, \boldsymbol{r}] = \boldsymbol{t}e_\infty\boldsymbol{r} - \boldsymbol{r}\boldsymbol{t}e_\infty$ is the commutator product. The fact that the bivectors $\boldsymbol{t}e_\infty$ and $\boldsymbol{r}$ do not generally commute makes this is an infinite series, and this is an obstacle to efficient statistical calculations in $\mathbb{SE}(3)$. To overcome it, we seek to refactor the motor in terms of versors that do commute. We therefore decompose the vector $\boldsymbol{t}$ into the sum of a part $\boldsymbol{u}$ that lies in the plane of $\boldsymbol{r}$ and a part $\boldsymbol{w}$ that is perpendicular to it, so that $\boldsymbol{t} = \boldsymbol{u} + \boldsymbol{w}$, where the translation by $\boldsymbol{w}$ commutes with the rotation in the plane of $\boldsymbol{r}$, but the translation by $\boldsymbol{u}$ does not. This is easy to do using the fact that $\boldsymbol{r}$ is a unit bivector, so $\boldsymbol{r}\tilde{\boldsymbol{r}} = 1$. Thus

$$\boldsymbol{t} = \boldsymbol{t}(\boldsymbol{r}\tilde{\boldsymbol{r}}) = (\boldsymbol{t}\boldsymbol{r})\tilde{\boldsymbol{r}} = (\boldsymbol{t}\cdot\boldsymbol{r})\tilde{\boldsymbol{r}} + (\boldsymbol{t}\wedge\boldsymbol{r})\tilde{\boldsymbol{r}} = \boldsymbol{u} + \boldsymbol{w} \quad (19)$$

We then define a new versor s by writing

$$m = tr = (wu)r = w(ur) = ws \tag{20}$$

where $u = 1 - \frac{1}{2}\boldsymbol{u}e_\infty$ and $w = 1 - \frac{1}{2}\boldsymbol{w}e_\infty$ are translation versors formed from the vectors $\boldsymbol{u}$ and $\boldsymbol{w}$. The versors w and s commute because $s = ur$ acts solely in the plane of $\boldsymbol{r}$ and w acts perpendicular to it.

We now seek a vector $\boldsymbol{v}$, from which we can form $v = 1 - \frac{1}{2}\boldsymbol{v}e_\infty$, allowing us to write $s = ur = vr\bar{v}$. From the following figure 1 below, it is clear that the product ws expresses the motor in screw form, whereby $\boldsymbol{v}$ must satisfy $\boldsymbol{u} = \boldsymbol{v} - rvr\bar{}$. Essentially, v translates the screw axis to the origin, r performs the rotation, $\bar{v}$ translates back, and w translates along the screw axis.

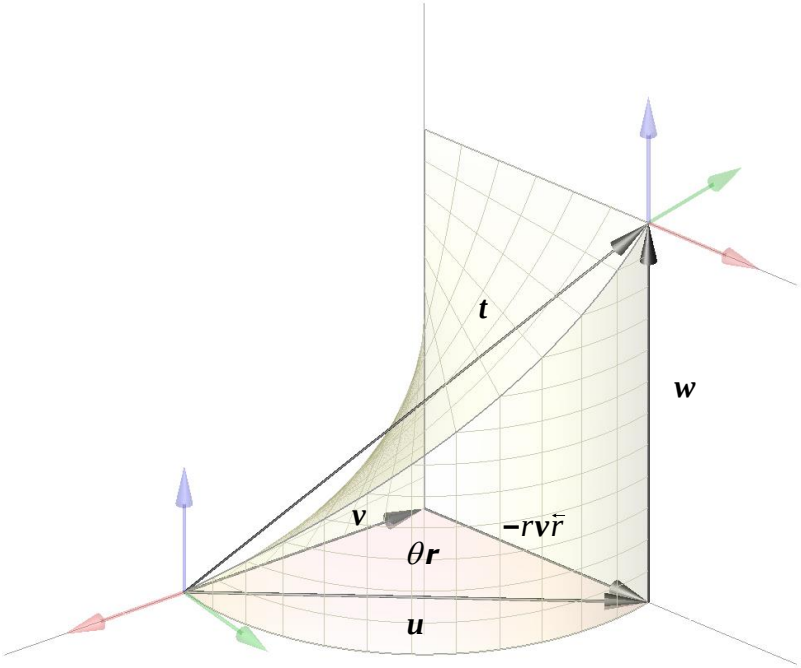

Figure 1 - Geometry of the screw transformation.

It is also clear from this figure that $v = |\boldsymbol{v}|$ is the radius of the screw, so $u = 2v\sin\frac{1}{2}\theta$. After some algebraic manipulations, which can be found in Appendix D, we obtain the motor in screw form:

$$m = ws = wvr\bar{v} = \exp(-\tfrac{1}{2}\boldsymbol{w}e_\infty)\exp(-\tfrac{1}{2}\theta v\boldsymbol{r}\bar{v}) = (1-\tfrac{1}{2}\boldsymbol{w}e_\infty)(\cos\tfrac{1}{2}\theta - \sin\tfrac{1}{2}\theta v\boldsymbol{r}\bar{v}) \quad (21)$$

Because w and s commute, the BCH formula terminates and we can write the logarithm very simply as

$$\log m = \log(ws) = \log(w) + \log(s) = -\tfrac{1}{2}\boldsymbol{w}e_\infty - \tfrac{1}{2}\theta v\boldsymbol{r}\bar{v} \quad (22)$$

which, after further algebra detailed in Appendix D, yields

$$\log m = -\tfrac{1}{2}(\boldsymbol{w} + (\operatorname{sinc}\tfrac{1}{2}\theta)^{-1}\bar{r}\boldsymbol{u})e_\infty - \tfrac{1}{2}\theta\boldsymbol{r} \quad (23)$$

Taking the squared magnitude of this quantity is straight forward:

$$|\log m|^2 = \tfrac{1}{4}(w^2 + (v^2+1)\theta^2) \quad (24)$$

In this form, it is easy to see that, when $\theta \Rightarrow 0$, we recover the flat metric of $\mathbb{R}^3$; when $\boldsymbol{t} \Rightarrow 0$ (forcing $w \Rightarrow 0$ and $v \Rightarrow 0$), we recover the bi-invariant metric of $\mathbb{SO}(3)$; in the general case, we have a smoothly varying blend of the two, which is a suitable affine parameter for geodesics of the Cartan-Schouten (0)-connection of $\mathbb{SE}(3)$ but does not constitute a metric of $\mathbb{SE}(3)$, as we have seen.

Estimating the Geodesic Barycentre

Let $\{m_k = (a_{0k}, a_{1k}, a_{2k}, a_{3k}, x_{1k}, x_{2k}, x_{3k})^T \in \mathbb{R}^7\}_{k=1}^N$ be a set of N data (either measurements or the result of a previous calculation) representing elements of $\mathbb{SE}(3)$ as motors, where the a_{ik} are the components of a quaternion a_k representing the rotation and the x_{ik} are the components of a vector $\boldsymbol{x}_k$ representing the translation, both with respect to a fixed reference frame $\{e_1, e_2, e_3\}$. We put $\cos\tfrac{1}{2}\alpha_k = a_{0k}/|a_k|$ and $\sin\tfrac{1}{2}\alpha_k = \varsigma_k|\boldsymbol{a}_k|/|a_k|$, with $|\boldsymbol{a}_k|^2 = a_{1k}^2 + a_{2k}^2 + a_{3k}^2$ and $|a_k|^2 = a_{0k}^2 + a_{1k}^2 + a_{2k}^2 + a_{3k}^2$, in which we have introduced $\varsigma_k = \pm 1$ to ensure that all rotations are uniformly oriented so

as to belong to the component of the group which is continuously connected to the identity, and thus corresponds to $\mathbb{SE}(3)$. This can easily be handled in preprocessing, so without loss of generality, we can absorb the ς_k into the $\boldsymbol{a}_k$ in the remainder of the development. The quaternion a_k then represents a rotation by angle α_k in the plane of the unit bivector $\hat{\boldsymbol{a}}_k = \boldsymbol{a}_k / |\boldsymbol{a}_k|$. Thus

$$\begin{aligned} a_k &= |a_k| \exp(-\tfrac{1}{2}\alpha_k \hat{\boldsymbol{a}}_k) = |a_k|(\cos\tfrac{1}{2}\alpha_k - \sin\tfrac{1}{2}\alpha_k \hat{\boldsymbol{a}}_k) \\ &= a_{0k} - \boldsymbol{a}_k = a_{0k} - a_{1k} e_{23} - a_{2k} e_{31} - a_{3k} e_{12} \end{aligned} \tag{25}$$

is a noisy estimate of a rotation versor,

$$x_k = \exp(-\tfrac{1}{2}\boldsymbol{x}_k) = 1 - \tfrac{1}{2}\boldsymbol{x}_k e_\infty = 1 - \tfrac{1}{2}x_{1k} e_{1\infty} - \tfrac{1}{2}x_{2k} e_{2\infty} - \tfrac{1}{2}x_{3k} e_{3\infty} \tag{26}$$

is a noisy estimate of a translation versor, and

$$\begin{aligned} z_k = z(m_k) = x_k a_k &= (1 - \tfrac{1}{2}\boldsymbol{x}_k e_\infty)(a_{0k} - \boldsymbol{a}_k) \\ &= |a_k|(1 - \tfrac{1}{2}\boldsymbol{x}_k e_\infty)(\cos\tfrac{1}{2}\alpha_k - \sin\tfrac{1}{2}\alpha_k \hat{\boldsymbol{a}}_k) \\ &= a_{0k} - \boldsymbol{a}_k - \tfrac{1}{2}a_{0k}\boldsymbol{x}_k e_\infty + \tfrac{1}{2}\boldsymbol{x}_k \boldsymbol{a}_k e_\infty \end{aligned} \tag{27}$$

is a noisy estimate of a motor with scalar, bivector, and quadvector parts

$$\begin{aligned} \langle z_k \rangle_0 &= a_{0k} && \text{(scalar part)} \\ \langle z_k \rangle_2 &= -\boldsymbol{a}_k - \tfrac{1}{2}(a_{0k}\boldsymbol{x}_k - \boldsymbol{x}_k \cdot \boldsymbol{a}_k) e_\infty && \text{(bivector part)} \\ \langle z_k \rangle_4 &= \tfrac{1}{2}\boldsymbol{x}_k \wedge \boldsymbol{a}_k e_\infty && \text{(quadvector part)} \end{aligned} \tag{28}$$

in which we have used $\boldsymbol{x}_k \boldsymbol{a}_k = \boldsymbol{x}_k \cdot \boldsymbol{a}_k + \boldsymbol{x}_k \wedge \boldsymbol{a}_k$. In components, this reads

$$
\begin{aligned}
z_k &= z_{0k} + z_{1k}e_{23} + z_{2k}e_{31} + z_{3k}e_{12} + z_{4k}e_{1\infty} + z_{5k}e_{2\infty} + z_{6k}e_{3\infty} + z_{7k}e_{123\infty} \\
&= a_{0k} && \text{(scalar part)} \\
&\quad - a_{1k}e_{23} - a_{2k}e_{31} - a_{3k}e_{12} \\
&\quad - \tfrac{1}{2}(a_{0k}x_{1k} - (x_{3k}a_{2k} - x_{2k}a_{3k}))e_{1\infty} \\
&\quad - \tfrac{1}{2}(a_{0k}x_{2k} - (x_{1k}a_{3k} - x_{3k}a_{1k}))e_{2\infty} && \text{(bivector part)} \\
&\quad - \tfrac{1}{2}(a_{0k}x_{3k} - (x_{2k}a_{1k} - x_{1k}a_{2k}))e_{3\infty} \\
&\quad - \tfrac{1}{2}(x_{1k}a_{1k} + x_{2k}a_{2k} + x_{3k}a_{3k})e_{123\infty} && \text{(quadvector part)}
\end{aligned}
\tag{29}
$$

The quadvector is completely determined by the scalar and the bivector, so it plays no further part in our analysis. The z_k and the m_k stand in 1-to-1 correspondence, so we refer to both as a motor, except when the context fails to make it clear which is meant.

Since the data are noisy, each given motor m_k differs from the unknown true value $\hat{m}_k$ by some unknown error term Δ_{m_k}. Thus $\hat{m}_k = m_k + \Delta_{m_k}$, meaning

$$
\begin{aligned}
\hat{a}_k = a_k + \Delta_{a_k} &= a_{0k} + \Delta_{a_{0k}} - (\boldsymbol{a}_k + \Delta_{\boldsymbol{a}_k}) \\
&= a_{0k} - a_{1k}e_{23} - a_{2k}e_{31} - a_{3k}e_{12} \\
&\quad + \Delta_{a_{0k}} - \Delta_{a_{1k}}e_{23} - \Delta_{a_{2k}}e_{31} - \Delta_{a_{3k}}e_{12}
\end{aligned}
\tag{30a}
$$

$$
\begin{aligned}
\hat{\boldsymbol{x}}_k = \boldsymbol{x}_k + \Delta_{\boldsymbol{x}_k} &= x_{1k}e_1 + x_{2k}e_2 + x_{3k}e_3 \\
&\quad + \Delta_{x_{1k}}e_1 + \Delta_{x_{2k}}e_2 + \Delta_{x_{3k}}e_3
\end{aligned}
\tag{30b}
$$

Also, each datum has a 7×7 covariance matrix

$$
\Sigma_{mm,k} = \begin{bmatrix} \Sigma_{aa,k} & \Sigma_{ax,k} \\ \Sigma_{xa,k} & \Sigma_{xx,k} \end{bmatrix} \tag{31}
$$

where $\Sigma_{aa,k}$ is the 4×4 auto-covariance of the quaternion, $\Sigma_{xx,k}$ is the 3×3 auto-covariance of the vector, and $\Sigma_{ax,k} = \Sigma_{xa,k}^T$ is their 4×3 cross-covariance. If the data are calculated values, then presumably a covariance matrix will have been calculated for

each one. If the data are measurements, then the sample covariance matrix may be used instead. If nothing else, a diagonal matrix, formed from the RMS measurement noise, can serve as a simple estimate of the covariance matrix.

Letting $p = yb = (1 - \frac{1}{2}\boldsymbol{y}e_\infty)(b_0 - \boldsymbol{b})$ denote the estimated geodesic barycentre of the m_k, we write the vector of parameters to be estimated as $(b_0, b_1, b_2, b_3, y_1, y_2, y_3) \in \mathbb{R}^7$. As with the data, we have $\hat{p} = p + \Delta_p$, meaning.

$$\begin{aligned} \hat{b} = b + \Delta_b &= b_0 + \Delta_{b_0} - (\boldsymbol{b} + \Delta_{\boldsymbol{b}}) \\ &= b_0 - b_1 e_{23} - b_2 e_{31} - b_3 e_{12} \\ &+ \Delta_{b_0} - \Delta_{b_1} e_{23} - \Delta_{b_2} e_{31} - \Delta_{b_3} e_{12} \end{aligned} \tag{32a}$$

$$\begin{aligned} \hat{\boldsymbol{y}} = \boldsymbol{y} + \Delta_{\boldsymbol{y}} &= y_1 e_1 + y_2 e_2 + y_3 e_3 \\ &+ \Delta_{y_1} e_1 + \Delta_{y_2} e_2 + \Delta_{y_3} e_3 \end{aligned} \tag{32b}$$

Our approach to finding $\hat{p}$ will be to use a linear mixed-effects model with constraints, expressed in Gauss-Helmert form. Petersen & Koch [2010] show that this is essentially a reformulation of the extended Kalman filter in block form. Further, it is robust against inhomogeneous and anisotropic noise [Kanatani & Niitsuma 2012]. Essentially, the idea is to estimate the true data and parameter values by varying the parameter and minimally varying the given data so as to exactly satisfy all the constraints which are operative in the problem. We now proceed to formulate an objective function which we can minimise to achieve this goal.

The condition of minimally varying the data will be realized by permitting data values to vary in inverse proportion to the precision with which they are known, and forcing more highly correlated values to covary more closely than less correlated ones. This can

be accomplished by scaling the variations by the inverse of the covariance matrix and minimizing the resulting sum. Thus each datum contributes a term

$$S_{m,k}(\Delta_{m,k}) = \tfrac{1}{2}\Delta_{m,k}^T \Sigma_{mm,k}^{-1} \Delta_{m,k} = \tfrac{1}{2}\begin{bmatrix}\Delta_{a,k}^T & \Delta_{x,k}^T\end{bmatrix}\begin{bmatrix}\Sigma_{aa,k} & \Sigma_{ax,k} \\ \Sigma_{xa,k} & \Sigma_{xx,k}\end{bmatrix}^{-1}\begin{bmatrix}\Delta_{a,k} \\ \Delta_{x,k}\end{bmatrix} \tag{33}$$

and the overall sum is just

$$S_m(\Delta_m) = \tfrac{1}{2}\sum_k S_{m,k}(\Delta_{m,k}) = \tfrac{1}{2}\Delta_{(1)}^T \Sigma_{(1)}^{-1} \Delta_{(1)} \tag{34}$$

where

$$\Delta_{(1)} = \begin{bmatrix}\Delta_{a,1} \\ \Delta_{x,1} \\ \Delta_{a,2} \\ \Delta_{x,2} \\ \vdots \\ \Delta_{a,N} \\ \Delta_{x,N}\end{bmatrix} \quad \text{and} \quad \Sigma_{(1)} = \begin{bmatrix}\Sigma_{aa,1} & \Sigma_{ax,1} & 0 & \cdots & 0 \\ \Sigma_{xa,1} & \Sigma_{xx,1} & & & \\ 0 & & \Sigma_{aa,2} & \Sigma_{ax,2} & \cdots & 0 \\ & & \Sigma_{xa,2} & \Sigma_{xx,2} & & \\ \vdots & & \vdots & & \ddots & \vdots \\ 0 & & 0 & & \cdots & \Sigma_{aa,N} & \Sigma_{ax,N} \\ & & & & & \Sigma_{xa,N} & \Sigma_{xx,N}\end{bmatrix} \tag{35}$$

but this leaves the $\Delta_{a,k}$ and $\Delta_{x,k}$ interleaved. While this gives the covariance matrix a nice block diagonal form, it turns out that separating the $\Delta_{a,k}$ and $\Delta_{x,k}$ is instrumental to putting the equations in a form that can be easily solved in closed form. Thus we put

$$\Delta_a = \begin{bmatrix}\Delta_{a,1} \\ \Delta_{a,2} \\ \vdots \\ \Delta_{a,N}\end{bmatrix} \qquad \Delta_x = \begin{bmatrix}\Delta_{x,1} \\ \Delta_{x,2} \\ \vdots \\ \Delta_{x,N}\end{bmatrix} \qquad \Delta_m = \begin{bmatrix}\Delta_a \\ \Delta_x\end{bmatrix} \tag{36}$$

and

$$\Sigma_{aa} = \begin{bmatrix} \Sigma_{aa,1} & 0 & \cdots & 0 \\ 0 & \Sigma_{aa,2} & \cdots & 0 \\ \vdots & \vdots & \ddots & \vdots \\ 0 & 0 & \cdots & \Sigma_{aa,N} \end{bmatrix} \quad \Sigma_{ax} = \begin{bmatrix} \Sigma_{ax,1} & 0 & \cdots & 0 \\ 0 & \Sigma_{ax,2} & \cdots & 0 \\ \vdots & \vdots & \ddots & \vdots \\ 0 & 0 & \cdots & \Sigma_{ax,N} \end{bmatrix} \tag{37a}$$

$$\Sigma_{xa} = \begin{bmatrix} \Sigma_{xa,1} & 0 & \cdots & 0 \\ 0 & \Sigma_{xa,2} & \cdots & 0 \\ \vdots & \vdots & \ddots & \vdots \\ 0 & 0 & \cdots & \Sigma_{xa,N} \end{bmatrix} \quad \Sigma_{xx} = \begin{bmatrix} \Sigma_{xx,1} & 0 & \cdots & 0 \\ 0 & \Sigma_{xx,2} & \cdots & 0 \\ \vdots & \vdots & \ddots & \vdots \\ 0 & 0 & \cdots & \Sigma_{xx,N} \end{bmatrix} \tag{37b}$$

whereby

$$\Sigma_{mm} = \begin{bmatrix} \Sigma_{aa} & \Sigma_{ax} \\ \Sigma_{xa} & \Sigma_{xx} \end{bmatrix} \quad \Sigma_{mm}^{-1} = \begin{bmatrix} A & B \\ B^T & C \end{bmatrix} \tag{38}$$

in which the definitions of A, B and C follow from the standard formula for the inverse of a partitioned matrix and the fact that $\Sigma_{xa} = \Sigma_{ax}^T$. Thus we can write the first part of our objective function as

$$S_m(\Delta_m) = \tfrac{1}{2}\Delta_m^T \Sigma_{mm}^{-1} \Delta_m \tag{39}$$

with partial derivative with respect to the residuals given by

$$\partial_{\Delta_m} S_m(\Delta_m) = \Sigma_{mm}^{-1} \Delta_m \tag{40}$$

Now, while this quantity is to be minimized, the constraints must be satisfied exactly. These fall into three types: those which constrain the data alone, those which constrain the parameter alone, and those which constrain them jointly. The first two simply require the rotors to be unitary. For each datum, this leads to a constraint $g_k(a_k, x_k) = g(a_k)$ $= a_k \tilde{a}_k - 1 = 0$, and for the parameter, we have $g(b, y) = g(b) = b\overleftarrow{b} - 1 = 0$. Thus, to first order, we have

$$g(\hat{a}_k) = g(a_k + \Delta_{a,k}) = \underbrace{g(a_k)}_{-c_{g,k}} + \underbrace{\partial_a g(a_k)^T}_{J_{g,k}} \Delta_{a,k} = 0 \tag{41a}$$

$$g(\hat{b}) = g(b + \Delta_b) = \underbrace{g(b)}_{-c_b} + \underbrace{\partial_b g(b)^T}_{J_{g,b}} \Delta_b = 0 \tag{41b}$$

Renaming the terms as indicated, this reads $J_{g,k}\Delta_{a,k} - c_{g,k} = 0$ and $J_{g,b}\Delta_b - c_b = 0$. We can now form the matrices

$$J_{g,a} = \begin{bmatrix} J_{g,1} & 0 & \cdots & 0 \\ 0 & J_{g,2} & \cdots & 0 \\ \vdots & \vdots & \ddots & \vdots \\ 0 & 0 & \cdots & J_{g,N} \end{bmatrix} \qquad c_a = \begin{bmatrix} c_{g,1} \\ c_{g,2} \\ \vdots \\ c_{g,N} \end{bmatrix} \tag{42}$$

and stack these equations to read $J_{g,a}\Delta_a - c_a = 0$. Since we are requiring that these constraints must be satisfied exactly, we introduce Lagrange multipliers $l_a \in \mathbb{R}^N$ and $l_b \in \mathbb{R}$ to obtain the next part of our objective function:

$$S_g(\Delta_a, \Delta_b, l_a, l_b) = (J_{g,a}\Delta_a - c_{g,a})^T l_a + (J_{g,b}\Delta_b - c_{g,b})^T l_b \tag{43}$$

with partial derivatives

$$\partial_{\Delta_a} S_g = J_{g,a}^T l_a \qquad \partial_{\Delta_b} S_g = J_{g,b}^T l_b \tag{44a}$$

$$\partial_{l_a} S_g = (J_{g,a}\Delta_a - c_a)^T \qquad \partial_{l_b} S_g = (J_{g,b}\Delta_b - c_b)^T \tag{44b}$$

The last constraint is a bit more involved. It is the one which requires the parameter being estimated to be the geodesic barycentre of the data. But we have already shown in eq. 16 that this means

$$f(m_k, p) = f(a_k, x_k, b, y) = \sum_{k=1}^{N} \omega_k \log(p^{-1} m_k)$$
$$= \tfrac{1}{2} \sum_{k=1}^{N} \omega_k ((\boldsymbol{w}_k - \theta \boldsymbol{v}_k) e_\infty + \theta \hat{\boldsymbol{r}}_k) = 0 \tag{45}$$

where, of course, $\boldsymbol{w}_k = \boldsymbol{w}_k(a_k, x_k, b, y)$, $\boldsymbol{v}_k = \boldsymbol{v}_k(a_k, x_k, b, y)$, and $\boldsymbol{r}_k = \boldsymbol{r}_k(a_k, x_k, b, y)$ are determined by writing the product $p^{-1} m_k$ in screw form and taking its logarithm as detailed above. Thus, to first order, we have

$$\begin{aligned} f(\hat{a}_k, \hat{x}_k, \hat{b}, \hat{y}) &= f(a_k + \Delta_{a,k}, x_k + \Delta_{x,k}, b + \Delta_b, y + \Delta_y) = 0 \\ &= \underbrace{f(a_k, x_k, b, y)}_{-c_f} \\ &+ \underbrace{\partial_{a,k} f(a_k, x_k, b, y)^T}_{J_{a,k}} \Delta_{a,k} + \underbrace{\partial_{x,k} f(a_k, x_k, b, y)^T}_{J_{x,k}} \Delta_{x,k} \\ &\underbrace{\partial_b f(a_k, x_k, b, y)^T}_{J_b} \Delta_b + \underbrace{\partial_y f(a_k, x_k, b, y)^T}_{J_y} \Delta_y \end{aligned} \tag{46}$$

Thus we form

$$\begin{aligned} J_a &= \begin{bmatrix} J_{a,1} & J_{a,2} & \cdots & J_{a,N} \end{bmatrix} \\ J_x &= \begin{bmatrix} J_{x,1} & J_{x,2} & \cdots & J_{x,N} \end{bmatrix} \end{aligned} \tag{47}$$

so the equation reads $J_a \Delta_a + J_x \Delta_x + J_b \Delta_b + J_y \Delta_y - c_f = 0$. Now we introduce one more Lagrange multiplier $l_f \in \mathbb{R}^7$ to obtain the last part of our objective function:

$$S_f(\Delta_a, \Delta_x, \Delta_b, \Delta_y, l_f) = (J_a \Delta_a + J_x \Delta_x + J_b \Delta_b + J_y \Delta_y - c_f)^T l_f \tag{48}$$

with partial derivatives

$$\partial_{\Delta_a} S_f = J_a^T l_f \qquad \partial_{\Delta_x} S_f = J_x^T l_f \qquad \partial_{\Delta_b} S_f = J_b^T l_f \qquad \partial_{\Delta_y} S_f = J_y^T l_f \tag{49a}$$

$$\partial_{k_f} S_f = (J_a \Delta_a + J_x \Delta_x + J_b \Delta_b + J_y \Delta_y - c_f)^T \tag{49b}$$

In total, then, we have

$$S(\Delta_a,\Delta_x,\Delta_b,\Delta_y,l_a,l_b,l_f)=S_m(\Delta_a,\Delta_x)+S_g(\Delta_a,\Delta_b,l_a,l_b)+S_f(\Delta_a,\Delta_x,\Delta_b,\Delta_y,l_f) \tag{50}$$

and we will find p by solving

$$(\Delta_a,\Delta_x,\Delta_b,\Delta_y,l_a,l_b,l_f)=\underset{\Delta'_a,\Delta'_x,\Delta'_b,\Delta'_y,l'_a,l'_b,l'_f}{\arg\min}\ S(\Delta'_a,\Delta'_x,\Delta'_b,\Delta'_y,l'_a,l'_b,l'_f) \tag{51}$$

This is achieved when the derivatives of S with respect to the residuals and the Lagrange multipliers all vanish. That is, when

$$\begin{aligned}
\partial_{\Delta_a}S &= A\Delta_a+B\Delta_x+J_{g,a}^T l_a+J_a^T l_f=0\\
\partial_{\Delta_x}S &= B^T\Delta_a+C\Delta_x+J_x^T l_f=0\\
\partial_{\Delta_b}S &= J_{g,b}^T l_b+J_b^T l_f=0\\
\partial_{\Delta_y}S &= J_y^T l_f=0\\
\partial_{l_a}S &= J_{g,a}\Delta_a-c_a=0\\
\partial_{l_b}S &= J_{g,b}\Delta_b-c_b=0\\
\partial_{l_f}S &= J_a\Delta_a+J_x\Delta_x+J_b\Delta_b+J_y\Delta_y-c_f=0
\end{aligned} \tag{52}$$

The first pair, second pair, and last three of these equations can be put in the form

$$\begin{bmatrix} A & B\\ B^T & C\end{bmatrix}\begin{bmatrix}\Delta_a\\ \Delta_x\end{bmatrix}+\begin{bmatrix} J_{g,a}^T & 0 & J_a^T\\ 0 & 0 & J_x^T\end{bmatrix}\begin{bmatrix} l_a\\ l_b\\ l_f\end{bmatrix}=0 \tag{53a}$$

$$\begin{bmatrix} 0 & J_{g,b}^T & J_b^T\\ 0 & 0 & J_y^T\end{bmatrix}\begin{bmatrix} l_a\\ l_b\\ l_f\end{bmatrix}=0 \tag{53b}$$

$$\begin{bmatrix} J_{g,a} & 0\\ 0 & 0\\ J_a & J_x\end{bmatrix}\begin{bmatrix}\Delta_a\\ \Delta_x\end{bmatrix}+\begin{bmatrix} 0 & 0\\ J_{g,b} & 0\\ J_b & J_y\end{bmatrix}\begin{bmatrix}\Delta_b\\ \Delta_y\end{bmatrix}=\begin{bmatrix} c_a\\ c_b\\ c_f\end{bmatrix} \tag{53c}$$

Now, putting

$$J_m = \begin{bmatrix} J_{g,a} & 0 \\ 0 & 0 \\ J_a & J_x \end{bmatrix} \quad J_p = \begin{bmatrix} 0 & 0 \\ J_{g,b} & 0 \\ J_b & J_y \end{bmatrix} \quad l = \begin{bmatrix} l_a \\ l_b \\ l_f \end{bmatrix} \quad c_l = \begin{bmatrix} c_a \\ c_b \\ c_f \end{bmatrix} \quad \Delta_p = \begin{bmatrix} \Delta_b \\ \Delta_y \end{bmatrix} \tag{54}$$

we have

$$\Sigma_{mm}^{-1}\Delta_m + J_m^T l = 0 \qquad J_p^T l = 0 \qquad J_m\Delta_m + J_p\Delta_p = c_l \tag{55}$$

The first of these immediately gives us $\Delta_m = -\Sigma_{mm}J_m^T l$. We substitute this into the third to get $l = (J_m\Sigma_{mm}J_m^T)^{-1}(J_p\Delta_p - c_l)$, which we substitute into the second to get an explicit, closed-form solution for Δ_p:

$$\Delta_p = \underbrace{(J_p^T \overbrace{(J_m\Sigma_{mm}J_m^T)^{-1}}^{Q} J_p)^{-1}}_{S^T} J_p^T \overbrace{(J_m\Sigma_{mm}J_m^T)^{-1}}^{Q} c_l = S^T J_p^T Q\, c_l \tag{56}$$

Now, we simply set $p = p + \Delta_p$ and repeat until convergence is achieved, taking final value of p as our best estimate of $\hat{p}$. It should be noted that this is the only iteration in the estimation process. Conformal geometric algebra has enabled us to eliminate iteration from the calculation of logarithms of group elements, eliminate the iterative BCH formula for the calculation of logarithms of products of group elements, and formulate the estimation problem so as to eliminate the iterative calculation of the residuals at each step of the minimization of the objective function.

Estimating the Covariance Matrix

Once we have the barycentre, the covariance matrix is very easily calculated from quantities we already have in hand. If we evaluate c_l at $\hat{p}$, where $\Delta_b = 0$ and $\Delta_y = 0$, we have

$$c_l = \begin{bmatrix} c_a \\ c_b \\ c_f \end{bmatrix} = \begin{bmatrix} J_{g,a}\Delta_a \\ J_{g,b}\Delta_b \\ J_a\Delta_a + J_x\Delta_x + J_b\Delta_b + J_y\Delta_y \end{bmatrix} = \begin{bmatrix} J_{g,a}\Delta_a \\ 0 \\ J_a\Delta_a + J_x\Delta_x \end{bmatrix} = \begin{bmatrix} J_{g,a} & 0 \\ 0 & 0 \\ J_a & J_x \end{bmatrix} \begin{bmatrix} \Delta_a \\ \Delta_x \end{bmatrix} \quad (57)$$
$$= J_m\Delta_m$$

and, by definition, $\Sigma_{pp} = \Sigma_{\Delta_p\Delta_p} = \Delta_p\Delta_p^T = S^T J_p^T Q c_l c_l^T Q^T J_p S$. Substituting the former into the later, we have

$$\Sigma_{pp} = S^T J_p^T Q J_m \Sigma_{mm} J_m^T Q^T J_p S = S^T J_p^T Q Q^{-1} Q^T J_p S = S^T \underbrace{J_p^T Q^T J_p}_{R} S = S^T R S$$
$$= \underbrace{(J_p^T (J_m \Sigma_{mm} J_m^T)^{-1} J_p)^{-1}}_{S^T} \underbrace{J_p^T (J_m \Sigma_{mm} J_m^T)^{-T} J_p}_{R} \underbrace{(J_p^T (J_m \Sigma_{mm} J_m^T)^{-1} J_p)^{-T}}_{S} \quad (58)$$

Application to Reach-to-Grasp Trajectories

We will now discuss an application of this novel methodology to an experiment in cognitive psychology, addressing the question of how competing action plans for reach-and-grasp responses are resolved over time. It is well-established that attending to a picture of a manipulable object evokes motor cortical activity; this finding is consistent with the view that the depicted object automatically leads to a mental representation of hand actions associated with it [e.g., Chao & Martin 2000; Grèzes, Tucker, Armony, Ellis & Passingham 2003; Handy, Grafton, Shroff, Ketay & Gazzaniga 2003]. Behavioural evidence supports the inference that manipulable objects evoke motor representations consistent with the objects' form and function [Bub, Masson, & Cree 2008; Bub & Masson 2010; Sumner & Husain 2008; Witt et al. 2010]. Of particular interest is the nature of these representations and their influence on the planning and execution of a subsequent action. One view holds that the mental representations of actions induced by a depicted object remain sufficiently abstract that the influence of such representations should be confined to the planning stages and effectively decoupled from the on-line control of movement [Glover 2004; Liu, Chua & Enns 2008; Milner & Goodale 2008]. The alternative view holds that an object evokes action representations coded in a form compatible with the actual execution of a motor program, which, once active, may then compete with and affect the entire course of an unrelated grasping action [Cisek 2007; Cisek & Kalaska 2005].

Evidence supporting the latter view is provided by behavioural studies, in which subjects are required to initiate a reaching response before one of a number of available targets is specified [Chapman et al. 2010a; Stewart et al. 2013]. Under these circumstances, the motor system can plan multiple reaches to the targets, and the initial movement appears to represent an average of these plans. So far, the evidence on the evocation of multiple action plans is limited to motor planning under conditions of uncertainty, characterized by competition between action plans that occurs when subjects do not know what the final target will be, and is fully resolved soon after the target is specified. Another form of competition arises when we attend to one object that evokes an action plan, but engage in a competing action applied to a separate object. For example, in a variant of the well known Eriksen flanker task [Eriksen & Eriksen 1974] a target arrow signals the direction of movement while irrelevant flanker arrows either conflict or agree with the intended action. Under these circumstances, the intended action is clearly specified but competition may occur from the action plan evoked by the irrelevant stimuli [Coulthard et al. 2008].

Characterizing the influence of a previously attended object on a grasping action requires that the trajectory of the hand under the influence of a competing object be compared with the trajectory of the hand when no such competition is present. The method described in this work allows the statistical analysis of dynamic changes in the motion of the hand against a complex background of substantial between- and within-subjects variation. As a result, we were able to capture very subtle perturbations of

reach-to-grasp trajectories and characterize their dependence on experimental manipulations. This is a significant methodological advance.

In some previous studies, analyses have been restricted to the measurement of the aperture between the thumb and forefinger [Glover & Dixon 2002; Glover, Rosenbaum, Graham & Dixon, 2004; Jakobson & Goodale 1991]. Others have relied on measuring joint angles to represent the shape of the hand as it approaches a target object [Santello, Flanders & Söchting, 1998, 2002; Santello & Söchting 1998]. These techniques, however, do not provide a means of statistically comparing the nature of the differences in hand trajectories between conditions. Hansen and colleagues [Hansen & Elliott 2009; Hansen, Elliott & Khan 2008] developed a method to measure, at various time points during a reach response, the variability across trials of the location of a sensor attached to the hand. Their analysis depicted the momentary variability of location along each axis in three-dimensional space. Their statistical method, however, did not consider rotations at all; nor was their analysis used to compare positional differences in trajectories across conditions. The methodology most closely resembling our approach used functional analysis of variance applied to the location of a single sensor during reach-and-point motions [Chapman et al. 2010a, 2010b]. This analysis was confined to two-dimensional projections of a three-dimensional trajectory, while Stewart et al. [2013] utilized two-dimensional projections of translation and of one rotational vs. one translational degree of freedom.

In contrast, our method captures, for the first time, moment-by-moment differences in the rotation and translation of the articulations of the hand, represented by a sequence of elements of $\mathbb{SE}(3)$, which a samples of a continuous trajectory lying in the six-dimensional group manifold of $\mathbb{SE}(3)$. To visualize experimental effects on the hand's movement, we represent statistical differences as a pair of three-dimensional projections of the full six-dimensional trajectory—one being the projection onto $\mathbb{R}^3$, the subgroup of three-dimensional translations, and the other being the projection onto $\mathbb{SO}(3)$, the subgroup of three-dimensional rotations. We refer to the former as a box plot, and the latter as a ball plot. These are described in the Data Analysis section.

Method

The experimental task allowed us to examine how a depiction of an object with a handle influences a horizontal or vertical power (clenched fist) grasp. In each trial sequence (see figure 2), a photo was shown of an object with a horizontal or vertical handle (e.g., frying pan or beer mug). The object could be in its canonical orientation (shown in the figure), rotated 90° clockwise, or rotated 90° counterclockwise. The object photo was followed by a cue indicating which one of two response elements the subject should reach for and grasp. One of the response elements was a horizontal handle and the other was a vertical handle, as shown at the bottom right of the figure. On each trial, the orientation of the object's handle in the photograph was either congruent or incongruent with the cued action (e.g., a beer mug is congruent with a vertical power grasp but incongruent with a horizontal one), for a total of four possible conditions. This

allowed us to measure the impact of this mental representation on the kinematics of the reach-and-grasp response.

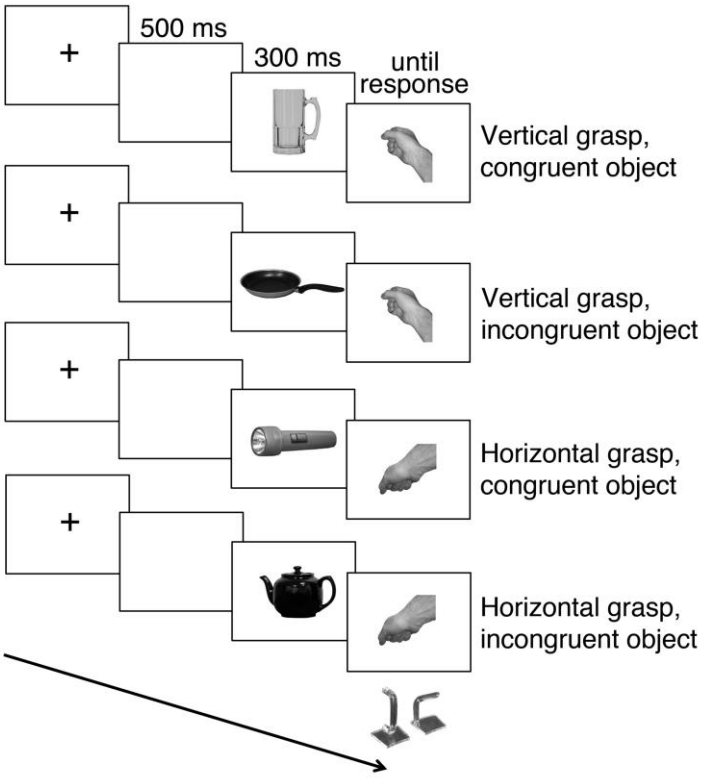

Figure 2 - Trial sequence for each of the four conditions.

The trajectories of fingertips, back of hand, and wrist were monitored using magnetic sensors that delivered information on position and rotation over time. Any condition-related variation in the trajectory of any of these articulations of the hand was termed a difference trajectory. In the absence of a difference, this trajectory would necessarily hover close to the origin of the box plot or ball plot, whereas a difference was deemed statistically significant whenever the difference trajectory moved at least 2 standard errors away from the origin. Because we were particularly interested in the effect of a competing action representation on the rotation of the hand, we emphasized conditions in

which moving from the start to the end position of a cued grasp required a 90° rotation of the hand (e.g., from a horizontal start, with the palm facing downward, to a vertical grasp, such as that used to grasp a teapot handle).

Experimental Set-up and Procedure

Stimuli were presented on a rear-projection display. A response box was located directly in front of the subject, and two acrylic response elements were mounted on a base located between the display and the response box, as shown in figure 3. The subject was seated facing the display and approximately 80 cm away from it, as shown in figure 4. Reach-and-grasp responses were made by lifting off from the response box and reaching forward about 30 cm to grasp one the response elements. Half of the subjects started from a horizontal position (hand flat with open palm facing downward and resting on the response box), and the other subjects started from a vertical position (flat hand with the wrist and hand in a vertical orientation, with the edge of the hand resting on the response box).

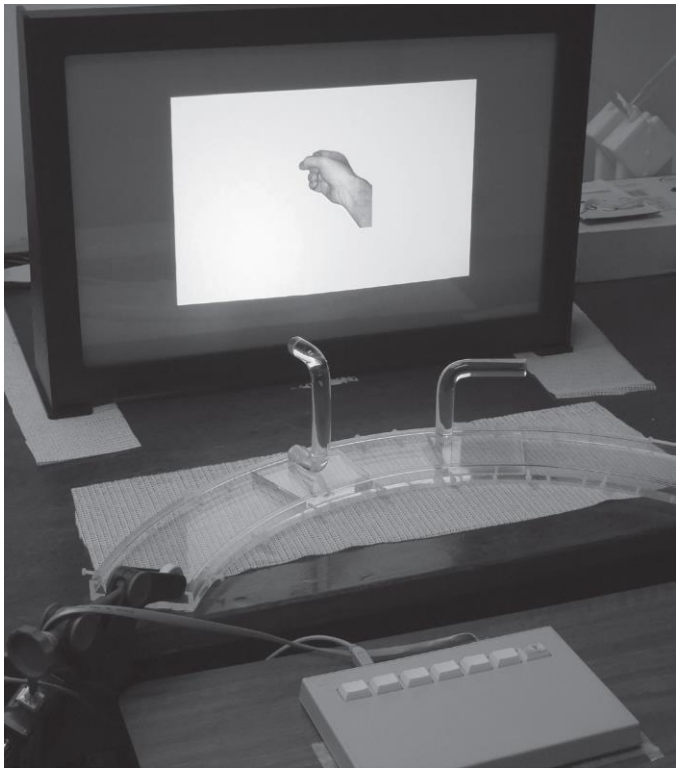

Figure 3 - The experimental set-up.

The response elements were displaced slightly from the midline, one to the left and the other to the right. The left-side element was a tall, C-shaped form 14 cm in height that afforded a vertical grasp. The right-side element was a right-angled form with a horizontal arm extending 9 cm rightward from a vertical post (9 cm in height) that afforded a horizontal grasp. The response elements occupied the same position for all subjects, rather than being counterbalanced with respect to position, so that reach-and-grasp trajectories across subjects would be as similar as possible.

Figure 4 - Placement of the subject.

In the first phase of the procedure, subjects practiced responding to the two hand cues by making vertical or horizontal reach-and-grasp response, as indicated by the cues. In the second phase of the testing session, subjects were familiarized with the priming objects to ensure that they could easily be named. The final phase of the experiment consisted of 24 practice and 288 critical trials. At the beginning of each trial, a fixation cross appeared on the display screen until the subject placed his or her right hand in the designated start position, resting on the response box. The fixation cross then disappeared, and 500 ms later, the image of the priming object was presented for 300 ms. The object's image was then replaced by the image of the hand cue indicating the

response that was to be made (see figure 2). The subject then executed the corresponding reach-and-grasp response as quickly as possible. The subject continued to hold the response element until an auditory signal indicated that the trial was over. Across the practice and critical trials, each of the two possible actions was performed equally often, and each was primed equally often by the 12 object images (4 objects × 3 versions). The trials were presented in a random order for each subject. To ensure that subjects attended to the priming object, we asked them to report the name of the object after completing the reach-and-grasp response on a randomly selected 20% of trials.

The complete set of object primes is shown in figure 5. Gray-scale digital photographs of a hand posed in a right-handed vertical power grasp and in a right-handed horizontal power grasp (palm down) were used as cues to indicate the action to be performed on a trial. Gray-scale digital photographs of four objects oriented for use with the right hand served as priming stimuli. Two objects were congruent with a vertical grasp when presented in their canonical orientation (beer mug and teapot), and two were congruent with a horizontal grasp when in their canonical orientation (frying pan and flashlight).

Figure 5 - Complete set of stimuli.

Two additional versions of the object photographs were created, but the trials using these images were not part of the analysis

reported here for reasons outlined below under Data Analysis and Filtering. One version was generated by rotating the object 90° (counterclockwise for the beer mug and teapot; clockwise for the frying pan and flashlight) to produce an image that was compatible with the alternate grasping action. An object in that orientation could be grasped, and a simple 90° rotation of the wrist to vertical or horizontal (palm down) would reorient the object so that it would be ready for use. The second version of the photographs was created by rotating the mirror-image view of the object 90° (clockwise for the beer mug and teapot; counterclockwise for the frying pan and flashlight). Again, these images afforded the alternate action, but now a grasp followed by a simple 90° rotation of the wrist to vertical or horizontal would result in the object being held in an upside-down position.

Subjects

Eighteen right-handed students at the University of Victoria participated for extra credit in an undergraduate psychology course. This sample size is consistent with those in previous studies of hand trajectories and was established before data collection began.

Data Acquisition

Five magnetic sensors were attached by surgical tape to subjects' right hand, positioned on the nails of the thumb, index finger, and middle finger; on the back of the hand; and on the dorsal surface of the wrist. A cable ran from each sensor up the arm and down the back; the cables were held in place by a fingerless glove, an upper-arm cuff, and a shoulder harness, all made of lightweight fabric. We used an Innovative Sports Training (Chicago, IL) MotionMonitor integrated system equipped with 8-mm Ascension

Technology (Burlington, VT) miniBird sensors that simultaneously measured position and orientation (to provide information about rotation). Figure 6 shows the positioning of the sensors on the hand, and the placement of the cables connecting the sensors to the data acquisition system can be seen in figure 4.

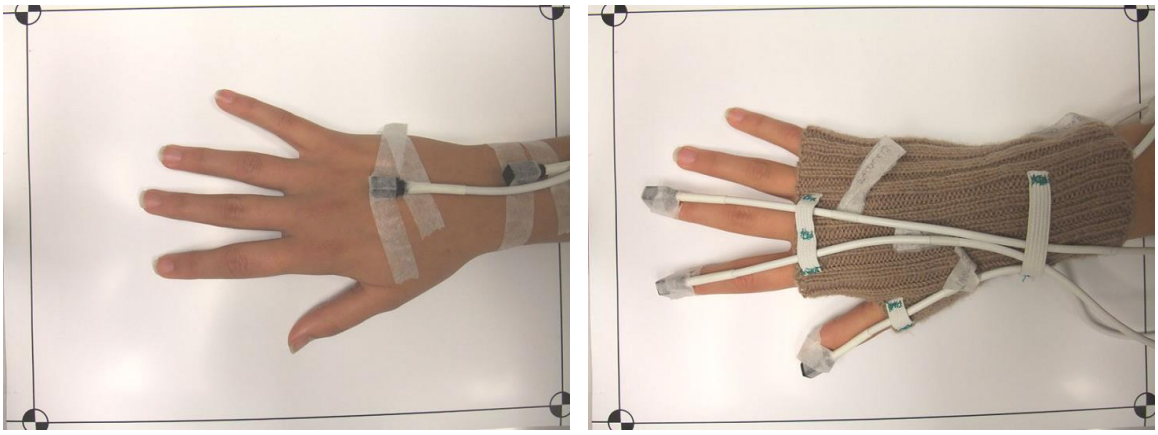

a) Sensors 4 and 5; respectively back of hand and wrist.

b) Sensors 1, 2, and 3; respectively thumb, index finger, and middle finger.

Figure 6 - Placement of the sensors on the hand.

Data from the sensors were collected at a 60-Hz sampling rate using MotionMonitor software. The recording epoch for a trial extended from 1 second prior to the hand lifting off the response box until 1.5 seconds after lift-off. This time range was adequate to capture normal reach-and-grasp responses.

Data Analysis and Filtering

Our design included a number of conditions, only some of which are relevant to the question of how a canonically viewed object affects the trajectory of a reach-and-grasp action. Although rotated objects were included as primes, they present a special interpretive problem that the present experimental design cannot adequately address.

Namely, an object such as a rotated beer mug invites a horizontal grasp on the basis of its visible form but a vertical grasp on the basis of its canonical properties. As a result, it is not possible to determine which of these influences affects the trajectory of the hand. Our interest was specifically in how canonically oriented objects influence the production of a reach-and-grasp response. Moreover, because our technique offered, for the first time, the possibility of assessing statistical differences in the rotation as well as the translation of the hand, we were particularly interested in actions that required a wrist rotation when moving from the starting position to the final grasp posture. Therefore, our primary analyses were restricted to trials on which the priming object was presented in its canonical view, and we emphasized conditions in which the reach-and-grasp response required a wrist rotation. In the next section we will, however, include a brief description of the priming results for trajectories that did not involve a wrist rotation.

Statistical outliers in the data set were identified on a sensor-by-sensor basis to reject invalid data while retaining good data from other sensors in the same trial. Data for a particular sensor in a specific trial were discarded if there were more than 30 missing samples in total (at a 60 Hz sampling rate), or more than 15 consecutive missing samples, both of which were artifacts of the sensor system. We also excluded a sensor's data for a trial if (a) it exhibited a sudden, physically implausible jump in position, velocity, or acceleration, (b) it contained a quaternion of non-unit magnitude, or (c) the lift-off or reach time was outside a defined range (100-1,000 ms for lift-off; 250-1,250 ms for reach). An entire trial was excluded if the subject made an incorrect reach and grasp

response. In all, 86% of the entire set of sensor records were retained. Any missing samples in a retained sensor record were interpolated in $\mathbb{SE}(3)$ so that translation and rotation were interpolated together.

Finally, retained sensor records were time-normalized as follows. The linear speed tangent to the trajectory was low-pass filtered using an 8th-order, zero-phase Butterworth filter with cut-off frequency of 8 Hz. Then the trajectory was followed forward and backward from the point of peak speed (near the midpoint of the trajectory), until the speed dropped below a threshold of 5 cm/s. These points were taken to be the start and end of the movement. The trajectory between these points was interpolated, again in $\mathbb{SE}(3)$, with a resolution of 100 intervals to generate a time-normalized path.

From the data obtained in this way, mean trajectories and a three-dimensional representation of the standard error of the mean at each sampled point in the trajectory (which we call an error volume) were calculated by subject and condition for each sensor. Difference trajectories representing the change in the paths followed by the hand in the congruent versus incongruent priming conditions, with error volumes based on these changes, were then calculated for each subject. Finally, difference trajectories were averaged across subjects, and aggregate error volumes were computed.

Results

The plots shown in figure 7 illustrate the nature of the trajectories produced by our reach-and-grasp task and the computational challenges associated with evaluating differences between those trajectories. Figure 7a is a three-dimensional depiction of

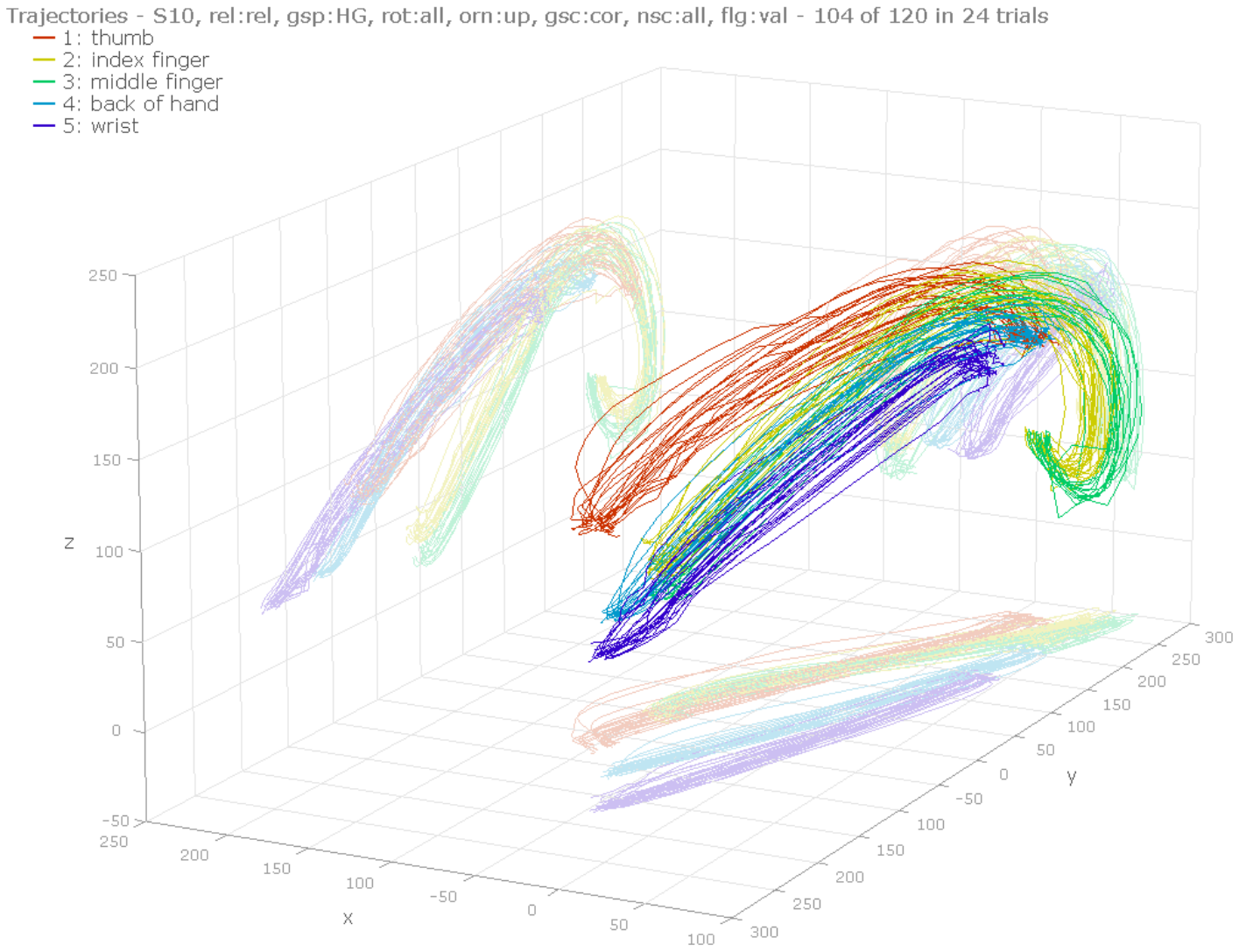

Figure 7a - Typical box plot showing the translation part of the trajectory. Raw data for subject 10.

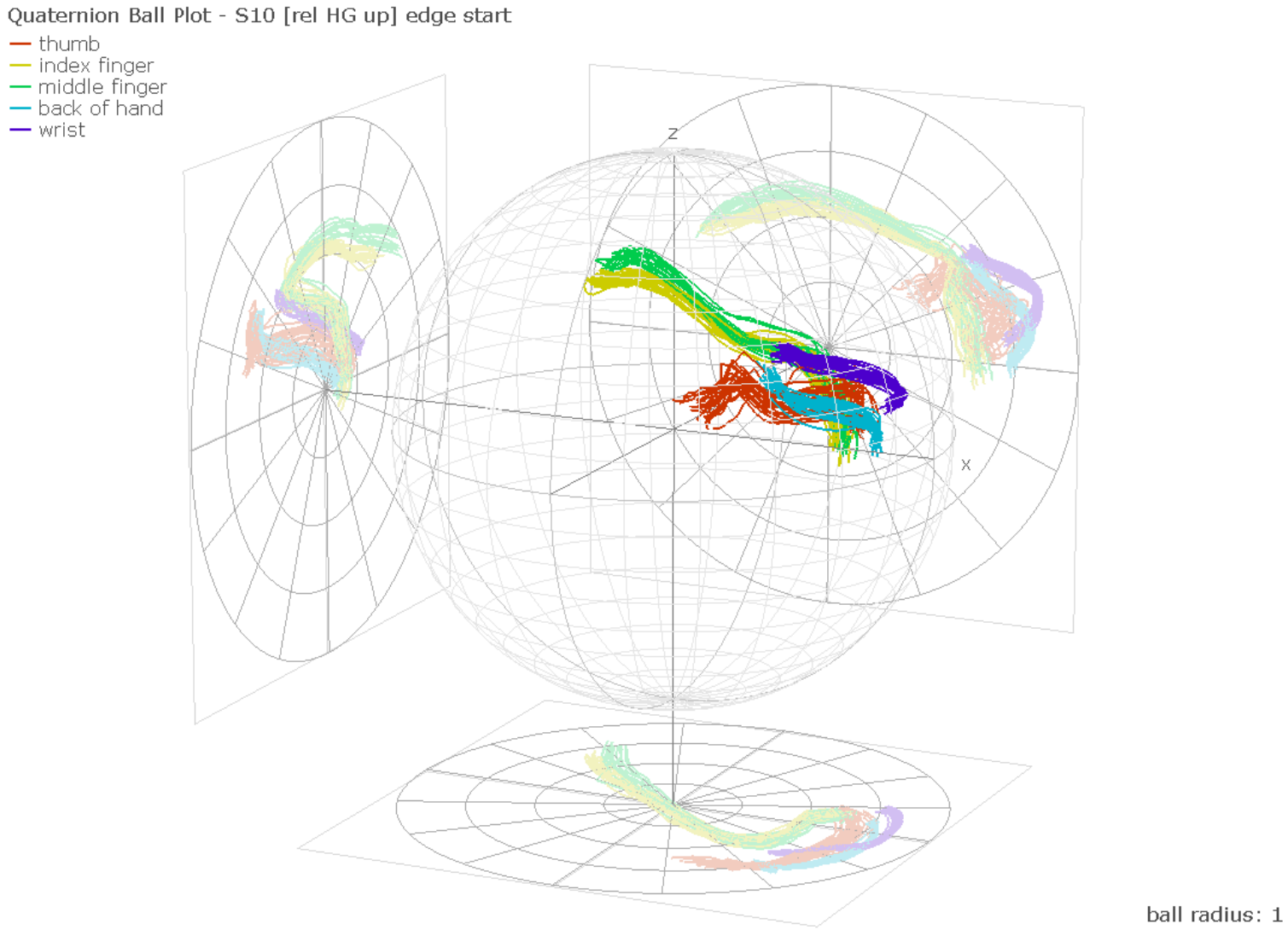

Figure 7b - Typical ball plot showing the rotation part of the trajectory. Raw data for subject 10.

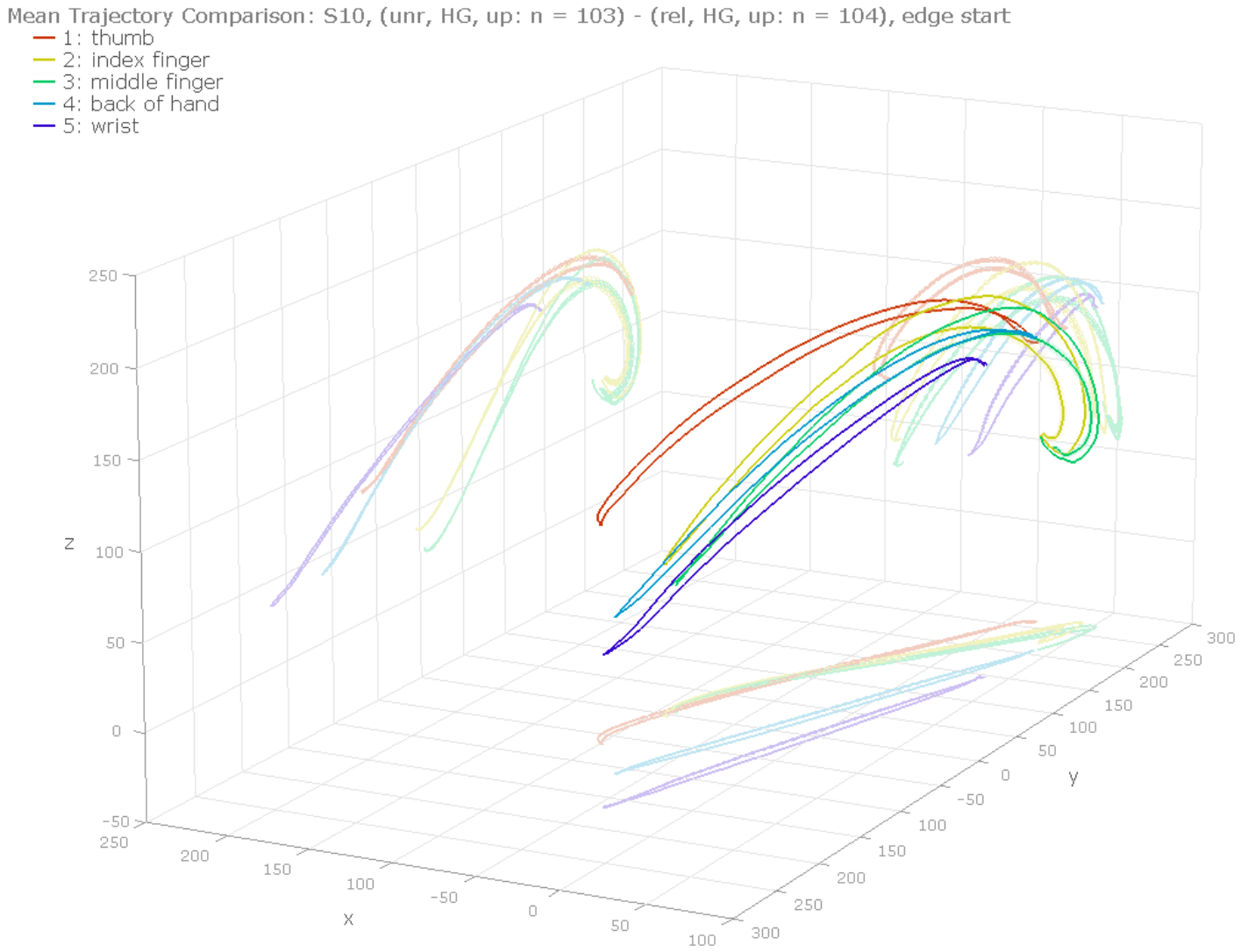

Figure 7c - Box plot showing the same data as figure 7a, averaged separately by condition.

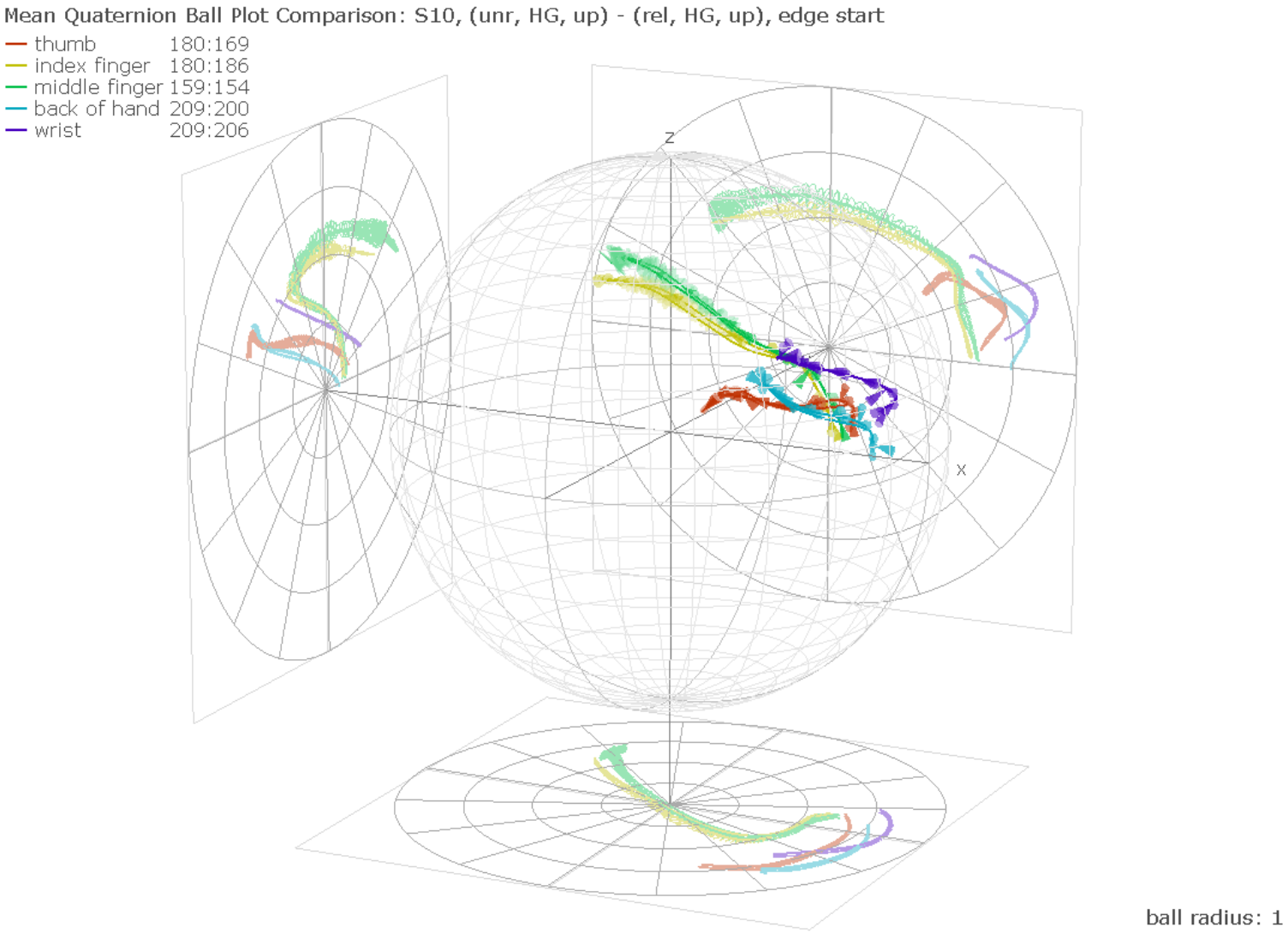

Figure 7d - Ball plot showing the same data as figure 7b, averaged separately by condition.

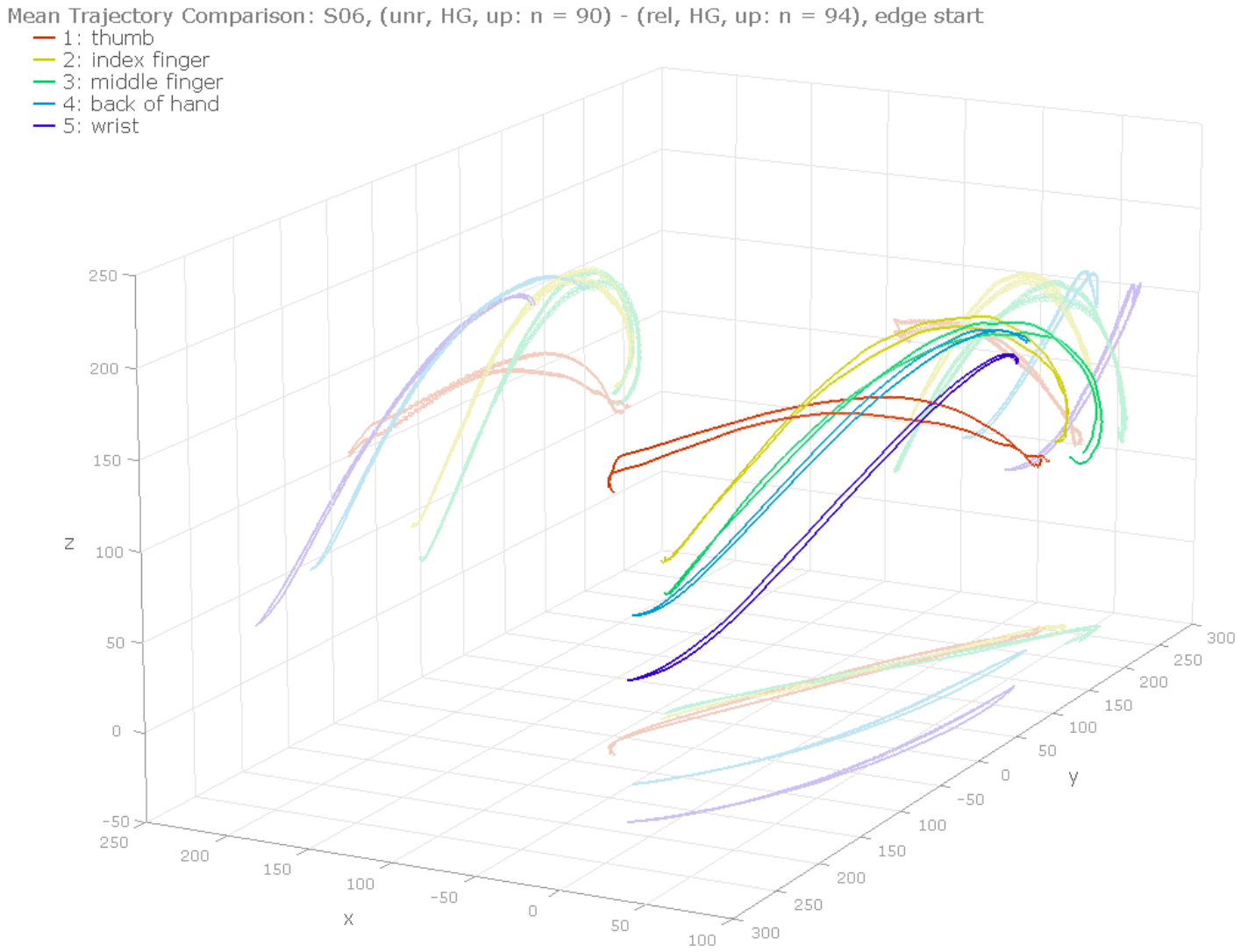

Figure 7e - Box plot with same parameters as figure 7c, but for a different subject.

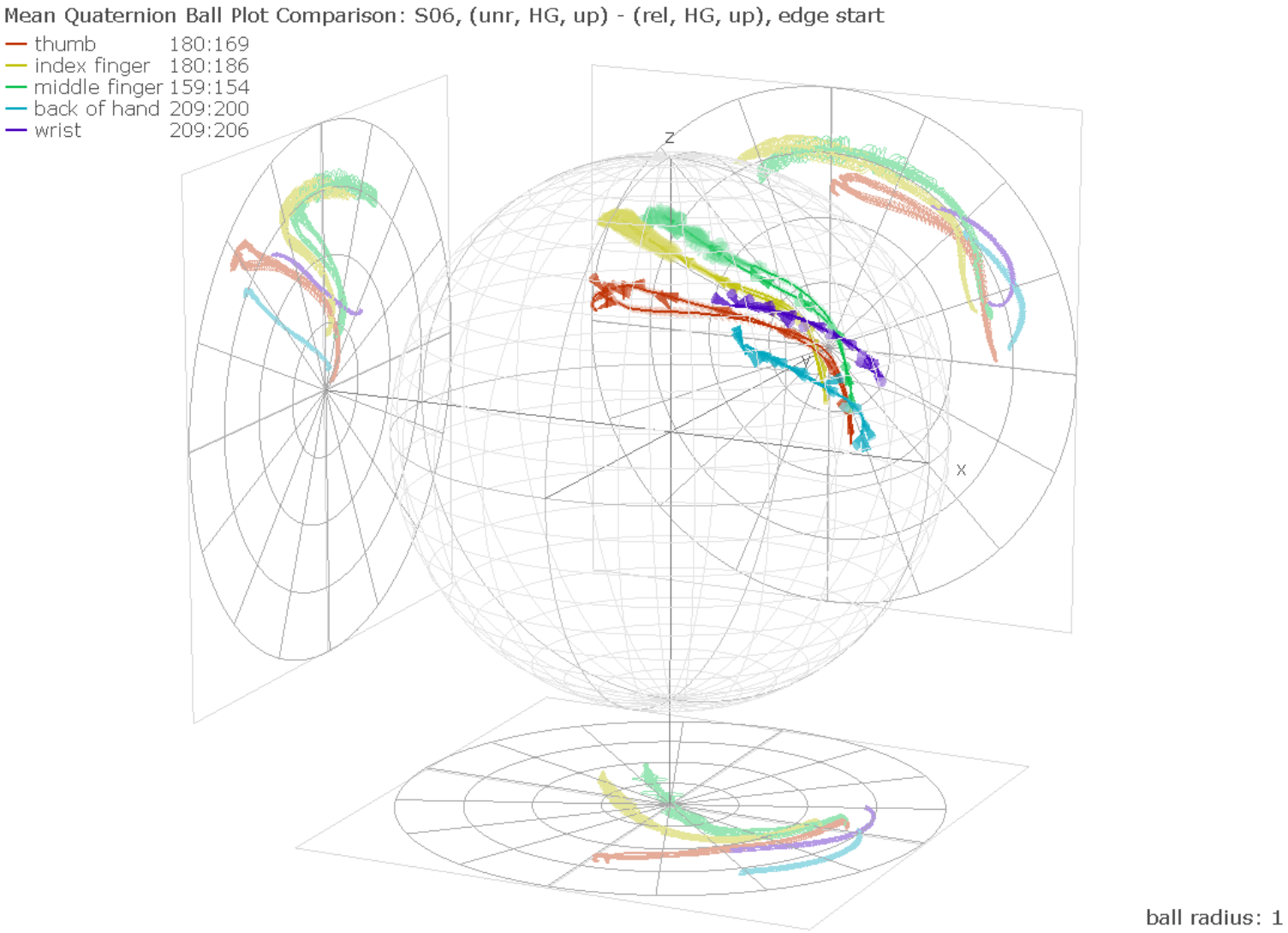

Figure 7f - Ball plot with same parameters as figure 7d, but for a different subject.

the position trajectory (i.e., position as a function of time) for each of the five sensors, which we call a box plot. The plot shows all trials from one subject making a horizontal grasp from a vertical starting position when the action associated with the prime object matched the grasping action being produced (congruent condition). The three dimensions represent forward motion (*y* axis), lateral motion (*x* axis), and vertical motion (*z* axis). The trajectories begin near the origin of the plot (i.e., $x = y = z = 0$) and move forward along the y-axis until the fingers curl around the response element (note the curved path reported by the sensors for the index and middle fingers). Trial-to-trial variability in movement is characterized by displacement among the individual trajectories. The plot also shows two-dimensional projections of the trajectory (in desaturated colour) on each of the three coordinate planes (i.e., *xy*, *yz*, and z*x*). These projections assist in visualizing the trajectory's three-dimensional shape and allow one to clearly see how it changes along two dimensions at a time. For example, on the *yz* plane (side view), one can easily see the curvature of the two fingers as they form themselves around the horizontal response element at the end of the movement.

Figure 7b is a three-dimensional depiction of the rotation trajectory (i.e., rotation as a function of time) of each sensor over the course of the movement for the same trials shown in figure 7a. We call this way of displaying rotation trajectories a ball plot. Each point on the rotation trajectory corresponds to the quaternion representing the momentary axis and amount of rotation experienced by a particular sensor.

As we have seen, a rotation can be represented by a unit versor of the form $a = \cos\frac{1}{2}\alpha - \sin\frac{1}{2}\alpha\,\hat{\boldsymbol{a}}$, where α is the angle of rotation and $\hat{\boldsymbol{a}} = a_1 e_{23} + a_2 e_{31} + a_3 e_{12}$ is a unit bivector spanning the plane of rotation. In three-dimensional space, this plane has a unique normal vector $\hat{\boldsymbol{a}}$, called its dual, and this is just the axis of rotation. Using geometric algebra, the dual of a multivector is easily calculated; we simply multiply by the inverse of the pseudoscalar, $e_{123}^{-1} = -e_{123}$. Thus

$$\hat{\boldsymbol{a}} = \hat{\boldsymbol{a}} e_{123} = (a_1 e_{23} + a_2 e_{31} + a_3 e_{12})(-e_{123}) = a_1 e_1 + a_2 e_2 + a_3 e_3 \qquad \text{(ps1)}$$

The vector $\boldsymbol{v} = \sin\frac{1}{2}\alpha\,\hat{\boldsymbol{a}}$ thus lies on the axis of rotation, and the angle of rotation is a function of its length: $\alpha = 2\sin^{-1}|\boldsymbol{v}|$, which is single-valued as long as we restrict the angle to lie in the range $-\pi \le \alpha \le +\pi$. The one drawback is that this function is nonlinear, but this is the price we pay for a three-dimensional representation of a four-dimensional object. We can do this because the unit-magnitude constraint reduces the number of degrees of freedom from four to three. Essentially, we have mapped the unit 3-sphere in four-dimensional space into the interior of the unit ball in three dimensional space.

Returning now to figure 7b, the trajectories begin at the right side of the plot and progress leftward from there. Near the end of the movement, for example, the index finger as it curls around the response element is still rotating into a horizontal position from the vertical starting point. This can be seen by consulting the *xy* and *yz* two-dimensional projections. In the *xy* projection (overhead view, lying below the ball plot), the end point of the index finger sensor's trajectory lies in the negative region of the *x*

axis and the positive region of the *y* axis. This captures the fact that as this finger curls inward, it is still rotating into the horizontal position. In addition, the *yz* projection, shown to the left of the ball plot (side view), indicates that this point also lies in the positive region of the *z* axis, which implies that the curling action occurred while the finger retained some vertical aspect.

Because the notion of a ball plot is likely to be unfamiliar to many, we provide a second example of how to interpret rotation, applied again to the index finger. Consider the starting point of its trajectory shown in figure 7b. As the ball plot and its two-dimensional projections imply, displacement of this starting point from the origin occurs almost exclusively along the *x* axis. This means that if we construct a vector from the origin to the initial point of the index finger's rotation trajectory, the direction of rotation would primarily be around the *x* axis pointing in the positive direction, which indicates that at the start of the movement, the index finger is moving upward and rotating toward the body.

Figure 7c shows the average position trajectory of each sensor for the congruent and incongruent conditions separately, and figure 7d shows the corresponding average rotation trajectories. Data are for the same subject and action as in figures 7a and 7b. Note that averaging across trajectories from different trials, which naturally vary in the time required to complete the action, necessitates defining trajectories in normalized time. That is, the full trajectory for a trial must be parceled into segments corresponding to particular proportions of the total time taken to complete the movement on that trial.

Averaging across trials can then be done for each of these portions of the trajectories. Error volumes representing one standard error of the mean in three dimensions are plotted for these trajectories. These volumes were particularly small for the position trajectory and therefore are occluded in the figure by the line drawn along the trajectory. The rotation trajectories also feature directional cones providing information on the temporal progression of the trajectory.

Figures 7e and 7f show the corresponding average trajectories and error volumes for a different subject. Notice that for both the position and rotation trajectories, the within-subjects differences between conditions are much more subtle than the between-subjects differences within conditions. Our analytic approach calculates difference trajectories (i.e., the difference between congruent and incongruent conditions) within subjects before aggregating them across subjects, which thereby allows subtle differences between conditions to be detected even in the presence of large between-subjects variation in trajectories. It should be noted that the word "difference" is used here in a suitably generalized sense. It applies literally only to the group of translations, which acts additively. The group of rotations, on the other hand, acts multiplicatively. To cover both cases, we define the difference between two displacements to be the displacement that takes us from the first to the second. Thus, the difference from $a \in \mathbb{SE}(3)$ to $b \in \mathbb{SE}(3)$ is $d \in \mathbb{SE}(3)$ such that $b = da$, or just $d = ba^{-1}$. We show the translation part of that difference in a box plot and the rotation part in a ball plot.

Congruency Effects for Conditions With Hand Rotation

We now discuss the prime object's effect on a grasping action using differences of average position trajectories. These difference trajectories show the position of a sensor in the incongruent condition at a given time point, relative to the position of that sensor in the congruent condition at that time. An effect of congruency will be revealed by a difference trajectory that progresses further away from the origin as the effect accrues over time. If there is no effect of the relationship between the object in working memory and the hand movement being executed, then the difference trajectory should remain near the origin, meaning that the origin should remain within the error volume throughout the time course of the movement.

As can be seen from the difference trajectories displayed in figure 8, the object in working memory had, indeed, a substantial impact on the reach-and-grasp response. These difference trajectories reveal positional and rotational differences (incongruent relative to congruent) and are shown as solid lines with directional cones placed at intervals of 10% of normalized time. The origin is indicated by a bright green ball of radius 1 mm. Because we are plotting difference trajectories, the scale of the axes in figure 8, though still in millimetres, is more fine-grained than in figure 7. Error volumes corresponding to differences of 1 standard error of the mean are depicted as semi-transparent ellipsoids around each trajectory and were computed independently at successive points along the trajectory. To assist with interpretation of these trajectories, we also provide two-dimensional projections as in figure 7. These projections show the error volumes as overlapping ellipses.

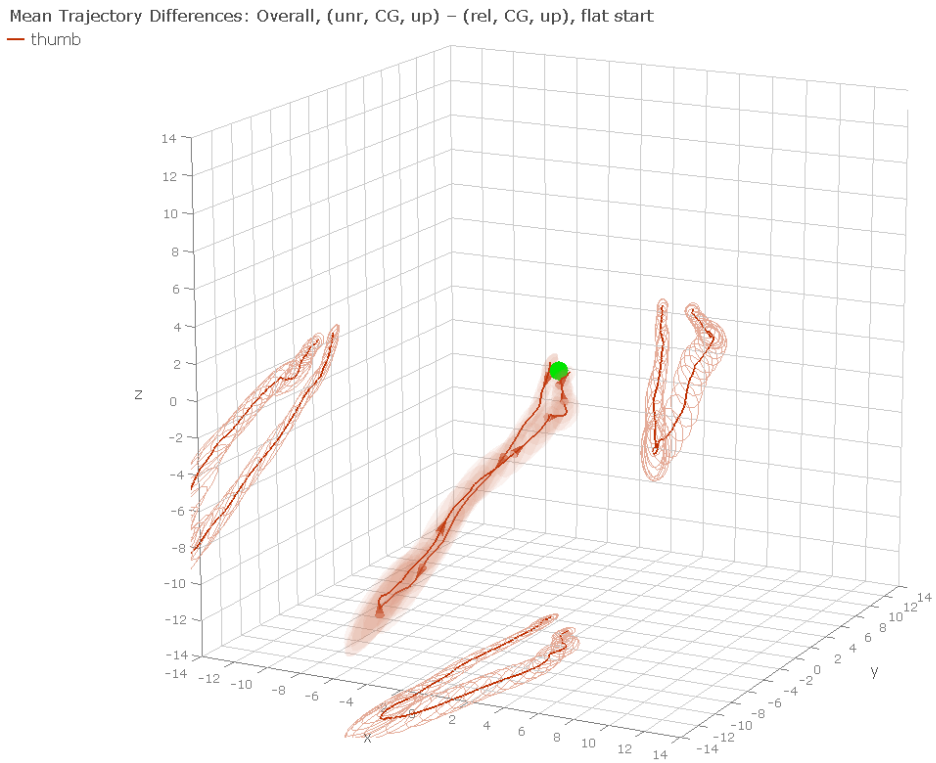

Figure 8a - Thumb position difference: vertical grasp from horizontal start.

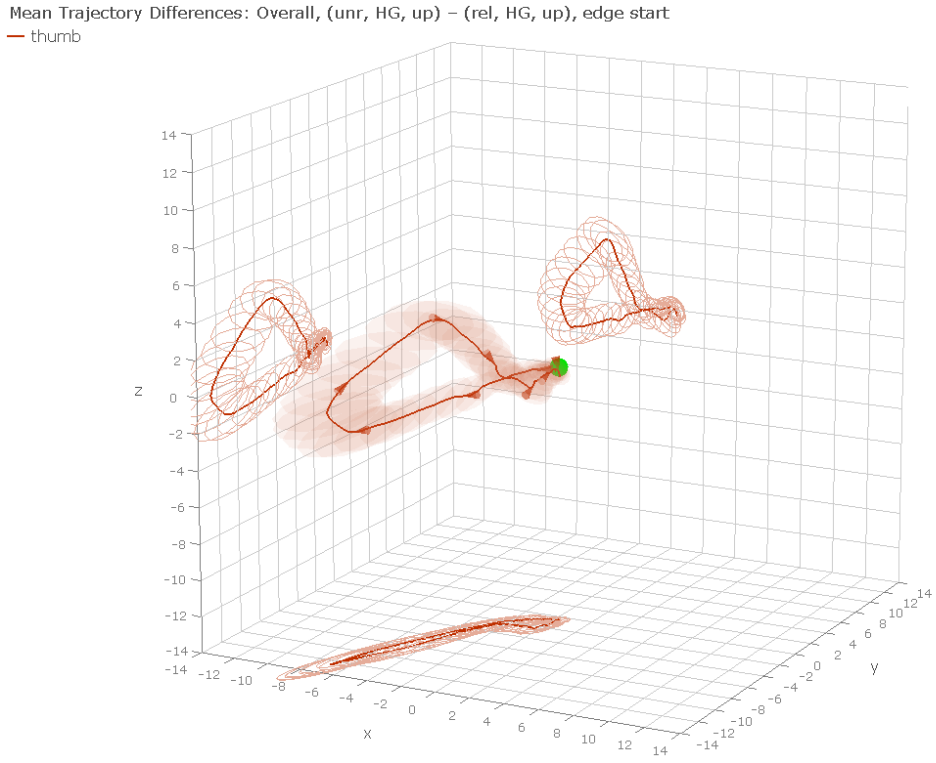

Figure 8f - Thumb position difference: horizontal grasp from vertical start.

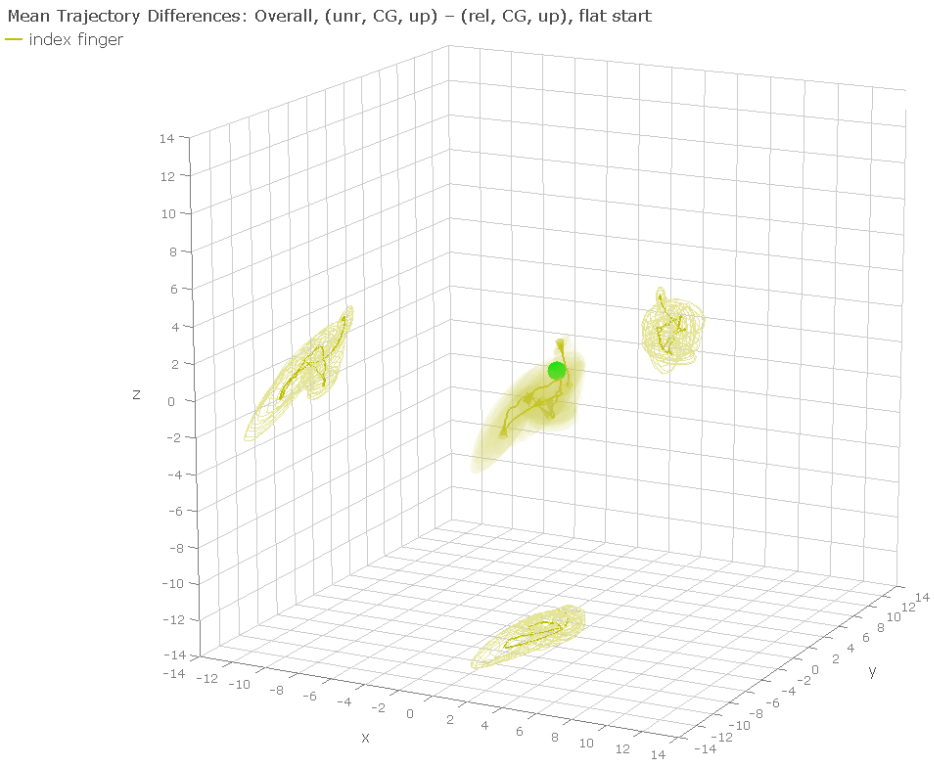

Figure 8b - Index finger position difference: vertical grasp from horizontal start.

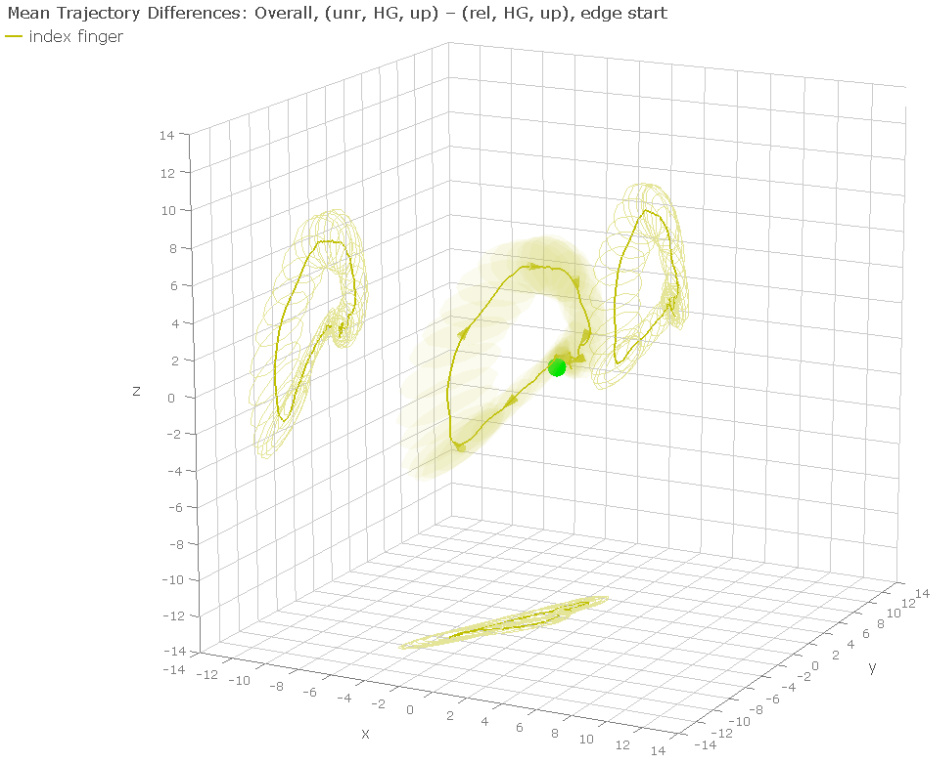

Figure 8g - Index finger position difference: horizontal grasp from vertical start.

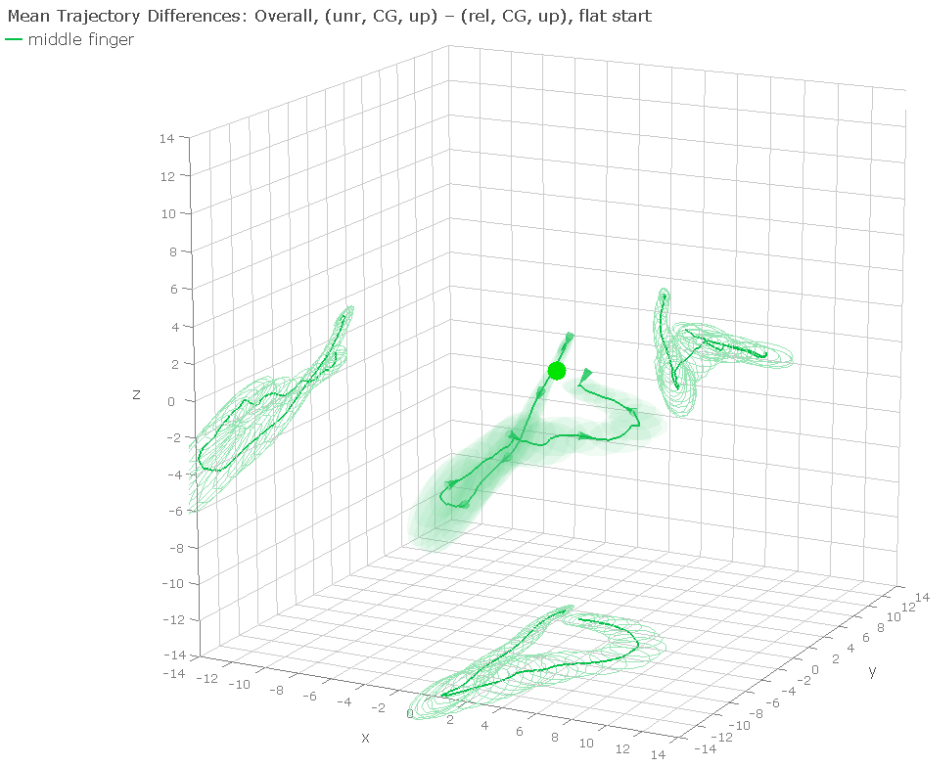

Figure 8c - Middle finger position difference: vertical grasp from horizontal start.

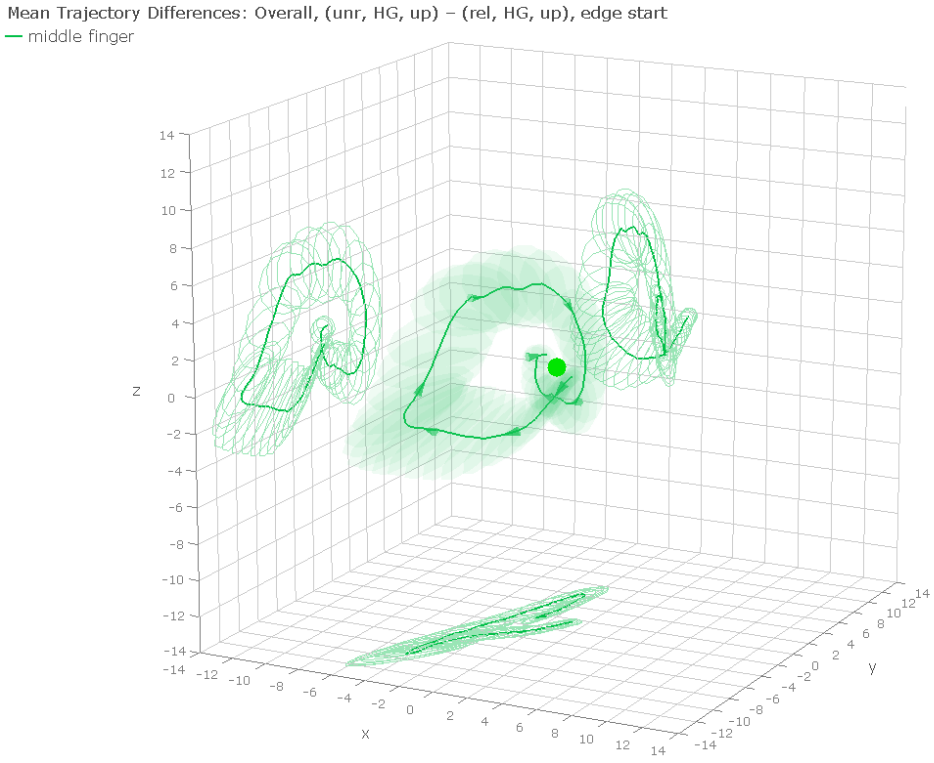

Figure 8h - Middle finger position difference: horizontal grasp from vertical start.

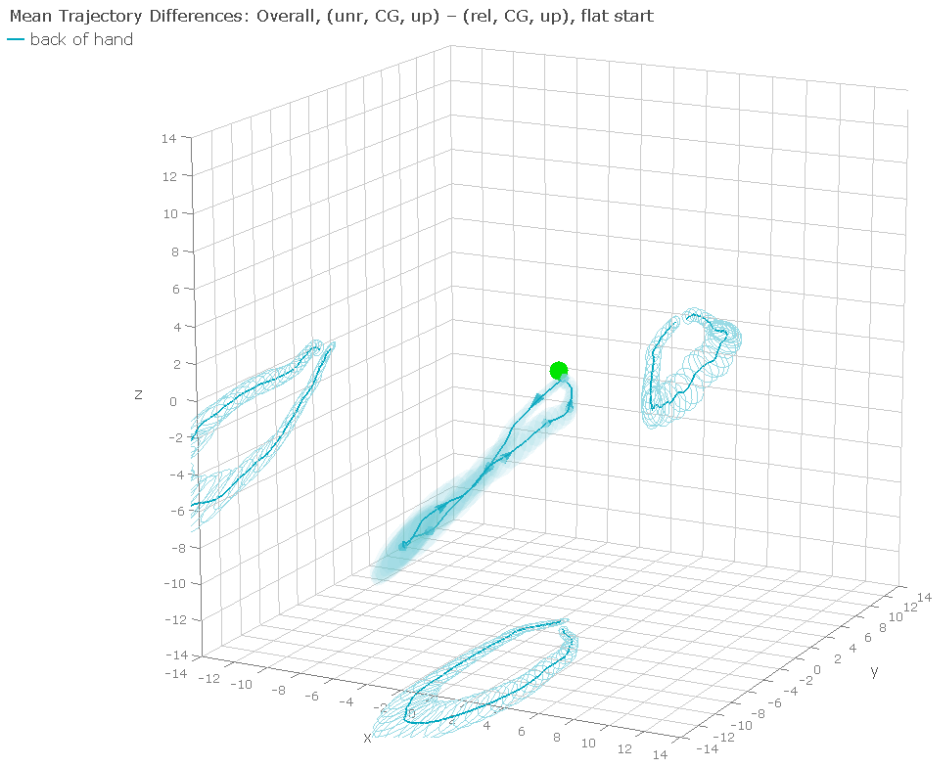

Figure 8d - Back of hand position difference: vertical grasp from horizontal start.

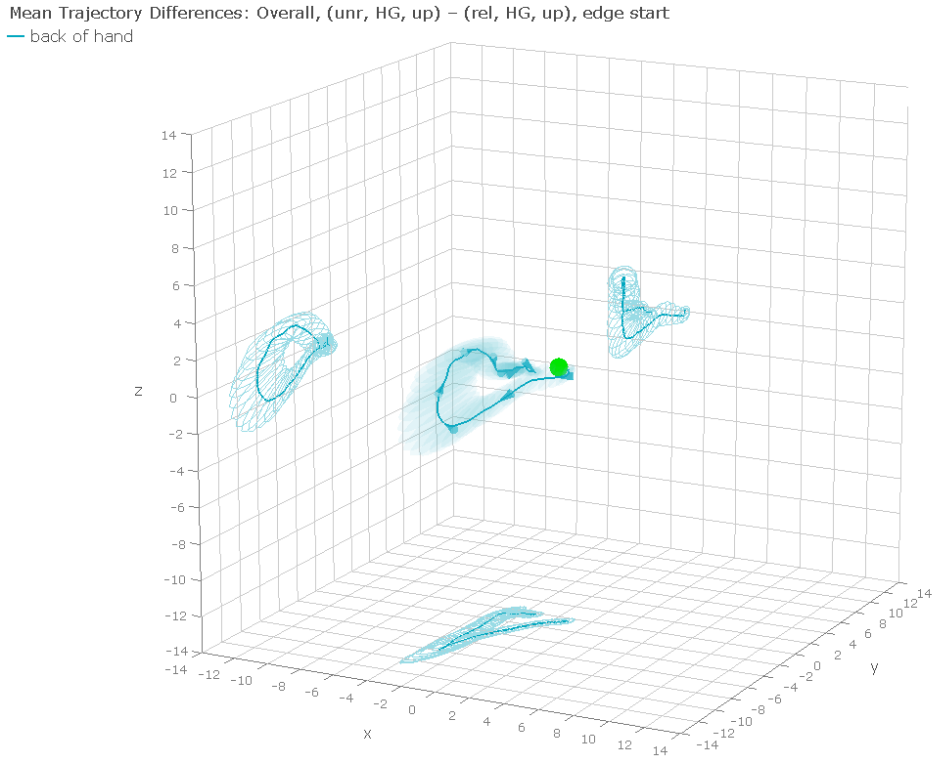

Figure 8i - Back of hand position difference: horizontal grasp from vertical start.

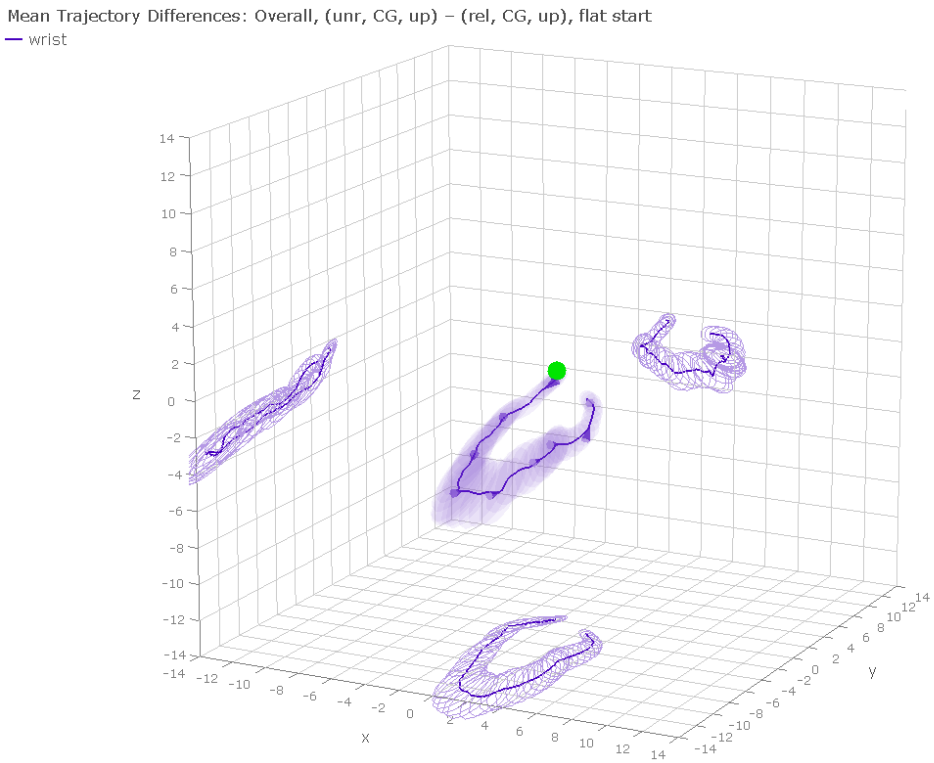

Figure 8e - Wrist position difference: vertical grasp from horizontal start.

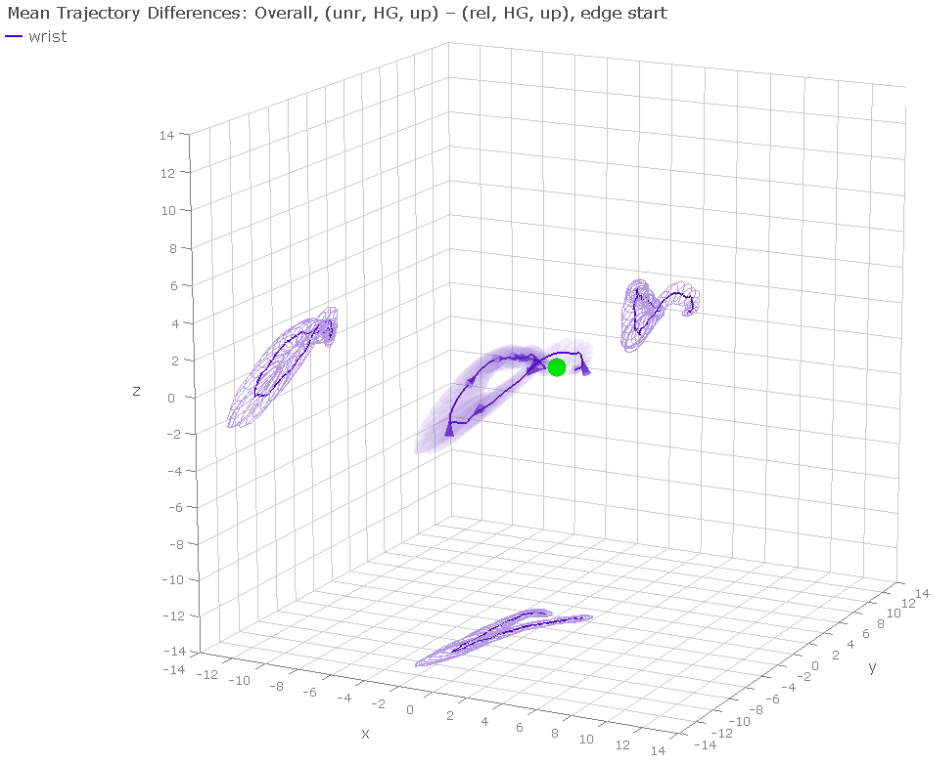

Figure 8j - Wrist position difference: horizontal grasp from vertical start.

Consider first the action in which subjects moved from a horizontal starting position (fingers extended, palm facing down) to a vertical power grasp (figures 8a-e). The figures show that for all of the sensors except the index finger, the difference trajectory moved a substantial distance away from the origin in the negative direction (backward) along the *y* axis, up to a maximum average exceeding 14 mm, before turning to the positive direction. As an example of this effect, consider the difference trajectory for the thumb. This trajectory begins near the origin and moves in the negative direction to a maximum of about 16 mm along the *y* axis. The directional cones indicate that this relative lag continues to increase until about the midpoint of the action (the fourth of ten cones), then the difference between the congruent and incongruent condition is progressively reduced until the grasp is completed. This pattern implies that in roughly the first half of the movement in the incongruent condition, there was less forward progress relative to the congruent condition. Over the remainder of the movement, this difference necessarily diminished in normalized time because the hand landed in approximately the same position at the end of both congruent and incongruent trials. This effect is especially clear when looking at the two-dimensional projection on the *xy* plane.

Notice that another effect is revealed both in the *xy* projection and in the projection on the *zx* plane. The trajectory is displaced to the right along the *x* axis during the second half of the movement. The same rightward displacement occurs for all the other sensors as well, although to only a minor extent for the index finger. This excursion to the right

in the incongruent condition appears to be due to an attraction to the alternate response element (horizontal handle), which was positioned to the right of midline and was compatible with the prime object presented in that condition.

A more interesting result concerns the effect of congruency on the thumb's position over the course of the trajectory. As indicated by the projection on the *zx* plane, the thumb was substantially lower in the incongruent than in the congruent condition (maximum average difference = 8 mm on the *z* axis during the middle part of the movement), more so than is seen with the other sensors. This exaggerated downward position of the thumb provides evidence that when the priming object invites a horizontal grasp, the thumb tends to remain in a pronated position as the hand moves into the vertical grasp. Positions of the middle finger along the *x* axis provide intriguing evidence on how this interference was overcome. This sensor displays an exaggerated rightward excursion in the last quarter of the movement (maximum average difference = 6 mm on the *x* axis), apparently counteracting the sustained pronation of the thumb. The segments of the mean difference trajectories described here are all more than 2 standard errors away from the origin.

An account of the effect of the object in working memory, consistent with the above, can be derived from the difference trajectory ball plots displayed in figure 9. Figure 9a plots differences in rotation between the congruent and incongruent conditions (i.e., rotation in the incongruent condition, relative to the congruent condition, as a function of

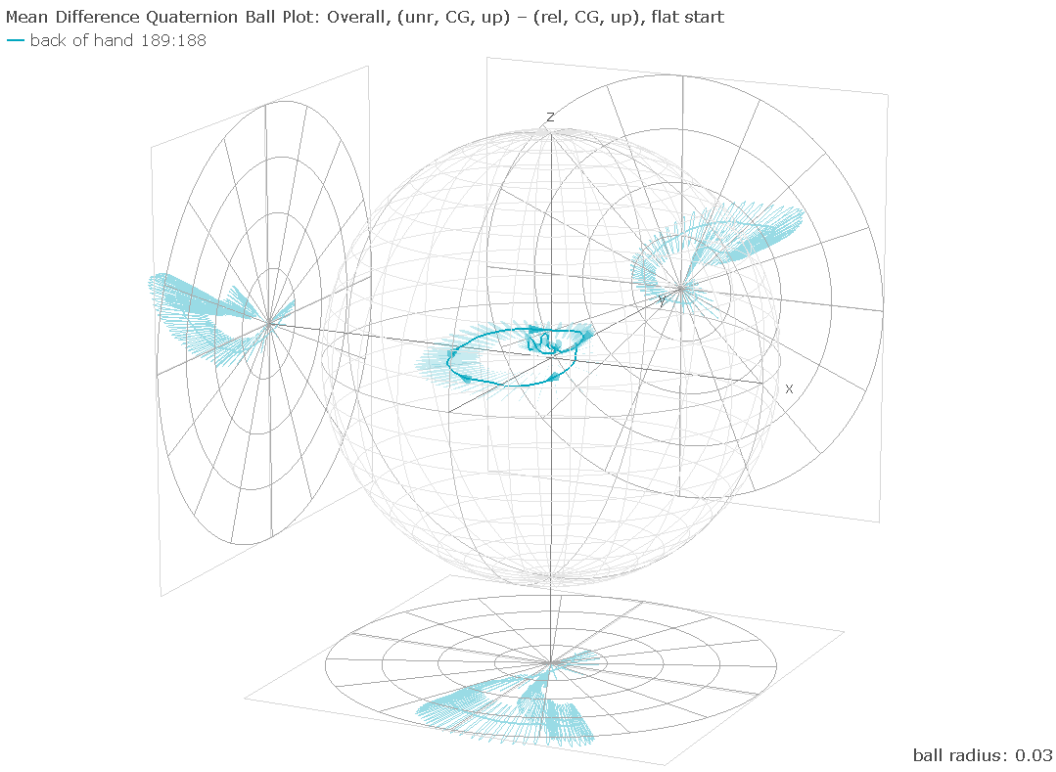

Figure 9a - Back of hand rotation difference: vertical grasp from horizontal start.

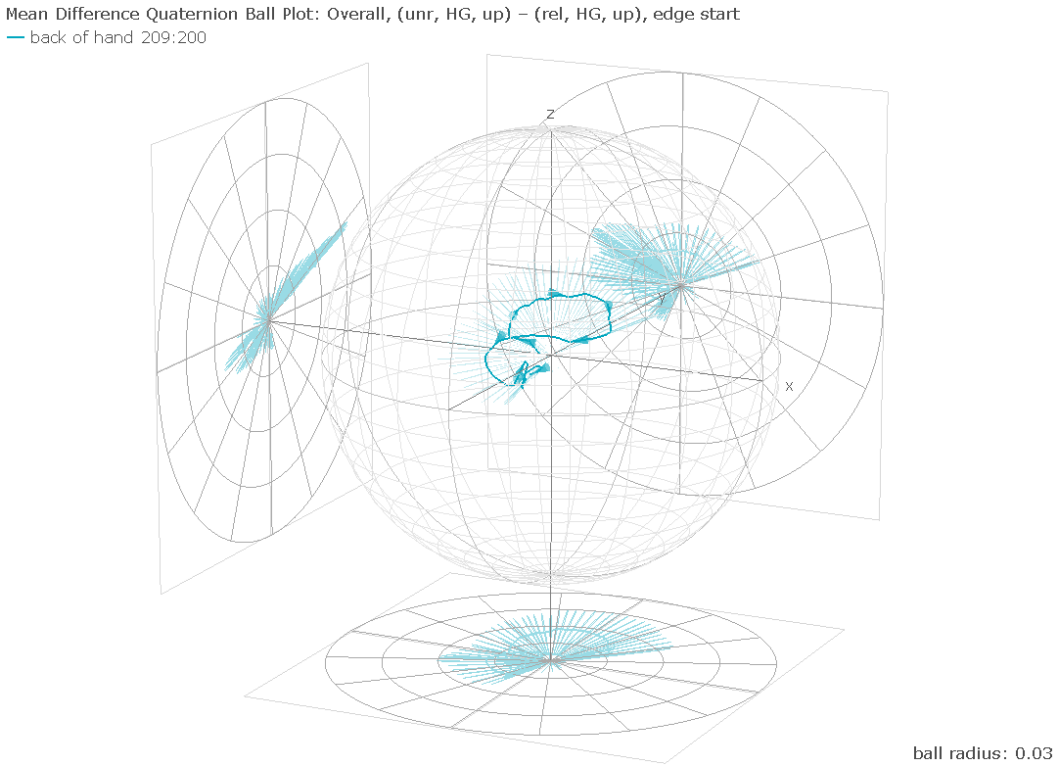

Figure 9b - Back of hand rotation difference: horizontal grasp from vertical start.

normalized time) for the vertical grasp. Once again, note the scale difference. The ball radius in figure 7 is 1, corresponding to a 180° rotation, while the ball radius in figure 9 is 0.03, corresponding to a rotation of only about 3.4°. Data are displayed for the sensor on the back of the hand because it provided the most stable estimate of rotational position. The form of the path, projected onto the horizontal (*xy*) plane, provides the clearest interpretation of the rotational effects. In this plane, the *y* axis projects from the origin toward the midline of the observer. To interpret the difference trajectory, one considers the axis and angle determined by the vector from the origin to each point on the trajectory, just as was done when interpreting figure 7.

The sense of the rotation is determined by the right hand rule: when the thumb of the right hand is aligned with the vector defining the axis, the fingers curl in the direction of the difference rotation (i.e., a counterclockwise rotation about the vector). This rotational difference indicates that in the incongruent condition, the sensor of interest lagged in its rotation from the horizontal starting position to the final vertical grasp. That is, relative to the position of the sensor in the congruent condition at a particular point in the trajectory, in the incongruent condition, the sensor was rotated counterclockwise away from that orientation (i.e., more toward a flat, horizontal position). In the latter part of the movement, this difference was resolved as the hand formed the vertical orientation required by the cued grasp posture.

It is highly significant that a pattern of effects complementary to those we have just discussed was obtained when the hand moved from a vertical start position to a horizontal

grasp. For the position trajectories (figures 8f-j), there was again a lag in the forward motion of the hand in the incongruent condition, which can be seen most clearly in the *xy* plane for the thumb sensor (maximum average = 12 mm on the *y* axis). There was also a leftward deviation for all sensors toward the location of the vertical response element (located to the left of midline), which was compatible with the incongruent object prime. This deviation can be most clearly seen in either the *xy* plane or the *zx* plane for each of the sensors, but especially for the thumb (maximum average = 6 mm on the *x* axis). In addition, the thumb and fingers remained relatively high on the *z* axis in the incongruent condition through the first half of the movement (compatible with the vertical grasp afforded by the depicted object in that condition). To see this, note that in the *yz* plane (corresponding to a side view of the box plot), the trajectories curve upward along the *z* axis after about the first third of the movement. In the case of the index finger, for example, the maximum average upward deviation is nearly 6 mm. These positional displacements were more than 2 standard errors from the origin over much of the trajectory. Then the thumb descended (the downward deflection began between the fifth and sixth directional cones), followed by the fingers (between the sixth and seventh directional cones). The early descent of the thumb appears to have counteracted the tendency for the index and middle fingers to remain in a vertical position.

The ball plot shown in figure 9b confirms this description of events. Examining the *yz* projection, one can see that the trajectory extends primarily away from the observer along the *y* axis (with some elevation on the *z* axis that remains within about 30°). A vector

extending from the origin away from the observer to the most extreme point on the trajectory together with the right-hand rule indicates that the rotational difference consists of a clockwise rotation primarily around the *y* axis. This direction of rotation for the difference trajectory is due to the fact that the position of the sensor in the incongruent condition, relative to the congruent condition, is closer to the upright starting position. In other words, the rotation of the back of the hand from upright to pronated is slower in the incongruent condition. We infer that the downward trajectory of the thumb, which begins prior to the downward trajectory of the other fingers, plays a role in counteracting the initial slowing of the hand's rotation.

Congruency Effects for Conditions With No Hand Rotation

When subjects made a reach and grasp response that did not require a rotation of the hand (e.g., a vertical grasp from a vertical starting position), there were two effects of the object held in working memory on movement trajectories. Plots of the difference trajectories for each sensor's position are shown in figure 10, with vertical action in figures 10a-e, horizontal action in figures 10f-j). Corresponding ball plots showing the difference trajectories for the rotation of each sensor are shown in figures 11a and 11b, respectively. For the horizontal grasp made from a horizontal start position, the index and middle fingers lagged in forward motion in the incongruent condition. Near the end of the response, the fingers made an upward excursion followed by a quick downward adjustment. This extra motion makes sense given that the object displayed in the

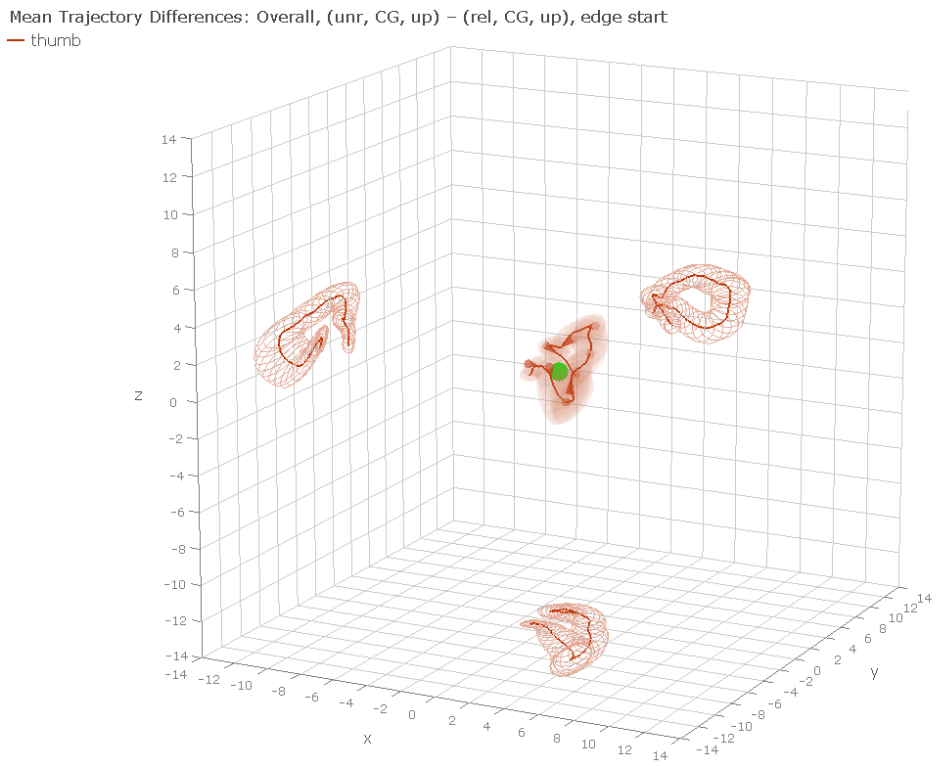

Figure 10a - Thumb position difference: vertical grasp from vertical start.

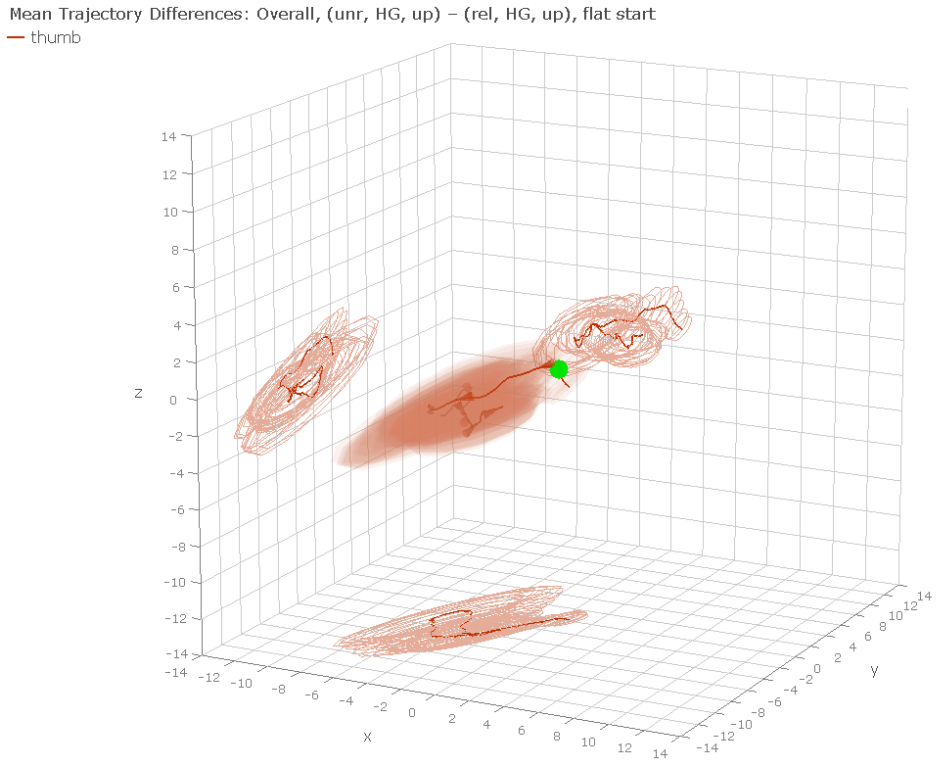

Figure 10f - Thumb position difference: horizontal grasp from horizontal start.

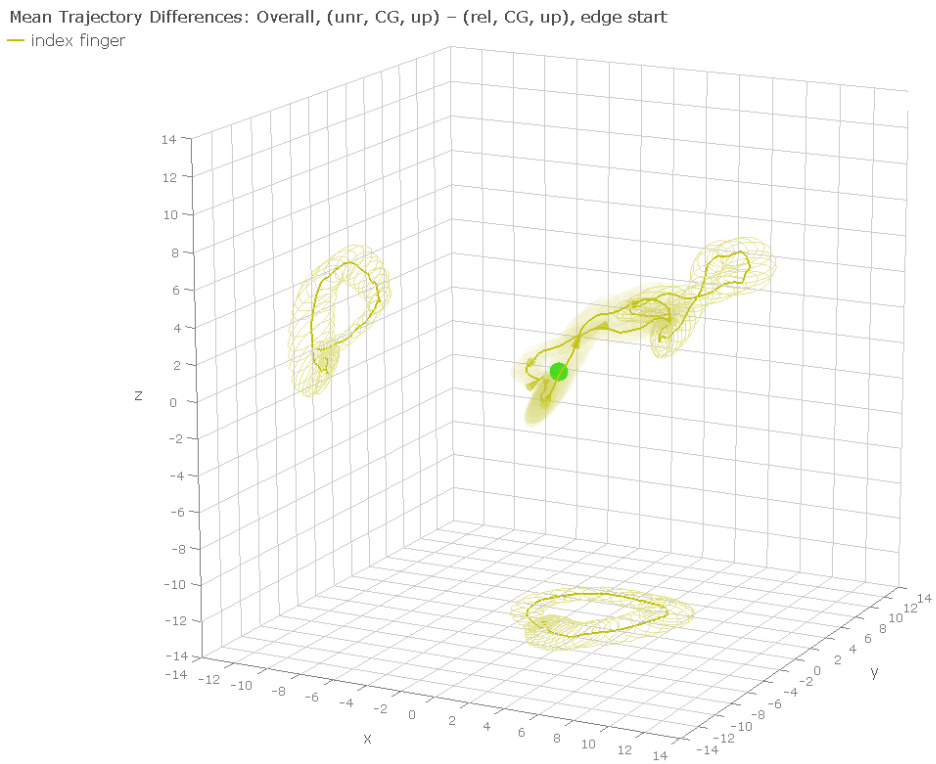

Figure 10b - Index finger position difference: vertical grasp from vertical start.

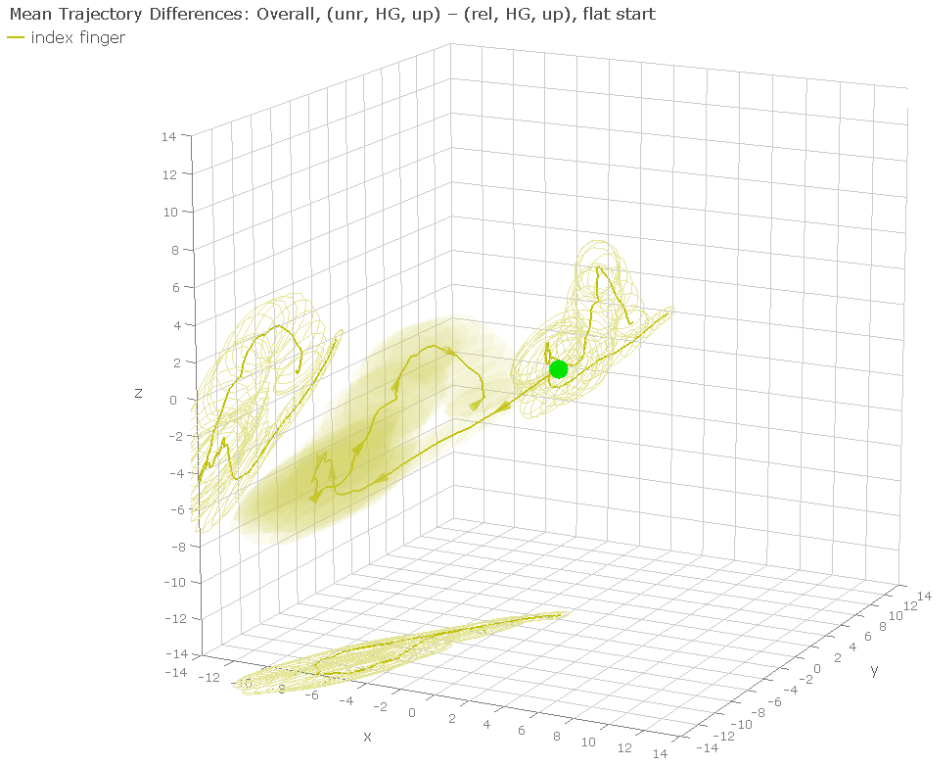

Figure 10g - Index finger position difference: horizontal grasp from horizontal start.

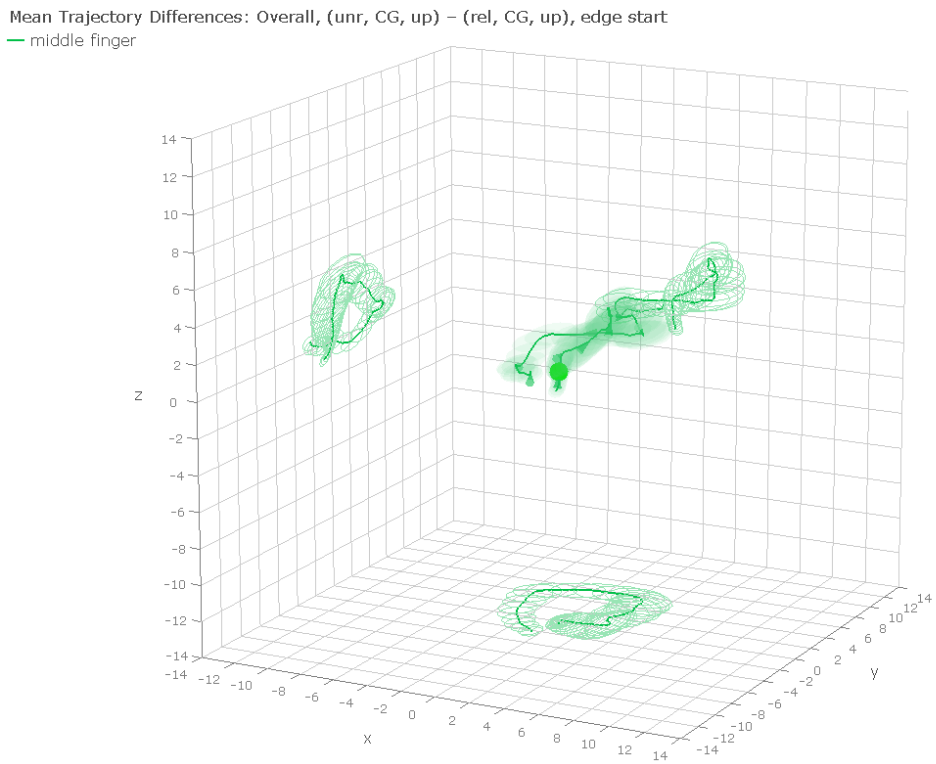

Figure 10c - Middle finger position difference: vertical grasp from vertical start.

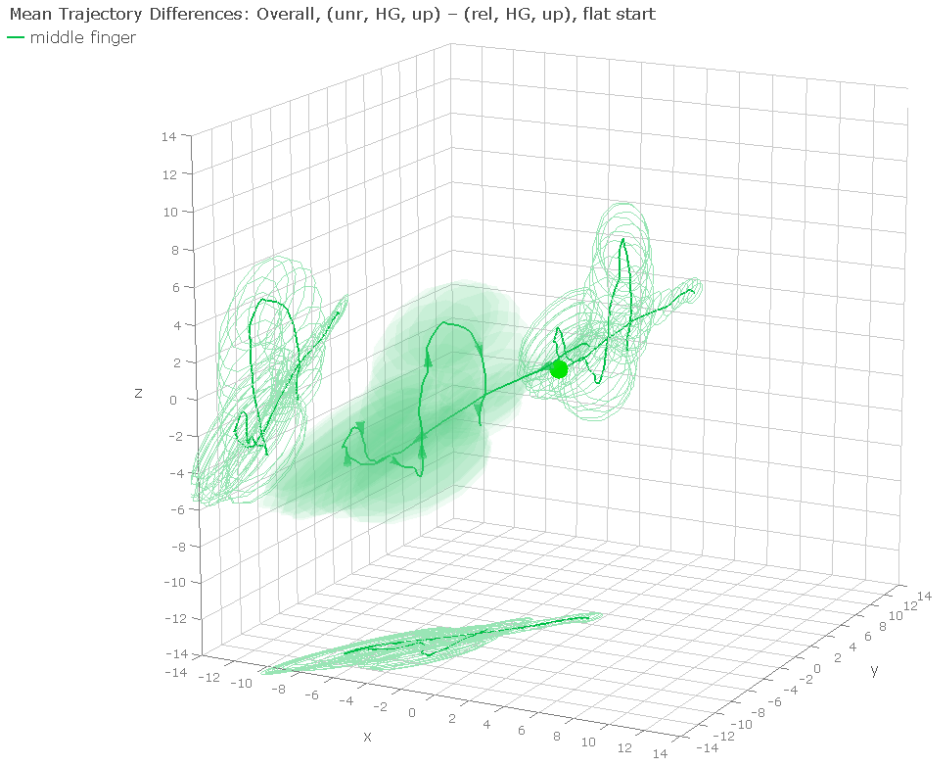

Figure 10h - Middle finger position difference: horizontal grasp from horizontal start.

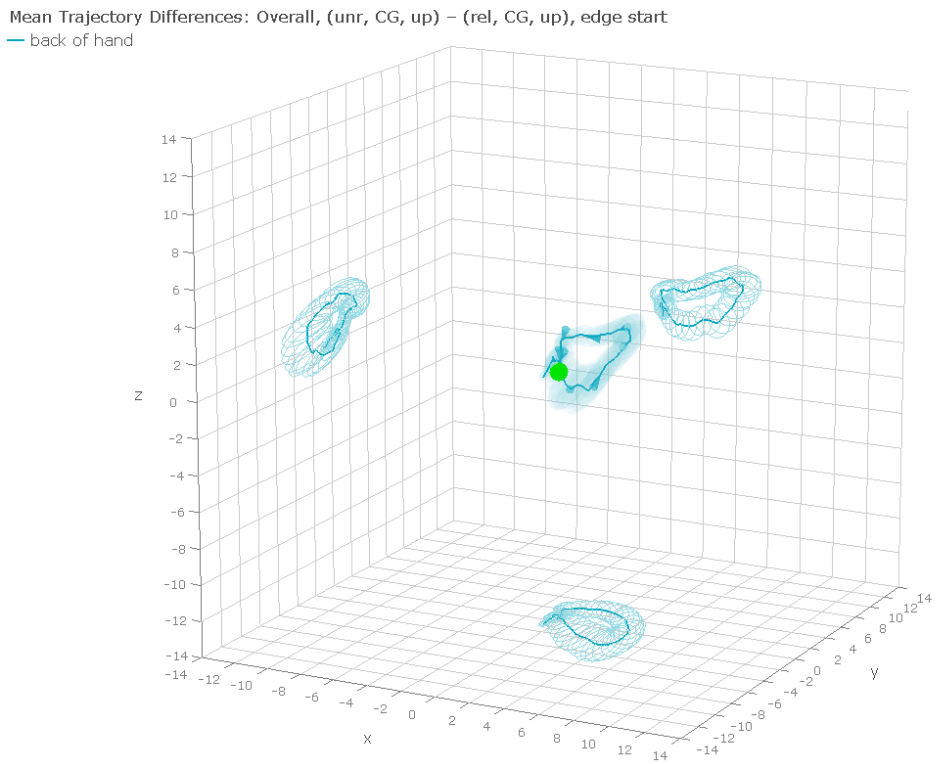

Figure 10d - Back of hand position difference: vertical grasp from vertical start.

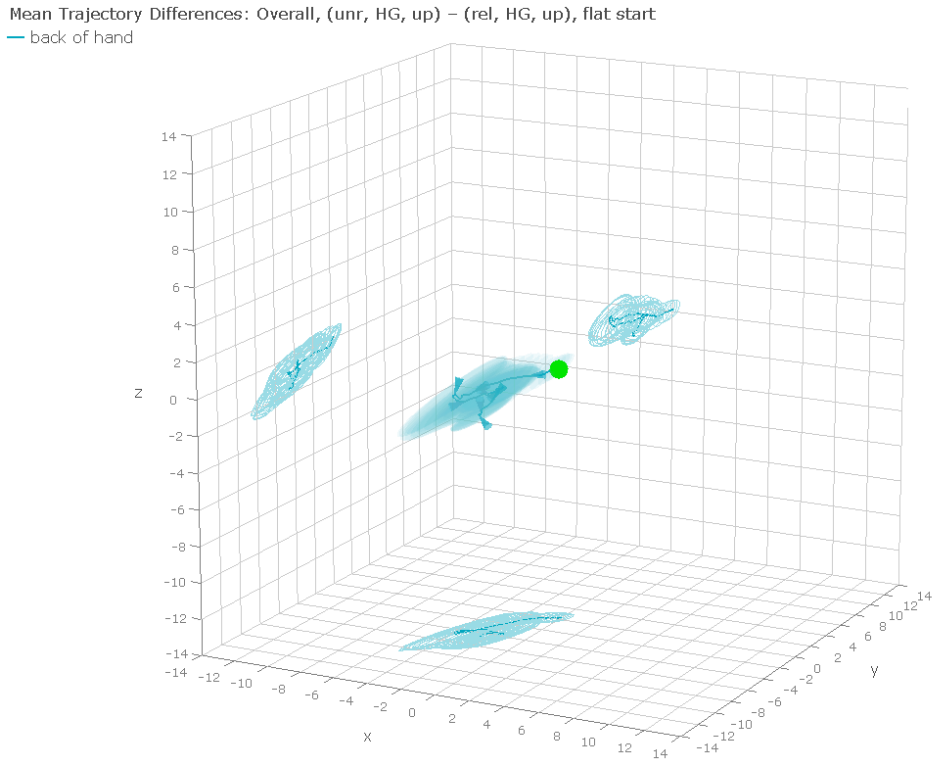

Figure 10i - Back of hand position difference: horizontal grasp from horizontal start.

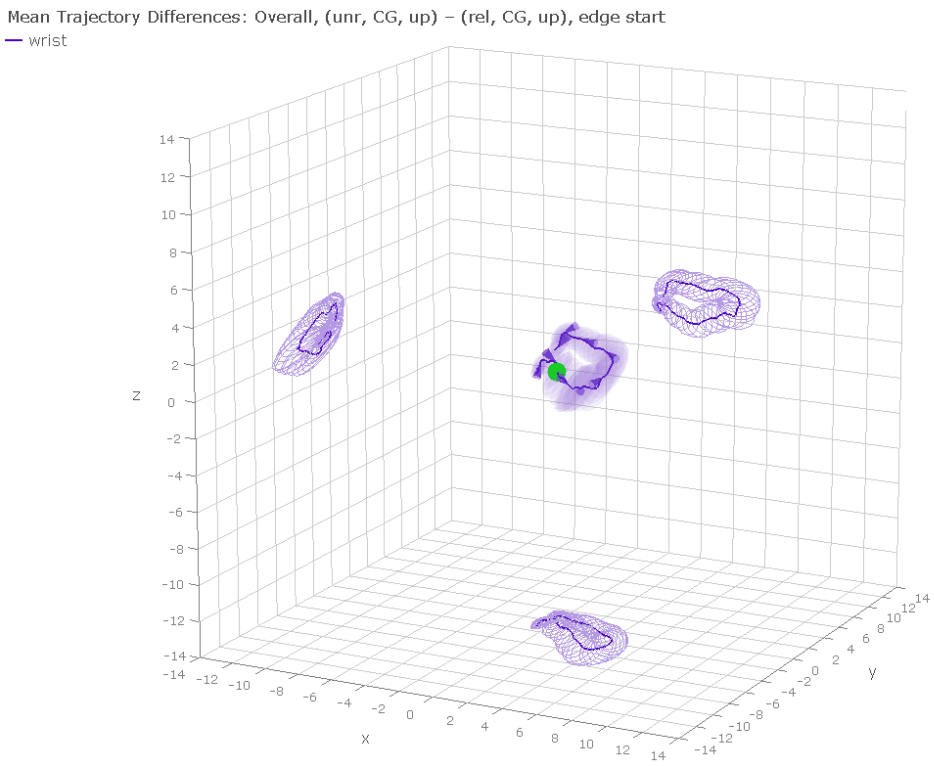

Figure 10e - Wrist position difference: vertical grasp from vertical start.

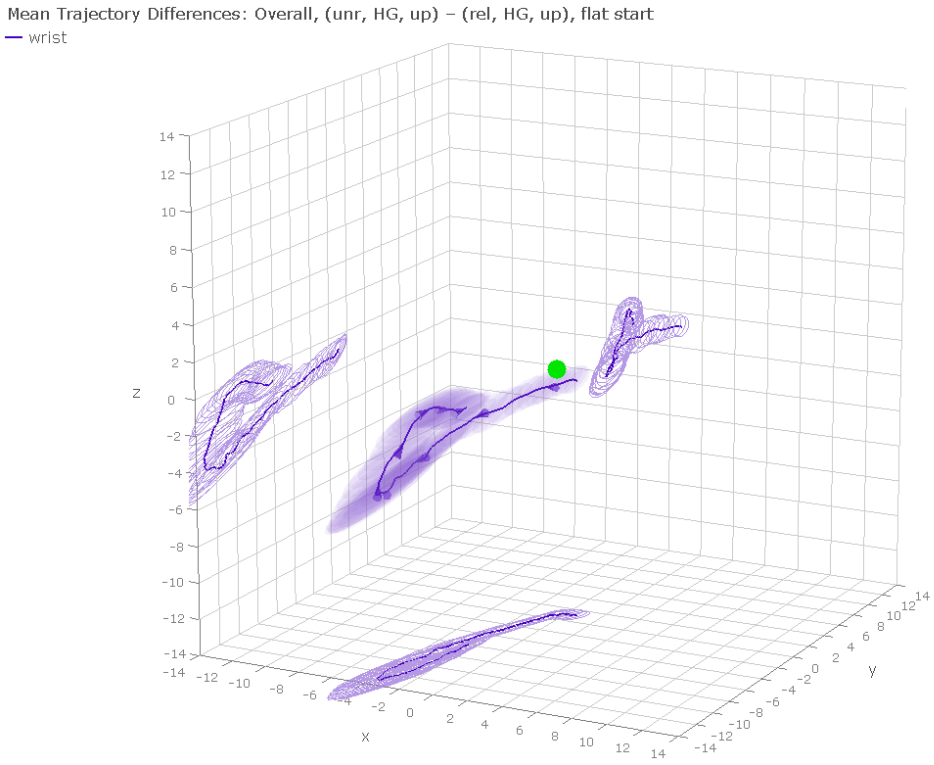

Figure 10j - Wrist position difference: horizontal grasp from horizontal start.

incongruent condition invites a vertical grasp. The rotation of the back of the hand is consistent with this interpretation. The ball plot of the corresponding sensor shows that the incongruent condition yields a slight flexion and supination of the wrist, presumably reflecting the influence of the irrelevant object on the trajectory of the horizontal grasp. The net result of the inadvertent influence of this conflicting motor representation was that the final position of the back of the hand was angled more toward a slightly more vertical posture. More obviously, all sensors showed a pronounced leftward excursion in the incongruent condition (maximum average = 8 mm for the index finger on the *x* axis). This can be understood by noting that the response element associated with the incongruent grasp was located to the left of body midline and, remarkably, the trajectory in the incongruent condition showed an attraction to that element en route to completion of the horizontal grasp. In the case of the vertical grasp made from a vertical start position, the incongruent object induced a brief excursion to the right for all sensors before the hand reached its final posture (maximum average = 5 mm for the index finger on the *x* axis). This outcome is pleasingly symmetrical with the result for the horizontal grasp; in both cases, the hand deviates in the direction of the response element associated with the incongruent grasp. The ball plot for rotation of the sensor attached to the back of the hand in this case showed a small clockwise rotation in the incongruent condition, again suggesting that the hand was inclined toward the incongruent response element.

Thus, in the absence of the need to rotate the hand to perform the required grasp, the only appreciable congruency effect on hand position that was apparent for those actions

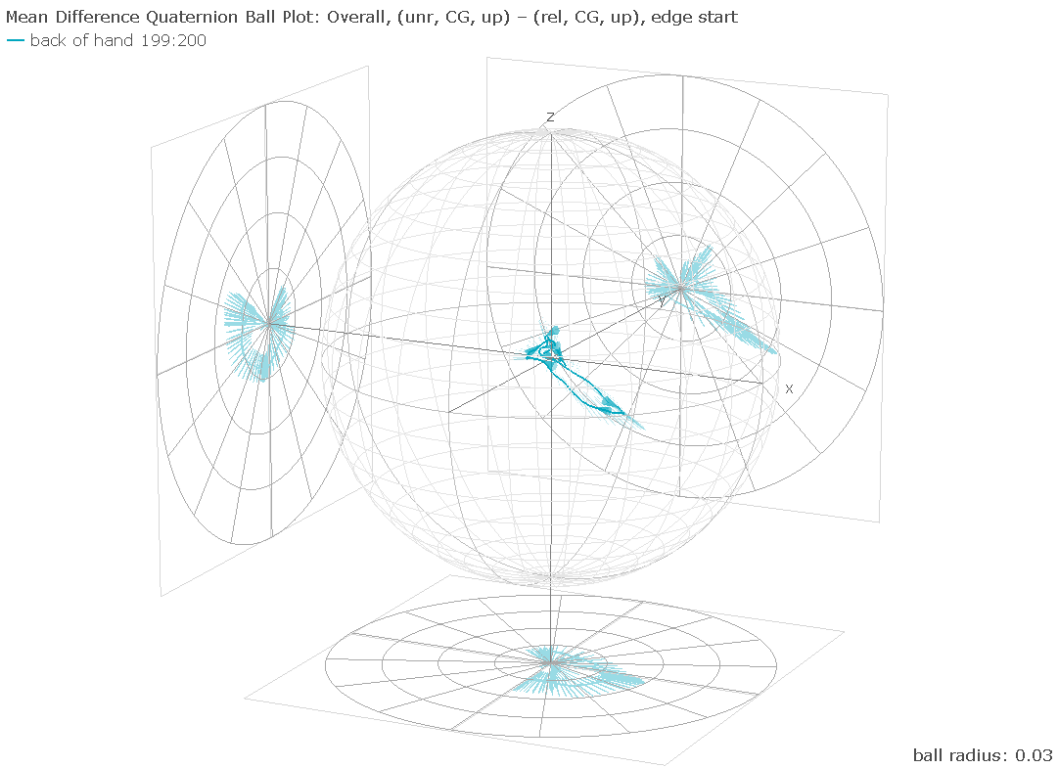

Figure 11a - Back of hand rotation difference: vertical grasp from vertical start.

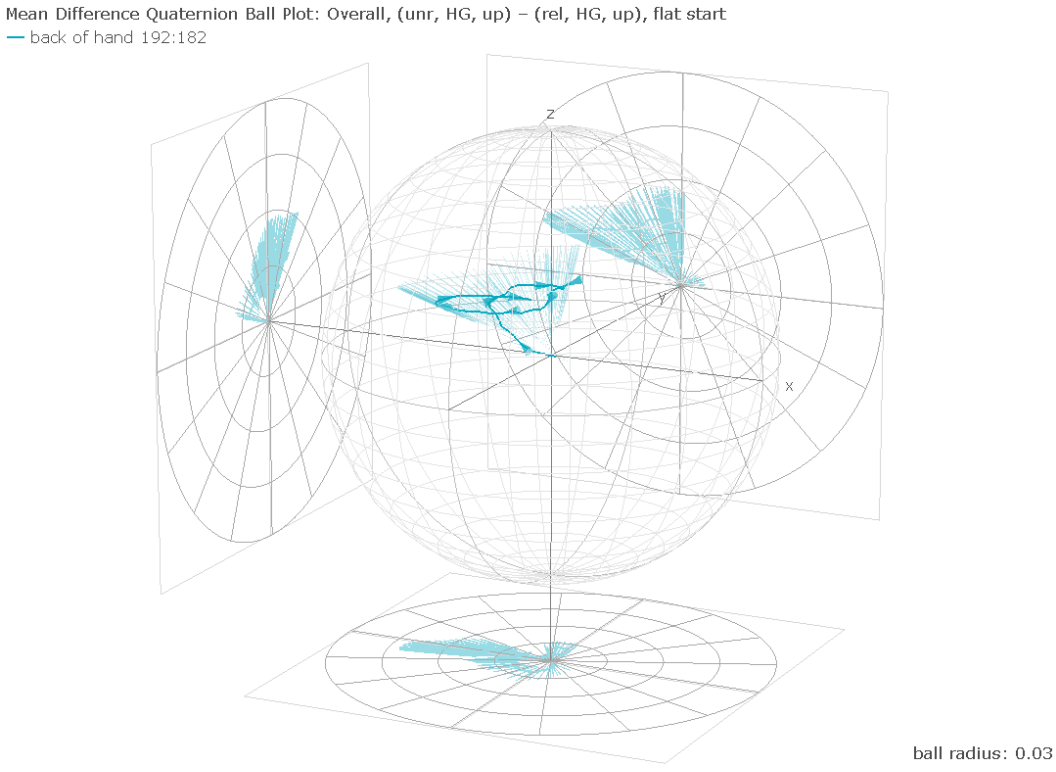

Figure 11b - Back of hand rotation difference: horizontal grasp from horizontal start.

was in the incongruent condition, in which the hand drifted laterally toward the incorrect response element in the first half of the trajectory, consistent with what was seen with the actions requiring a rotation as described above. With respect to rotational differences, during a vertical grasp, the sensor on the back of the hand indicated that the hand rotated around the *x* axis so that the fingers were elevated slightly in the incongruent relative to the congruent condition. When making a horizontal grasp, there was a tendency in the incongruent condition to rotate the hand slightly forward, away from the body.

Statistical Effect Size

To address the question of whether the effects of the object context extended throughout the hand's trajectory, rather than being confined to the early stages of movement, we plotted the combined translation and rotation effect size for each sensor as a function of normalized time in figure 12.

This was calculated as the Hotelling distance, defined as the square root of Hotelling's [1931] T^2 statistic, which is just the squared difference between the means divided by the pooled variance. This quantity can be thought of as a generalized signal-to-noise ratio; it is essentially the heteroscedastic generalization of the square of the Mahalanobis [1936] distance. These measures are in accord with the Riemannian geometry of the manifold of multivariate normal distributions as laid down by Skovgaard [1984] and finally subsumed by the very elegant information geometry of Amari [1990]. This work does not call for the full generality of Amari's information geometric methods, however, because second order statistics are assumed throughout.

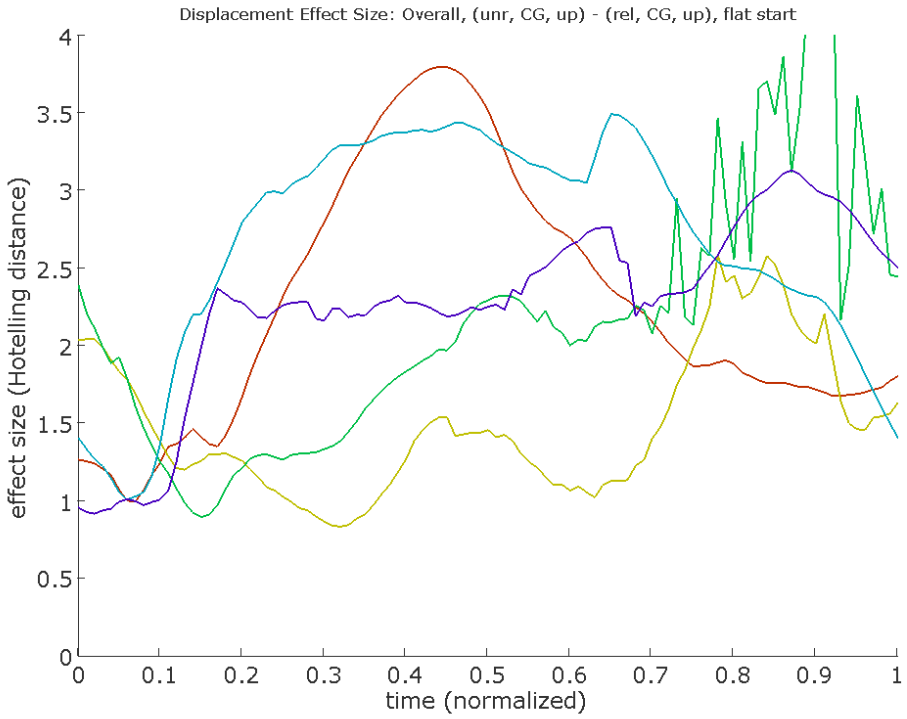

Figure 12a - Overall effect size: vertical grasp from horizontal start.

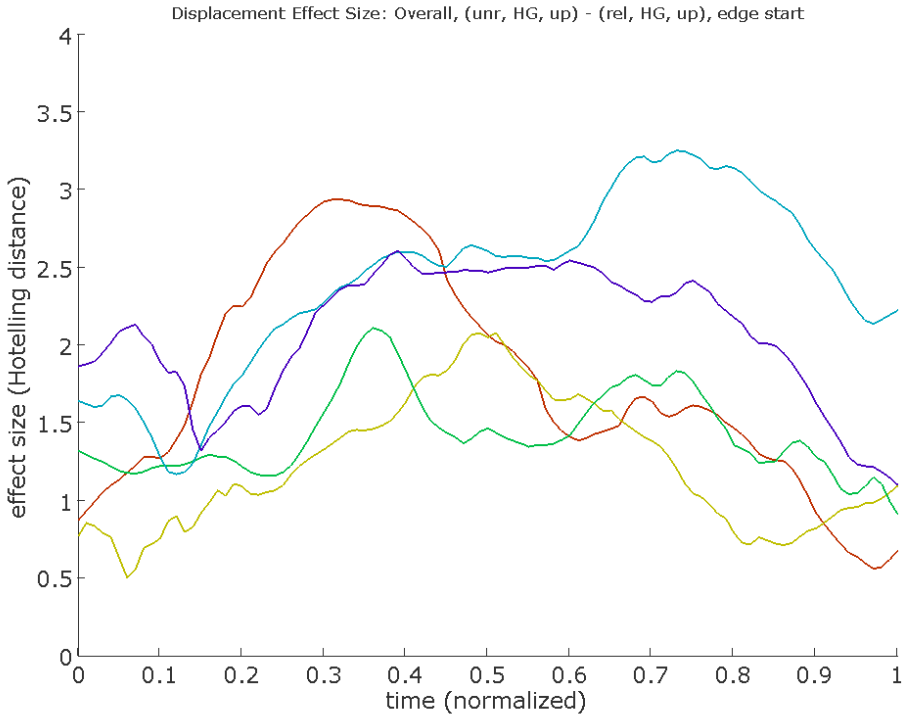

Figure 12b - Overall effect size: horizontal grasp from vertical start.

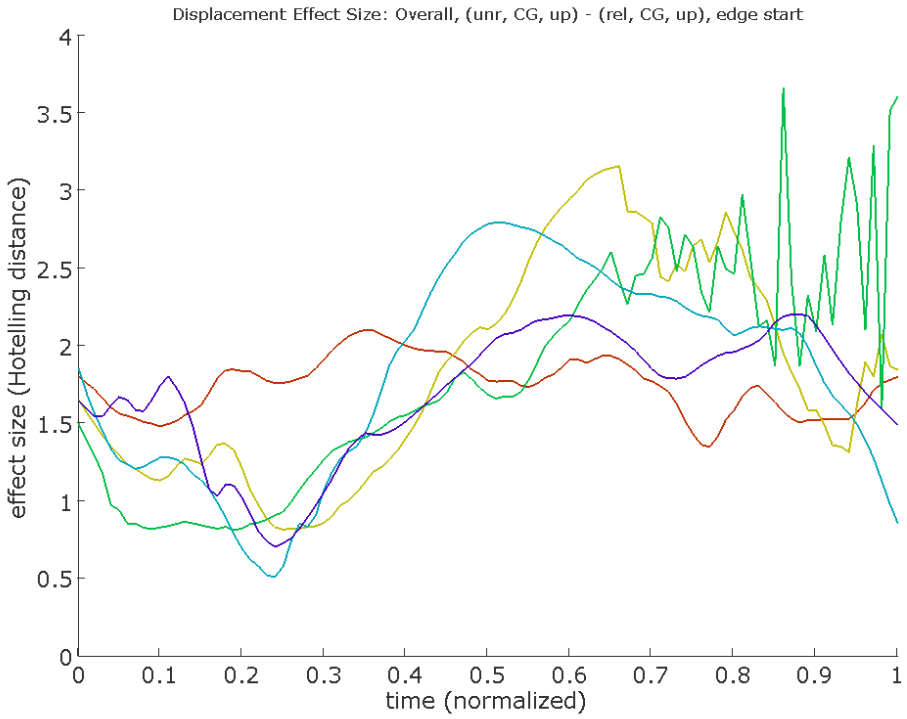

Figure 12c - Overall effect size: vertical grasp from vertical start.

Figure 12d - Overall effect size: horizontal grasp from horizontal start.

Figure 12a shows that, for the vertical grasp made from a horizontal starting position, the congruency effect for all sensors but the index finger was greater than 2 standard errors of the mean even after the midpoint of the trajectory. Near the end of the trajectory, the effect for some sensors was still greater than 2 standard errors above zero. Note that the middle finger in the vertical-grasp condition shows some perturbations in the last part of the trajectory. These are likely caused by small movements of the sensor due to its imperfect attachment to the finger for some subjects. This artifact appears in both conditions requiring a vertical grasp. For the horizontal grasp made from the vertical starting position (figure 12b), the maximal effect size occurred in the last quarter of the trajectory for the sensor on the back of the hand, and the effect remained over 2 standard errors away from zero for that sensor even at the end of the movement.

In the two conditions not requiring rotation (figures 12c and 12d), the effect sizes were somewhat smaller, and tended either to hover at the threshold of significance, (e.g., the thumb in figure 12c) or to trend roughly towards greater significance in the second half of the movement.

Discussion of Experimental Results

Previous reports have shown that the trajectory of the hand in a pointing task and of an eye movement to a target can deviate toward or away from the spatial location of a distractor [Song & Nakayama 2008; Tipper, Howard & Houghton 1998; Van der Stigchel 2010; Weaver, Lauwereyns & Theeuwes 2011]. Computational models of trajectories that curve away from a distractor are based on the idea of localized areas of inhibition

that operate on neuronal populations responsible for encoding the distractor location [Doyle & Walker 2001; Tipper, Howard & Paul 2001]. A further mechanism is required to counteract the influence of the distractor so that the trajectory curves back toward the target location [McSorley, Haggard & Walker 2004]. Situations in which the hand or eye curves toward instead of away from a distractor occur when attention is forced to the distractor because of task demands [Song & Nakayama 2008]. For example, selecting a target using its unique colour as the cue inevitably generates internal competition from among a set of homogeneously coloured distractors. This competition is the result of lateral interactions between the neuronal populations that separately encode the locations of the target and distractors [McPeek & Keller 2001].

In our experiment, attention was forced to the visual object that had to be held in memory while the reach-and-grasp action was programmed and executed. Remarkably, the competition we observed was generated at least in part by a mental representation of a potential action to an object held in working memory. Thus, analogously to visual search experiments that have examined hand and eye trajectories attracted toward a spatial distractor, the dynamics of the grasp posture of the hand in our task was affected by the "virtual grasp" associated with the object. This competition between the intended and the virtual grasps altered both the translation and rotation of the articulations of the hand in principled ways. We observed three qualitatively distinct effects. When the grasping response required a rotation, an incongruent object in working memory appeared to generate a virtual counterforce that was compensated for during the movement. For

example, pronation of the hand was altered when the distracting object invited supination, and vice versa. Regardless of whether rotation was required, during the first half of the reach action, an incongruent object in working memory slowed forward progress and attracted the hand toward the competing response element. The latter result converges nicely with previous demonstrations showing analogous effects for both hand and eye movements in two dimensions [McSorley et al. 2004; Song & Nakayama 2008].

The evidence we obtained goes well beyond previous work that has shown effects of physically present distractor objects on the trajectory of a hand or eye movement toward a target location [McSorley et al. 2004; Song & Nakayama 2008; Tipper et al. 1998; Weaver et al. 2011]. The distracting action representation in our task was evoked by an object in memory that was no longer visible when the grasping action was planned and executed. Nevertheless, the entire trajectory of the movement, as well as the articulation of the hand, were altered under the competing influence of the distracting object (see figure 12).

Other research examining the effect of an irrelevant word or object on the trajectory of hand actions has relied on traditional kinematic measures, such as time to peak velocity and thumb-forefinger aperture [e.g., Gentilucci, Benuzzi, Bertolani, Daprati & Gangitano 2000; Gentilucci & Gangitano 1998; Glover & Dixon 2002; Glover et al. 2004]. These results indicate that effects are confined to relatively early stages of the trajectory and dissipate during the course of the movement. Measures such as velocity and aperture, however, are inherently constrained by the fact that the hand must arrive at an end point

with the thumb and forefinger spaced in accordance with the size of the grasped object. It is inevitable, then, that these kinematic measures eventually must be determined by the parameters of the target and can admit no influence of context on later stages of the movement. Our statistical methodology allowed us to track changes as small as a fraction of a degree in the rotation of the hand and a few millimetres in its position, and it clearly established that the on-line control of movement is continuously modulated by conceptually driven representations of action, in much the same way that movement is continuously informed by the presence of competing objects in space. Overcoming the competing affordances of an object in working memory when carrying out an intended action is much like resolving competition between action plans evoked by objects in space.

Summary and Conclusions

We have seen how geometric algebra provides an approach to the representation of geometric objects and the transformations acting on them which allows us to arrive at some of the more advanced results from the theory of Lie groups by a greatly simplified path, and thereby to define barycentres and dispersion in non-commutative, non-compact Lie groups without a bi-invariant metric. In the specific case of $\mathbb{SE}(3)$, we have applied these tools to the formulation of a random-effects statistical model of the trajectories swept out in the group manifold by the motions of the articulations of the human hand during reach-to-grasp movements carried out in differing cognitive states. We have introduced the combination of box plots and ball plots to aid in data visualization and interpretation of these results. The new results we have been able to establish in this way have proven the robustness and usefulness of the methodology.

Bibliography

Amari, S-I, 1990: *Differential-Geometrical Methods in Statistics, 2nd edition*. Lecture Notes in Statistics, vol 28. Springer.

Aristidou, A, 2010: *Tracking and Modelling Motion for Biomechanical Analysis*, Ph.D. Dissertation, Cambridge University Engineering Department.

Bicchi, A, Gabiccini, M, & Santello, M, 2011: Modelling natural and artificial hands with synergies. *Phil. Trans. Roy. Soc. B, Biol. Sci.* 366(1581):3153-3161.

Blinn, J F, 2002: Using tensor diagrams to represent and solve geometric problems. *Short Course, SIGGRAPH 2002*.

Brillinger, D R, 2010: Modeling spatial trajectories. ed: Gelfand, A E, Diggle, P, Guttorp, P, & Fuentes, M, *Handbook of Spatial Statistics*, CRC Press.

Bub, D N, & Masson, M E J, 2010: Grasping beer mugs: on the dynamics of alignment effects induced by handled objects. *J. Experim. Psychol. Hum. Percept. Perform.* 36(2):341-358.

Bub, D N, Masson, M E J, & Cree, G S, 2008: Evocation of functional and volumetric gestural knowledge by objects and words. *Cognition*, 106(1):27-58.

Buchholz, S, & Sommer, G, 2005: On averaging in Clifford groups. ed: Li, H, Olver, P J, & Sommer, G, *Computer Algebra and Geometric Algebra with Applications*, Lecture Notes in Computer Science, 3519:229-238, Springer.

Buss, S R, & Fillmore, J P, 2001: Spherical averages and applications to spherical splines and interpolation. *ACM Trans. Graphics*, 20(2):95-126.

Cardoso, J R, & Leite, F S, 2010: Exponentials of skew-symmetric matrices and logarithms of orthogonal matrices. *J. Computational & Appl. Math.* 233(11):2867-2875.

Cartan, E, & Schouten, J A, 1926: On the geometry of the group-manifold of simple and semi-simple groups. *Proc. Kon. Ned. Akad. v. Wetensch.* 29:803-815.

Chao, L L, & Martin, A, 2000: Representation of manipulable man-made objects in the dorsal stream. *NeuroImage*, 12:478-484.

Chapman, C S, Gallivan, J P, Wood, D K, Milne, J L, Culham, J C, & Goodale, M A, 2010a: Reaching for the unknown: Mutliple-target encoding and real-time decision-making in a rapid reach task. *Cognition*, 116(2):168-176.

Chapman, C S, Gallivan, J P, Wood, D K, Milne, J L, Culham, J C, & Goodale, M A, 2010b: Short-term motor plasticity revealed in a visuomotor decision-making task. *Behavioural Brain Research*, 214:130-134.

Chasles, M, 1830: Note sur les propriétés générales du système de deux corps semblables entr'eux et placés d'une manière quelconque dans l'espace; et sur le déplacement fini ou infiniment petit d'un corps solide libre. *Bulletin des Sciences Mathematiques, Astronomiques, Physiques et Chimiques*, 14:321-326.

Chavarria-Fabila, M A, 2009: Monocular pose estimation based on global and local features. *Technical Report 0922*, Institut für Informatik, Christian-Albrechts-Universität zu Kiel.

Chirikjian, G S, 2012: *Stochastic Models, Information Theory, & Lie Groups, Volume 2: Analytic Methods and Modern Applications*, Springer.

Chirikjian, G S, 2010: Information-theoretic inequalities on unimodular Lie groups. *J. Geom. Mech.* 2(2):119-158.

Chirikjian, G S, & Kyatkin, A B, 2001: *Engineering Applications of Noncommutative Harmonic Analysis With Emphasis on Rotation and Motion Groups*, CRC Press.

Choe, S B, 2006: *Statistical analysis of orientation trajectories via quaternions with applications to human motion*, Ph.D. Thesis, University of Michigan.

Cisek, P, 2007: Cortical mechanisms of action selection: The affordance competition hypothesis. *Phil. Trans. Roy. Soc. B: Biol. Sci.* 362:1585-1599.

Cisek P, & Kalaska, J F, 2005: Neural correlates of reaching decisions in dorsal premotor cvortex: Specification of multiple directoin choices and final selection of action. *Neuron*, 45:801-814.

Clifford, W K, 1878: Applications of Grassmann's extensive algebra. *Am. J. Math.* 1(4):350-358.

Coulthard, E J, Nachev, P, & Husain, M, 2008: Control over conflict during movement preparation: Role of posterior parietal cortex. *Neuron*, 58:144-157.

Doran, C J L, & Lasenby, A N, 2007: *Geometric Algebra for Physicists*, Cambridge University Press.

Dorst, L, 2005: First order error propagation of the Procrustes method for 3D attitude estimation. *IEEE Trans. Pattern Analysis & Machine Intelligence*, 27(2):221-229.

Dorst, L, Fontijne, D, & Mann, S, 2009: *Geometric Algebra for Computer Science: An Object-Oriented Approach to Geometry, Revised Edition*, Morgan-Kaufmann.

Dorst, L, & Mann, S, 2002: Geometric Algebra: A computational framework for geometrical applications, part 1 - algebra. *IEEE Computer Graphics & Applications*, 22(3):24-31.

Doyle, M, & Walker, R, 2001: Curved saccade trajectories: Voluntary and reflexive saccades curve away from irrelevant distractors. *Experimental Brain Research*, 139:333-344.

Eriksen, B A, & Eriksen, C,W, 1974: Effects of noise letters upon identification of a target letter in a nonsearch task. *Perception & Psychophysics*, 16:143-149.

Faraway, J, Reed, M, & Wang, J, 2007: Modeling 3D trajectories using Bézier curves with application to hand motion. *J. Roy. Statist. Soc. Ser. C: Appl. Statist.* 56(5):571-585.

Fiori, S, 2010: A closed-form solution to the problem of averaging over the Lie group of special orthogonal matrices. *Advances in Neural Networks - ISNN 2010*, Lecture Notes in Computer Science, 6063:185-192.

Fontijne, D, & Dorst, L, 2003: Modelling 3D Euclidean geometry. *IEEE Comput. Graph. Appl.* 23(2):68-78.

Fréchet, M, 1948: Les éléments aléatoires de nature quelconque dans un espace distancié. *Ann. Inst. Henri Poincaré*, 10(4):215-310.

Gebken, C, & Sommer, G, 2008: Perspective pose estimation with geometric algebra. *AIP Conf. Proc.* 1046:95-98.

Gentilucci, M, Benuzzi, F, Bertolani, L, Daprati, E, & Gangitano, M, 2000: Language and motor control. *Experimental Brain Research*, 133:468-490.

Gentilucci, M, & Gangitano, M, 1998: Influence of automatic word reading on motor control. *Eur. J. Neurosci.* 10:752-756.

Glover, S, 2004: Separate visual representations in the planning and control of action. *Behavioural and Brain Sciences*, 27:3-78.

Glover, S, & Dixon, P, 2002: Semantics affect the planning but not control of grasping. *Experimental Brain Research*, 146:383-387.

Glover, S, Rosenbaum, D A, Graham, J, & Dixon, P, 2004: Grasping the meaning of words. *Experimental Brain Research*, 154:103-108.

Goldman, R, 2003: Computer graphics in its fifth decade: ferment at the foundations. *Proc. 11th Pacific Conf. Computer Graphics and Applications*, 4-21.

Govindu, V M, 2004: Lie-algebraic averaging for globally consistent motion estimation. *Proc. IEEE Conf. Computer Vision & Pattern Recognition (CVPR 2004)*, 1:684-691.

Grassmann, H, 1877: Der Ort der Hamilton'schen Quaternionen in der Ausdehnungslehre. *Math. Ann.* 12(3):375-386.

Grassmann, H, 1844: *Die Lineale Ausdehnungslehre, ein neuer Zweig der Mathematik*, Leipzig: Otto Wigand.

Grèzes, J, Tucker, M, Armony, J, Ellis, R, & Passingham, R E, 2003: Objects automatically potentiate action: An fMRI study of implicit processing. *Eur. J. Neurosci.* 17, 2735–2740.

Handy, T C, Grafton, S T, Shroff, N M, Ketay, S, & Gazzaniga, M S, 2003: Graspable objects grab attention when the potential for action is recognized. *Nature Neurosci.* 6:421-427.

Hansen, S, & Elliott, D, 2009: Three-dimensional manual responses to unexpected target perturbations during rapid aiming. *J. Motor Behavior*, 41:16-29.

Hansen, S, Elliott, D, & Khan, M A, 2008: Quantifying the variability of three-dimensional aiming movements using ellipsoids. *Motor Control*, 12:241-251.

Hestenes, D, 2010: New tools for computational geometry and rejuvenation of screw theory. ed: Bayro-Corrochano, E, & Scheuermann, G, *Geometric Algebra Computing in Engineering and Computer Science*, 3-33, Springer.

Hestenes, D, 2001: Old wine in new bottles: A new algebraic framework for computational geometry. ed: Bayro-Corrochano, E, & Sobczyk, G, *Geometric Algebra: A geometric approach to computer vision, neural and quantum computing, robotics and engineering*, 3-18, Birkhäuser.

Hestenes, D, 1991: The design of linear algebra and geometry. *Acta Appl. Math.* 23(1):65-93.

Hestenes, D, 1988: Universal geometric algebra. *Simon Stevin*, 62(3-4):253-274.

Hestenes, D, & Sobczyk, G, 1987: *Clifford Algebra to Geometric Calculus: A Unified Language for Mathematics and Physics*, Springer.

Hotelling, H, 1931: The generalization of Student's ratio. *Ann. Math. Statist.* 2(3):360-378.

Jakobson, L S, & Goodale, M A, 1991: Factors affecting higher-order movement planning: A kinematic analysis of human prehension. *Experimental Brain Research*, 86:199-208.

Kanatani, K, & Niitsuma, H, 2012: Optimal computation of 3-D similarity: Gauss-Newton vs.Gauss-Helmert. *Memoirs of the Faculty of Engineering, Okayama University*, 46:21-33.

Karcher, H, 1977: Riemannian center of mass and mollifier smoothing. *Commun. Pure & Appl. Math.* 30(5):509-541.

Laquer, H T, 1992: Invariant affine connections on Lie groups. *Trans. Amer. Math. Soc.* 331(2):541-551.

Lasenby, A N, Lasenby, J, & Wareham, R, 2004: A covariant approach to geometry using geometric algebra. *Technical Report CUED/F-INFENG/TR-483*, Cambridge University Engineering Department.

Liu, G, Chua, R, & Enns, J T, 2008: Attention for perception and action: Task interference for action planning but not for online control. *Experimental Brain Research*, 185:709-717.

Mahalanobis, P, 1936: On the generalized distance in statistics. *Proc. Nat'l Inst. Sci. Calcutta*, 2:49-55.

Mann, S & Dorst, L, 2002: Geometric Algebra: A computational framework for geometrical applications, part 2 - applications. *IEEE Computer Graphics & Applications*, 22(4):58-67.

Maroulas, V, 2012: Error analysis of stochastic flight trajectory prediction models. *J. Appl. Stat.* 39(8):1825-1841.

McCarthy, J M, & Soh, G S, 2011: Clifford algebra synthesis of serial chains. *Geometric Design of Linkages*, Interdisciplinary Applied Mathematics, 11:357-392, Springer.

McPeek, R M, & Keller, E L, 2001: Short-term priming, concurrent processing, and saccade curvature during a target selection task in the monkey. V*ision Research*, 41:785-800.

McSorley, E, Haggard, P, & Walker, R, 2004: Distractor modulation of saccade trajectories: Spatial separation and symmetry effects. *Experimental Brain Research*, 155:320-333.

Milner, A D, & Goodale, M A, 2008: Two visual systems re-viewed. *Neuropsychologia*, 46:774-785.

Moakher, M, 2002: Means and averaging in the group of rotations. *SIAM J. Matrix Anal. Appl.* 24(1):1-16.

Mozzi, G, 1763: *Discorso Matematico Sopra il Rotamento Momentaneo dei Corpi*, Stamperia di Donato Campo, Napoli.

Nomizu, K, 1956: *Lie Groups and Differential Geometry*, Mathematical Society of Japan.

Nomizu, K, 1954: Invariant affine connections on homogeneous spaces. *Am. J. Math.* 76(1):33-65.

Pennec, X, & Arsigny, V, 2013: Exponential barycenters of the canonical Cartan connection and invariant means on Lie groups. ed: Nielsen, F, & Bhatia, R, *Matrix Information Geometry*, 123-166, Springer.

Petersen, A, & Koch, R, 2010: Statistical analysis of Kalman filters by conversion to Gauss-Helmert models with applications to process noise estimation. *Proc. 20th Int'l Conf. Pattern Recognition (ICPR 2010)*, 2386-2389.

Ramsay, J O, & Silverman, B W, 2005: *Functional Data Analysis, 2nd ed.*, Springer.

Santello, M, Flanders, M, & Söchting, J F, 1998: Postural hand synergies for tool use. *J. Neurosci.* 18:10105-10115.

Santello, M, Flanders, M, & Söchting, J F, 2002: Patterns of hand motion during grasping and the influence of sensory guidance. *J. Neurosci.* 22:1426-1435.

Santello, M, & Söchting, J F, 1998: Gradual molding of the hand to object contours. *J. Neurophysiol.* 79:1307-1320.

Selig, J M, & Bayro-Corrochano, E, 2009: Rigid body dynamics using Clifford algebra. *Adv. Appl. Clifford Algebras*, 20(1):141-154.

Sharf, I, Wolf, A, & Rubin, M B, 2010: Arithmetic and geometric solutions for average rigid-body rotation. *Mech. Mach. Theory*, 45(9):1239-1251.

Skovgaard, L T, 1984: A Riemannian geometry of the multivariate normal model. *Scand. J. Statist.* 11(4):211-223.

Sobczyk, G, 2013: *New Foundations in Mathematics: The Geometric Concept of Number*, Springer.

Song, J-H, & Nakayama, K, 2008: Target selection in visual search as revealed by movement trajectories. *Vision Research*, 48:853-861.

Stewart, B M, Baugh, L A, Gallivan, J P, & Flanagan, J R, 2013: Simultaneous encoding of the direction and orientation of potential targets during reach planning: Evidence of multiple competing reach plans. *J. Neurophysiol.* 110:807-816.

Sumner, P, & Husain, M, 2008: At the edge of consciousness: Automatic motor activation and voluntary control. *The Neuroscientist*, 14:474-486.

Till, B C, Masson, M E J, Bub, D N, & Driessen, P F, 2014: Embodied effects of conceptual knowledge continuously perturb the hand in flight. *Psych. Sci.* 25(8):1637-1648.

Tipper, S P, Howard, L A, & Houghton, G, 1998: Action-based mechanisms of attention. *Phil. Trans. Roy. Soc. B: Biol. Sci.* 353:1385-1393.

Tipper, S P, Howard, L A, & Paul, M A, 2001: Reaching affects saccade trajectories. *Experimental Brain Research*, 136:241-249.

Valkenburg, R, & Dorst, L, 2011: Estimating motors from a variety of geometric data in 3D conformal geometric algebra. ed: Dorst, L, & Lasenby, J, *Guide to Geometric Algebra in Practice*, 25-45, Springer.

Van der Stigchel, S, 2010: Recent advances in the study of saccade trajectory deviations. *Vision Research*, 50:1619-1627.

Weaver, M D, Lauwereyns, J, & Theeuwes, J, 2011: The effect of semantic information on saccade trajectory deviations. *Vision Research*, 51:1124-1128.

Weyrauch, A, & Scholz, D, 2009: Computing the Baker-Campbell-Hausdorff series and the Zassenhaus product. *Computer Phys. Commun.* 180(9):1558-1565.

Witt, J K, Kemmerer, D, Linkenauger, S A, & Culham, J, 2010: A functional role for motor simulation in identifying tools. *Psych. Sci.* 21:1215-1219.

Zhao, Y, Valkenburg, R, Klette, R, & Rosenhahn, B, 2006: Target calibration and tracking using conformal geometric algebra. ed: Chang,V, & Lie, W-N, *Advances in Image and Video Technology*, Lecture Notes in Computer Science, 4319:74-83.

Zefran, M, Kumar, R V, & Croke, C, 1999: Metrics and connections for rigid body kinematics. *Int'l J. Robotics Research*, 18(2):243-258.

Graded Algebra of Geometric Primitives

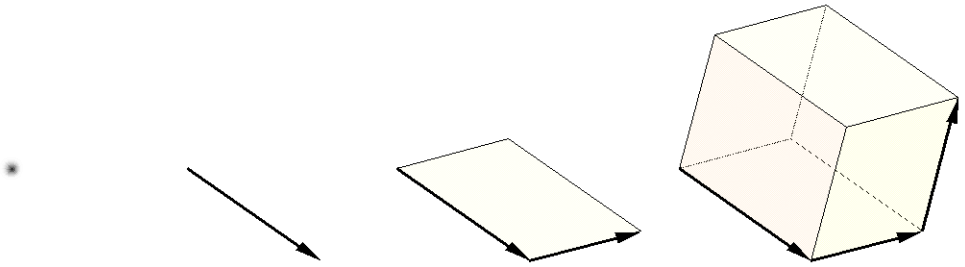

point	line	area	volume
scalar	vector	bivector	trivector
0-blade	1-blade	2-blade	3-blade
a	a	$a \wedge b$	$a \wedge b \wedge c$

The Commutative Vector Product

inner product: parallel parts give a ***scalar***

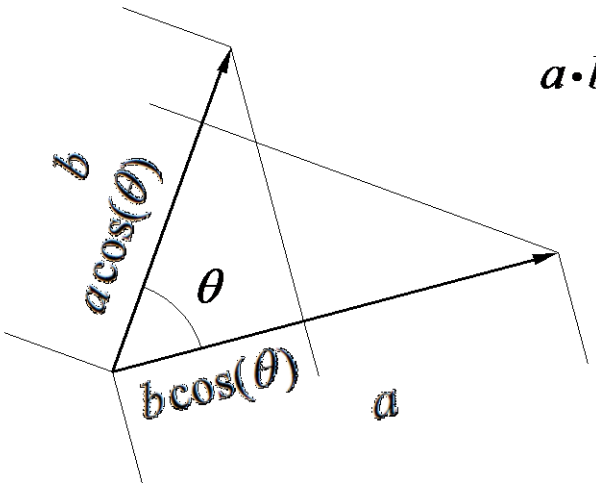

$$a \cdot b = b \cdot a = |a||b|\cos(\theta)$$

The Anti-commutative Vector Product

outer product: perpendicular parts give a ***bivector***

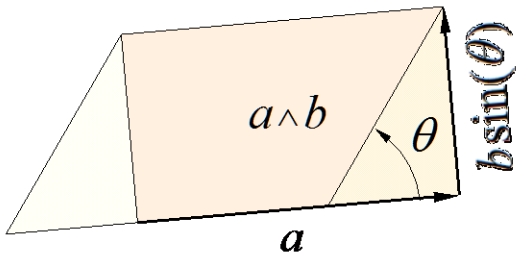

$$a \wedge b = -b \wedge a = ab\sin(\theta)$$

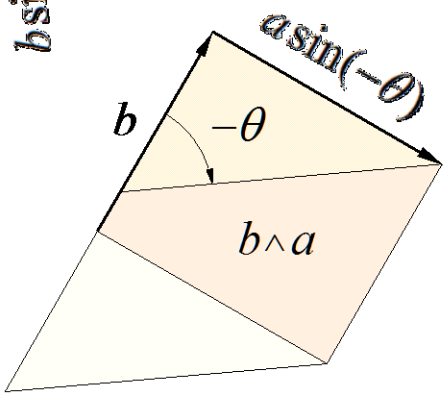

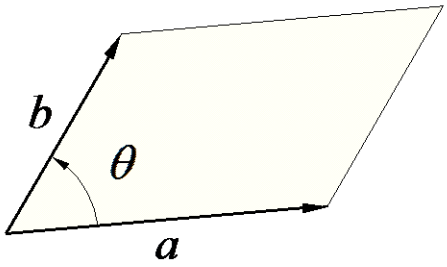

The Geometric Product

geometric product: sum of inner and outer products

$$ab = a \cdot b + a \wedge b$$

$$a \cdot b = \frac{1}{2}(ab + ba)$$

dot product

- ▷ parallel parts
- ▷ yields a scalar
- ▷ commutes

$$a \wedge b = \frac{1}{2}(ab - ba)$$

wedge product

- ▷ perpendiculars
- ▷ yields a bivector
- ▷ anticommutes

The Geometric Product is Invertible

every vector squares to a scalar ...

$$(a+b)^2 = a^2 + ab + ba + b^2$$

$$(a+b)^2 - a^2 - b^2 = ab + ba = 2a \cdot b$$

... and this lets us ***divide by vectors***

$$aa^{-1} = a^{-1}a = 1 \quad \Rightarrow \quad a^{-1} = \frac{1}{a^2}a$$

The Inverse of an Arbitrary Blade

inverting a bivector leads us to define ***reversion***

$$(uv)(v^{-1}u^{-1}) = u(vv^{-1})u^{-1} = u(1)u^{-1} = uu^{-1} = 1$$

$$(uv)^{-1} = v^{-1}u^{-1} = \frac{vu}{v^2u^2} = \frac{vu}{uvvu} = \frac{\overleftarrow{uv}}{uv\overleftarrow{uv}}$$

and this generalizes ***inversion*** to any arbitrary blade

$$b^{-1} = \frac{\overleftarrow{b}}{b\overleftarrow{b}} = \frac{\overleftarrow{b}}{|b|^2} \quad \Rightarrow \quad |b| = \sqrt{b\overleftarrow{b}}$$

Signature (2 ,0): Unit Bivectors Square To –1

unit bivectors are ***geometric*** **roots of –1**

$$\boldsymbol{b}^2 = (uv)^2 = uvuv = -uvvu = -\boldsymbol{b}\tilde{\boldsymbol{b}} = -u^2v^2$$

$$u^2 = 1, v^2 = 1 \quad \Rightarrow \quad \boldsymbol{b}^2 = -1$$

these bivectors lead to circular functions

wherever i appears in formulae, look for a bivector!

Signature (1 ,1): Unit Bivectors Square To +1

unit bivectors are ***geometric*** **roots of unity**

$$\boldsymbol{b}^2 = (uv)^2 = uvuv = -uvvu = -\boldsymbol{b}\tilde{\boldsymbol{b}} = -u^2v^2$$

$$u^2 = 1, v^2 = -1 \quad \Rightarrow \quad \boldsymbol{b}^2 = 1$$

these bivectors lead to hyperbolic functions

The Geometric Elements of the Plane

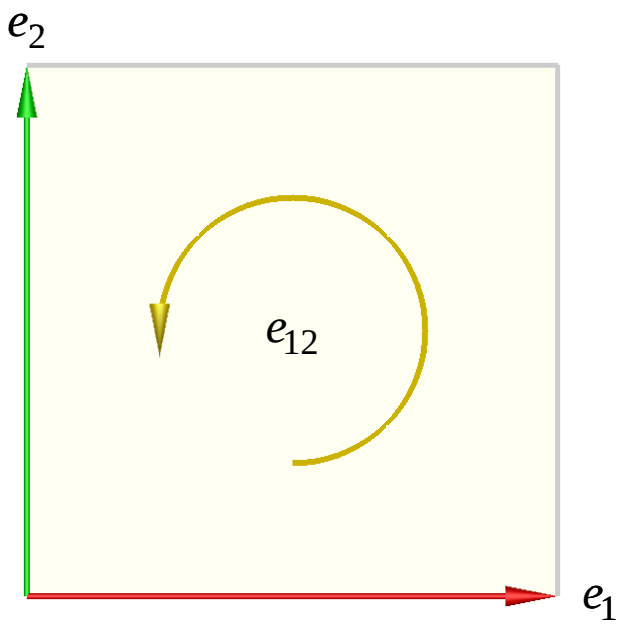

▷ the unit square (bivector)

$$e_{12} = e_1 e_2 = e_1 \wedge e_2$$

▷ the axes (vectors)

$$\{e_1, e_2\} = \{\hat{x}, \hat{y}\}$$

The Geometric Algebra of the Plane, $\mathcal{G}_2$

	1	e_1	e_2	e_{12}
1	1	e_1	e_2	e_{12}
e_1	e_1	1	e_{12}	e_2
e_2	e_2	$-e_{12}$	1	$-e_1$
e_{12}	e_{12}	$-e_2$	e_1	-1

▷ The algebra has 4 elements:

- ▷ scalar: 1
- ▷ vectors: e_1 and e_2
- ▷ bivector: e_{12} (pseudoscalar)

	1	e_1	$e_1 i$	i
1	1	e_1	$e_1 i$	i
e_1	e_1	1	i	$e_1 i$
$e_1 i$	$e_1 i$	$-i$	1	$-e_1$
i	i	$-e_1 i$	e_1	-1

▷ writing the pseudoscalar as i makes it obvious that

$$\mathcal{G}_2^+ \simeq \mathbb{C}$$

(even subalgebra)

Other Signatures: $\mathcal{G}_{1,1}$ *and* $\mathcal{G}_{0,0,2}$

	1	e_+	e_-	e_{+-}
1	1	e_+	e_-	e_{+-}
e_+	e_+	1	e_{+-}	e_-
e_-	e_2	$-e_{+-}$	-1	e_1
e_{+-}	e_{+-}	$-e_-$	$-e_+$	1

▷ Minkowski plane:

$$\mathcal{G}^+_{1,1} \simeq \{\text{hyperbolic numbers}\}$$

▷ Transform to null basis

$$e_o = \tfrac{1}{2}(e_- - e_+)$$
$$e_\infty = \quad (e_- + e_+)$$

	1	e_o	e_∞	$e_{o\infty}$	$e_{\infty o}$
1	1	e_o	e_∞	$e_{o\infty}$	$e_{\infty o}$
e_o	e_o	0	$e_{o\infty}$	0	$-2e_o$
e_∞	e_∞	$e_{\infty o}$	0	$-2e_\infty$	0
$e_{o\infty}$	$e_{o\infty}$	$-2e_o$	0	$-2e_{o\infty}$	0
$e_{\infty o}$	$e_{\infty o}$	0	$-2e_\infty$	0	$-2e_{\infty o}$

$$e_{o\infty} = (-1 - e_{+-})$$
$$e_{\infty o} = (-1 + e_{+-})$$

$$\{1, e_\infty\} \simeq \{\text{dual numbers}\}$$

The Null Basis Vectors, e_o *and* e_∞

$$\begin{aligned} e_\infty^2 &= (e_- + e_+)(e_- + e_+) \\ &= (e_-^2 + e_- e_+ + e_+ e_- + e_+^2) \\ &= (-1 - e_{+-} + e_{+-} + 1) \\ &= 0 \end{aligned}$$

$$\begin{aligned} e_0^2 &= \tfrac{1}{4}(e_- - e_+)(e_- - e_+) \\ &= \tfrac{1}{4}(e_-^2 - e_- e_+ - e_+ e_- + e_+^2) \\ &= \tfrac{1}{4}(-1 + e_{+-} - e_{+-} + 1) \\ &= 0 \end{aligned}$$

$$\begin{aligned} e_{0\infty} &= \tfrac{1}{2}(e_- - e_+)(e_- + e_+) \\ &= \tfrac{1}{2}(e_-^2 + e_- e_+ - e_+ e_- - e_+^2) \\ &= \tfrac{1}{2}(-1 - e_+ e_- - e_+ e_- - 1) \\ &= -1 - e_{+-} \end{aligned}$$

$$\begin{aligned} e_{\infty 0} &= \tfrac{1}{2}(e_- + e_+)(e_- - e_+) \\ &= \tfrac{1}{2}(e_-^2 - e_- e_+ + e_+ e_- - e_+^2) \\ &= \tfrac{1}{2}(-1 + e_+ e_- + e_+ e_- - 1) \\ &= -1 + e_{+-} \end{aligned}$$

$$\begin{aligned} e_\infty \cdot e_0 &= \tfrac{1}{2}(e_\infty e_0 + e_0 e_\infty) \\ &= \tfrac{1}{2}(-1 + e_{+-} - 1 - e_{+-}) \\ &= -1 \end{aligned}$$

$$\begin{aligned} e_\infty \wedge e_0 &= \tfrac{1}{2}(e_\infty e_0 - e_0 e_\infty) \\ &= \tfrac{1}{2}(-1 + e_{+-} + 1 + e_{+-}) \\ &= e_{+-} \end{aligned}$$

The Geometric Elements of Space

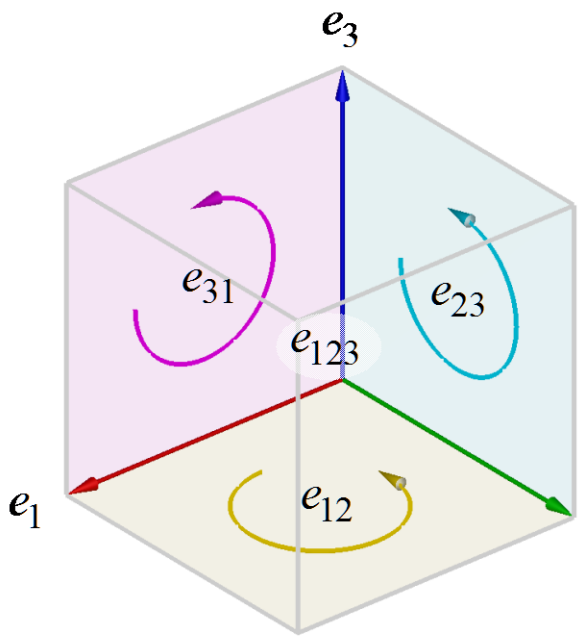

▷ unit cube (trivector)

$$e_{123} = e_1 e_2 e_3 = e_1 \wedge e_2 \wedge e_3$$

▷ unit squares (bivectors)

$$e_{12} = e_1 e_2 = e_1 \wedge e_2$$

$$e_{23} = e_2 e_3 = e_2 \wedge e_3$$

$$e_{31} = e_3 e_1 = e_3 \wedge e_1$$

▷ axes (unit vectors)

$$\{e_1, e_2, e_3\} = \{\hat{x}, \hat{y}, \hat{z}\}$$

The Geometric Algebra of Space, $\mathcal{G}_3$

	1	e_1	e_2	e_3	e_{12}	e_{31}	e_{23}	e_{123}
1	1	e_1	e_2	e_3	e_{12}	e_{31}	e_{23}	e_{123}
e_1	e_1	1	e_{12}	$-e_{31}$	e_2	$-e_3$	e_{123}	e_{23}
e_2	e_2	$-e_{12}$	1	e_{23}	$-e_1$	e_{123}	e_3	e_{31}
e_3	e_3	e_{31}	$-e_{23}$	1	e_{123}	e_1	$-e_2$	e_{12}
e_{12}	e_{12}	$-e_2$	e_1	e_{123}	-1	e_{23}	$-e_{31}$	$-e_3$
e_{31}	e_{31}	e_3	e_{123}	$-e_1$	$-e_{23}$	-1	e_{12}	$-e_2$
e_{23}	e_{23}	e_{123}	$-e_3$	e_2	e_{31}	$-e_{12}$	-1	$-e_1$
e_{123}	e_{123}	e_{23}	e_{31}	e_{12}	$-e_3$	$-e_2$	$-e_1$	-1

▷ the pseudoscalar is a trivector, and $\mathcal{G}_3^+ \simeq \mathbb{H}$

Appendix B: The Conformal Model of $\mathbb{E}^3$

The Conformal Geometric Algebra, $\mathcal{G}_{3,0,2}$

▷ we start with $\mathcal{G}_3 : \{e_1, e_2, e_3\}$ and append $\mathcal{G}_{1,1} : \{e_+, e_-\}$ to form $\mathcal{G}_{4,1} : \{e_1, e_2, e_3, e_+, e_-\}$

▷ then a simple change of basis

$$\begin{aligned} e_o &= \tfrac{1}{2}(e_- - e_+) \\ e_\infty &= \quad (e_- + e_+) \end{aligned} \quad \Leftrightarrow \quad \begin{aligned} e_+ &= \tfrac{1}{2} e_\infty - e_o \\ e_- &= \tfrac{1}{2} e_\infty + e_o \end{aligned}$$

results in $\mathcal{G}_{3,0,2} : \{e_1, e_2, e_3, e_o, e_\infty\}$, which has two ***null basis vectors***:

e_o : the origin and e_∞ : the point at infinity

Stereographic Projection in 1D

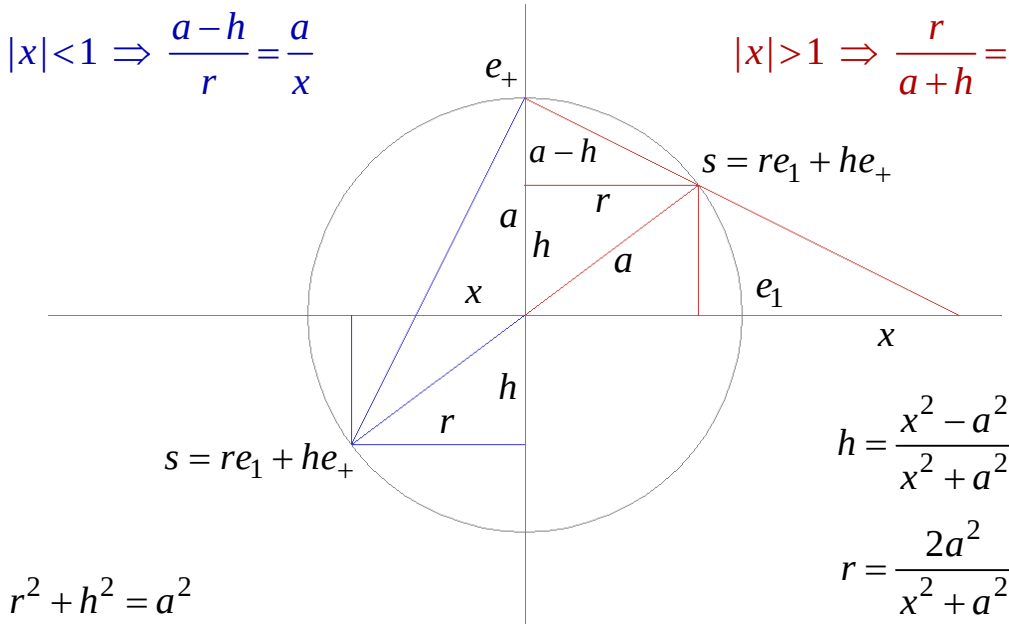

Stereographic Projection in 2D

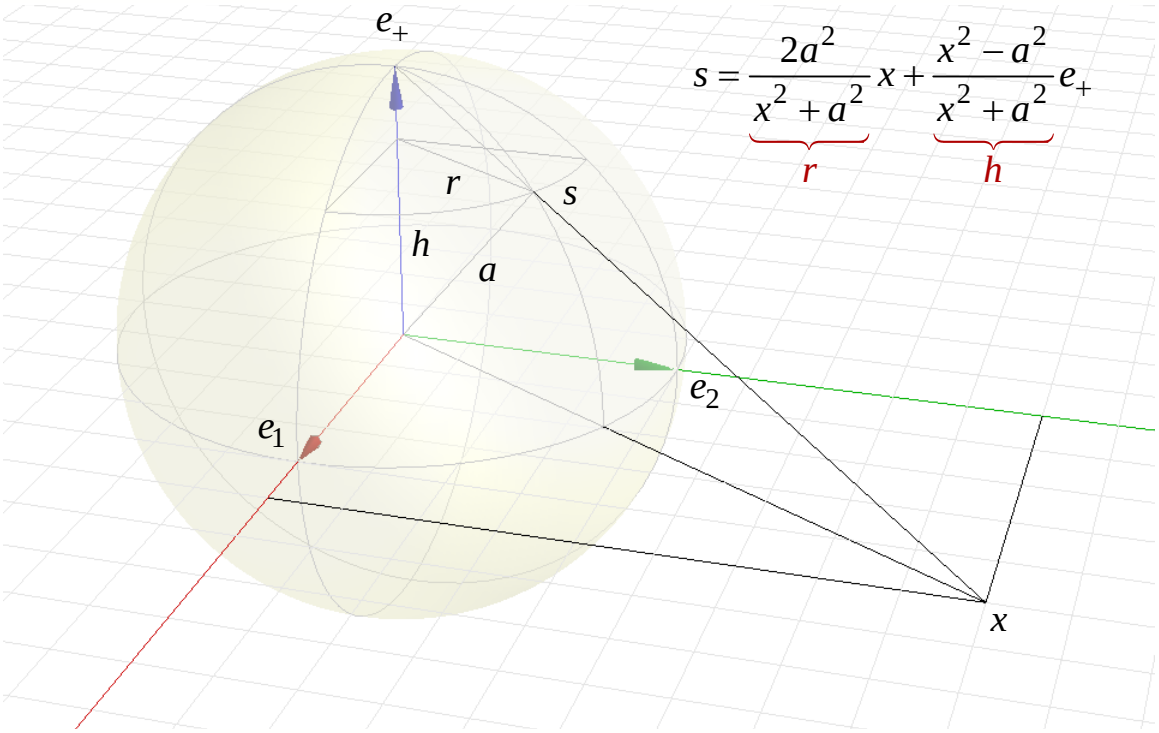

The Projective Null Cone

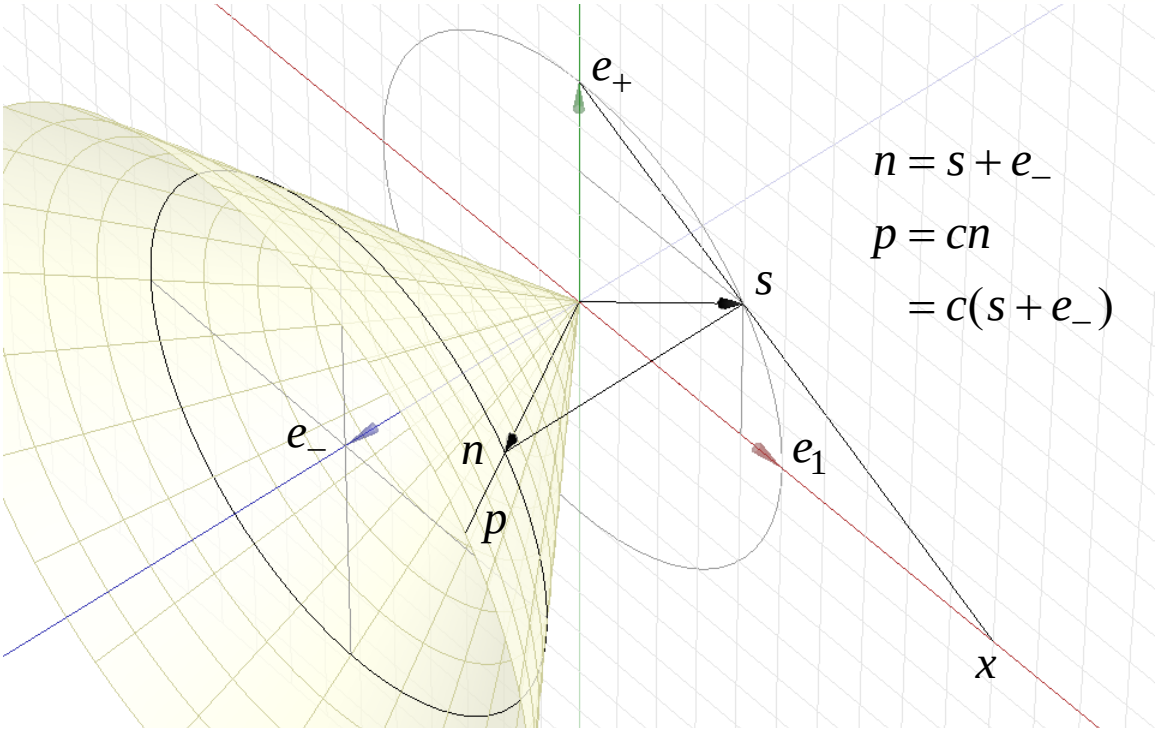

The Horosphere

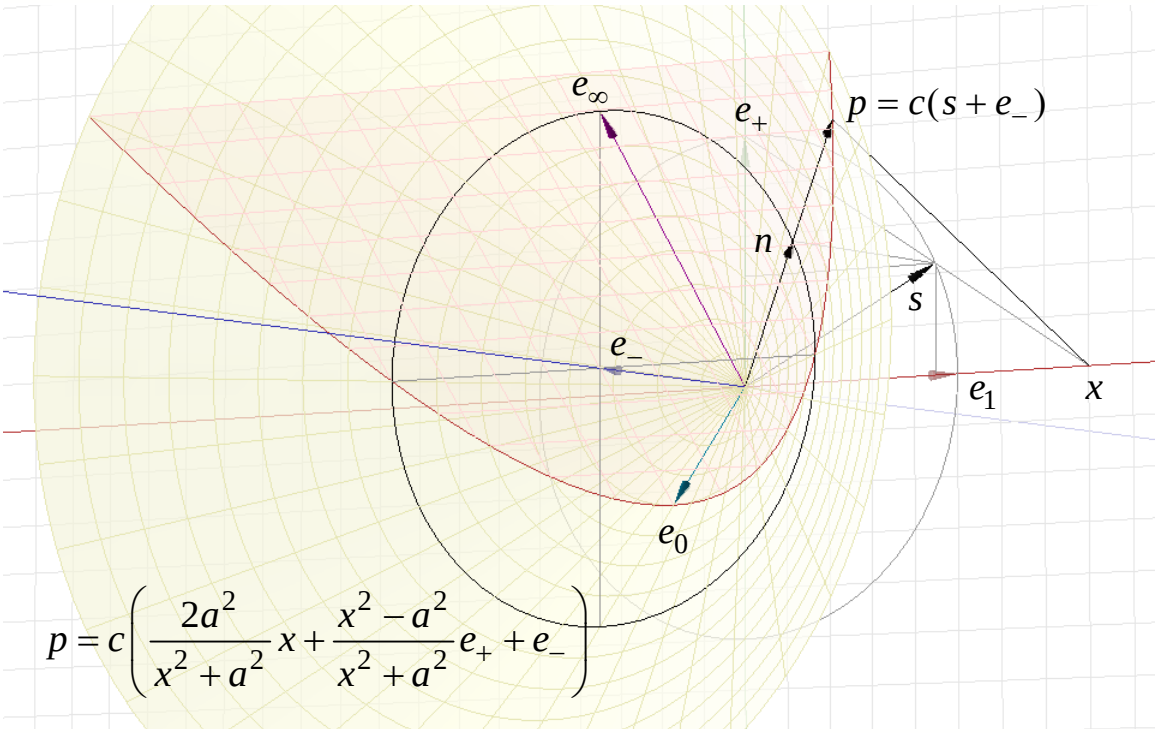

The Horosphere - Another View

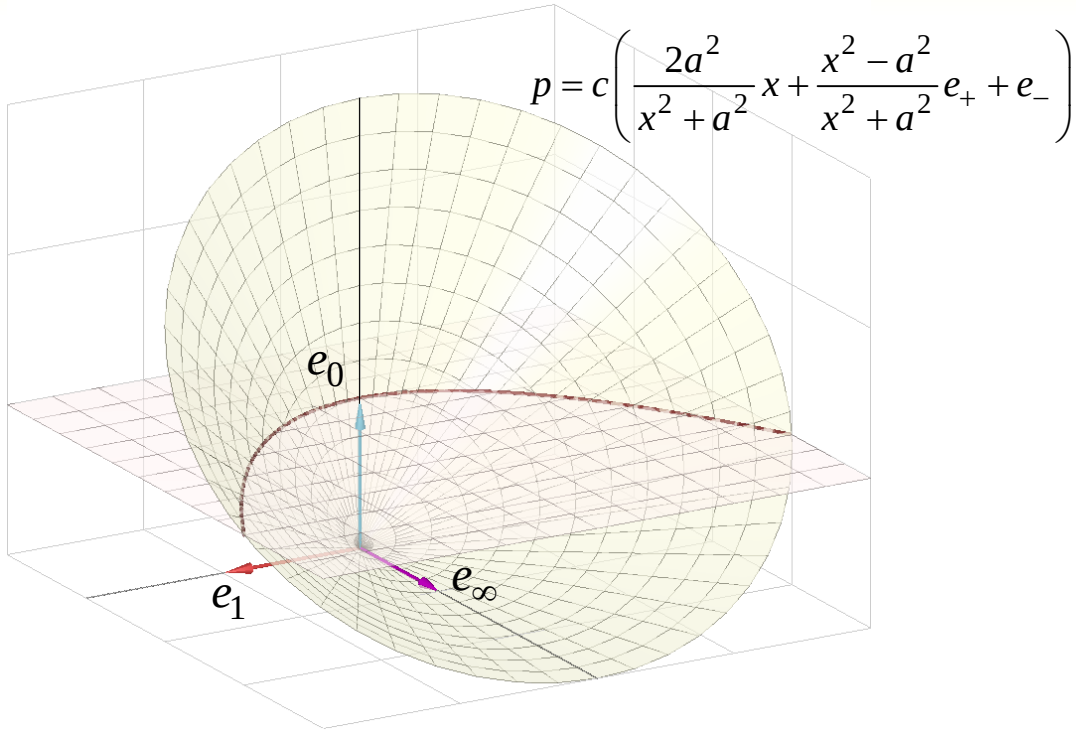

Expressing the Horosphere Mapping in $\mathcal{G}_{3,0,2}$

▷ set $c = (x^2 + a^2)/2a^2$ to get

$$p = x + \frac{x^2 - a^2}{2a^2} e_+ + \frac{x^2 + a^2}{2a^2} e_-$$
$$= x + x^2 \frac{e_- + e_+}{2a^2} + \frac{e_- - e_+}{2}$$
$$= x + \tfrac{1}{2} x^2 e_\infty + e_0$$

using

$$e_\infty = \tfrac{1}{a^2}(e_- + e_+)$$
$$e_0 = \tfrac{1}{2}(e_- - e_+)$$
$$\Updownarrow$$
$$e_- = \tfrac{a^2}{2} e_\infty + e_0$$
$$e_+ = \tfrac{a^2}{2} e_\infty - e_0$$

▷ then set $a = 1$ to get back to

$$e_o = \tfrac{1}{2}(e_- - e_+) \quad \Leftrightarrow \quad e_+ = \tfrac{1}{2} e_\infty - e_o$$
$$e_\infty = (e_- + e_+) \quad \Leftrightarrow \quad e_- = \tfrac{1}{2} e_\infty + e_o$$

The Conformal Point $p = x + \frac{1}{2} x^2 e_\infty + e_0$

▷ being null vectors, points have no magnitude

$$p^2 = p \cdot p = (x + \tfrac{1}{2} x^2 e_\infty + e_0)(x + \tfrac{1}{2} x^2 e_\infty + e_0)$$
$$= \tfrac{1}{2} x^2 (\cancel{x e_\infty + e_\infty x}) + (\cancel{x e_0 + e_0 x}) + \tfrac{1}{4} x^4 \overbrace{\cancel{e_\infty^2}}^{=0} + \overbrace{\cancel{e_0^2}}^{=0}$$
$$+ x^2 + \tfrac{1}{2} x^2 \underbrace{(e_\infty e_0 + e_0 e_\infty)}_{-2}$$
$$= 0$$

▷ dot product of two points = distance between them

$$p \cdot q = (x + \tfrac{1}{2} x^2 e_\infty + e_0)(y + \tfrac{1}{2} y^2 e_\infty + e_0)$$
$$= (x - y)^2$$

The Geometric Primitives in CGA

solutions of $x \wedge (p_1 \wedge p_2 \wedge \cdots \wedge p_n) = 0$ represent primitives

grade	rounds		flats	
0	scalar	1		
1	point	p_1	infinity	e_∞
2	point pair	$p_1 \wedge p_2$	flat point	$p_1 \wedge e_\infty$
3	circle	$p_1 \wedge p_2 \wedge p_3$	line	$p_1 \wedge p_2 \wedge e_\infty$
4	sphere	$p_1 \wedge p_2 \wedge p_3 \wedge p_4$	plane	$p_1 \wedge p_2 \wedge p_3 \wedge e_\infty$
5			pseudoscalar	$p_1 \wedge p_2 \wedge p_3 \wedge p_4 \wedge e_\infty$

for details, see Lasenby et al., 2004

Appendix C: Multivectors as Operators

Vectors Generate Reflections

$$a = (1)a = (v^{-1}v)a = v^{-1}(va) = v^{-1}(v\cdot a + v\wedge a)$$

$$= \underbrace{v^{-1}(v\wedge a)}_{a_\perp} + \underbrace{v^{-1}(v\cdot a)}_{a_\parallel}$$

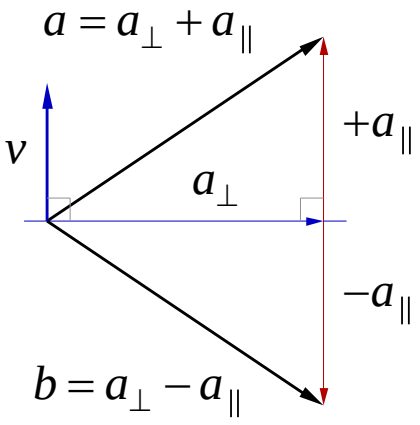

$$\begin{aligned} b &= a_\perp - a_\parallel \\ &= v^{-1}(v\wedge a) - v^{-1}(v\cdot a) \\ &= -v^{-1}(a\wedge v) - v^{-1}(a\cdot v) \\ &= -v^{-1}(a\cdot v + a\wedge v) \\ &= -v^{-1}av \end{aligned}$$

Bivectors Generate Rotations

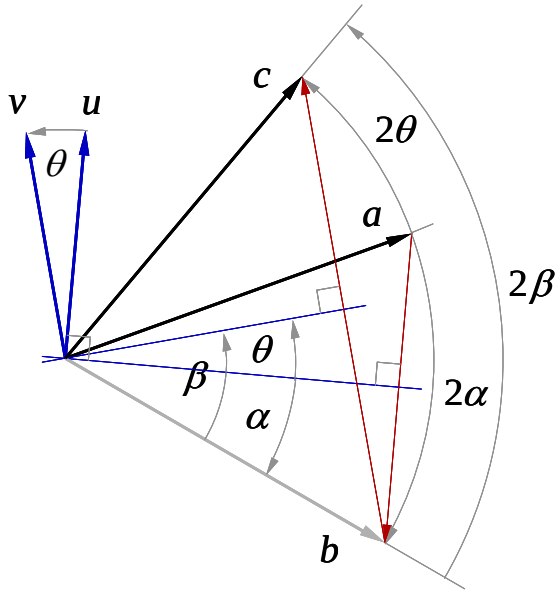

$$b = -u^{-1}au$$

$$\begin{aligned} c &= -v^{-1}bv \\ &= -v^{-1}(-u^{-1}au)v \\ &= (v^{-1}u^{-1})a(uv) \\ &= (uv)^{-1}a(uv) \\ &= \boldsymbol{b}^{-1}a\boldsymbol{b} \end{aligned}$$

Exponential of a Negative Bivector

▷ for unit bivector $\boldsymbol{b}$, $\boldsymbol{b}^2 = -1$, and scalar α we have

$$r = e^{\alpha \boldsymbol{b}} = 1 + \frac{(\alpha \boldsymbol{b})}{1!} + \frac{(\alpha \boldsymbol{b})^2}{2!} + \frac{(\alpha \boldsymbol{b})^3}{3!} + \frac{(\alpha \boldsymbol{b})^4}{4!} + \frac{(\alpha \boldsymbol{b})^5}{5!} + \ldots$$

$$= \left(1 - \frac{\alpha^2}{2!} + \frac{\alpha^4}{4!} - \ldots\right) + \boldsymbol{b}\left(\frac{\alpha}{1!} - \frac{\alpha^3}{3!} + \frac{\alpha^5}{5!} - \ldots\right)$$

$$= \cos\alpha + \boldsymbol{b}\sin\alpha$$

▷ $e^{\alpha \boldsymbol{b}} = \cos\alpha + \boldsymbol{b}\sin\alpha \quad \Leftrightarrow \quad \cos\alpha + i\sin\alpha = e^{i\alpha}$

▷ Lie algebra $\Rightarrow$ exp $\Rightarrow$ Lie group $\Rightarrow$ log $\Rightarrow$ Lie algebra

Rotation Versors

▷ rotation is takes place in the plane of the bivector

$$r\boldsymbol{x}\tilde{r} = e^{-\frac{\alpha}{2}\boldsymbol{b}}\boldsymbol{x}e^{\frac{\alpha}{2}\boldsymbol{b}} = (\cos\tfrac{\alpha}{2} - \boldsymbol{b}\sin\tfrac{\alpha}{2})(\boldsymbol{x}_\perp + \boldsymbol{x}_\parallel)(\cos\tfrac{\alpha}{2} + \boldsymbol{b}\sin\tfrac{\alpha}{2})$$

$$= (\cos\tfrac{\alpha}{2} - \boldsymbol{b}\sin\tfrac{\alpha}{2})(\cos\tfrac{\alpha}{2} + \boldsymbol{b}\sin\tfrac{\alpha}{2})\boldsymbol{x}_\perp$$

$$+ (\cos\tfrac{\alpha}{2} - \boldsymbol{b}\sin\tfrac{\alpha}{2})(\cos\tfrac{\alpha}{2} - \boldsymbol{b}\sin\tfrac{\alpha}{2})\boldsymbol{x}_\parallel$$

$$= (\cos^2\tfrac{\alpha}{2} + \sin^2\tfrac{\alpha}{2})\boldsymbol{x}_\perp + (\cos^2\tfrac{\alpha}{2} - \sin^2\tfrac{\alpha}{2} - 2\boldsymbol{b}\sin\tfrac{\alpha}{2}\cos\tfrac{\alpha}{2})\boldsymbol{x}_\parallel$$

$$= \boldsymbol{x}_\perp + (\cos\alpha - \boldsymbol{b}\sin\alpha)\boldsymbol{x}_\parallel$$

$$= \boldsymbol{x}_\perp + (\cos\alpha - \boldsymbol{u}\boldsymbol{v}\sin\alpha)(a\boldsymbol{u} + b\boldsymbol{v})$$

$$= \boldsymbol{x}_\perp + \boldsymbol{u}a\cos\alpha - \boldsymbol{u}\boldsymbol{v}^2 b\sin\alpha + \boldsymbol{v}\boldsymbol{u}^2 a\sin\alpha + \boldsymbol{v}b\cos\alpha$$

$$= \boldsymbol{x}_\perp + (a\cos\alpha - b\sin\alpha)\boldsymbol{u} + (a\sin\alpha + b\cos\alpha)\boldsymbol{v}$$

$$= \boldsymbol{x}_\perp + \mathrm{rot}_{\alpha,\boldsymbol{b}}(\boldsymbol{x}_\parallel)$$

Rotation of Conformal Points

▷ the horosphere is closed under rotation

$$\begin{aligned} rp(\boldsymbol{x})\tilde{r} &= r(\boldsymbol{x} + \tfrac{1}{2}\boldsymbol{x}^2 e_\infty + e_0)\tilde{r} \\ &= r\boldsymbol{x}\tilde{r} + \tfrac{1}{2}\boldsymbol{x}^2 r\tilde{r}e_\infty + r\tilde{r}e_0 \\ &= r\boldsymbol{x}\tilde{r} + \tfrac{1}{2}(r\boldsymbol{x}\tilde{r})^2 e_\infty + e_0 \\ &= p(r\boldsymbol{x}\tilde{r}) \end{aligned}$$

Exponential of a Null Bivector

▷ for a unit vector $\boldsymbol{a}$ and a scalar d we have

$$\begin{aligned} t &= e^{d\boldsymbol{a}e_\infty} \\ &= 1 + \frac{(d\boldsymbol{a}e_\infty)}{1!} + \frac{(d\boldsymbol{a}e_\infty)^2}{2!} + \frac{(d\boldsymbol{a}e_\infty)^3}{3!} + \frac{(d\boldsymbol{a}e_\infty)^4}{4!} + \ldots \\ &= 1 + d\boldsymbol{a}e_\infty - d^2\boldsymbol{a}^2 \underbrace{e_\infty^2}_{=0}\left(\frac{1}{2!} + \frac{(d\boldsymbol{a}e_\infty)}{3!} + \frac{(d\boldsymbol{a}e_\infty)^2}{4!} + \ldots\right) \\ &= 1 + d\boldsymbol{a}e_\infty \end{aligned}$$

Translation Versors

▷ the horosphere is closed under translation

$$tp(\boldsymbol{x})\overleftarrow{t} = e^{-\frac{1}{2}d\boldsymbol{a}e_\infty}\, p(\boldsymbol{x})\, e^{\frac{1}{2}d\boldsymbol{a}e_\infty} = (1-\tfrac{1}{2}d\boldsymbol{a}e_\infty)(\boldsymbol{x}+\tfrac{1}{2}\boldsymbol{x}^2e_\infty+e_0)(1+\tfrac{1}{2}d\boldsymbol{a}e_\infty)$$

$$= (1-\tfrac{1}{2}d\boldsymbol{a}e_\infty)(\boldsymbol{x}+\tfrac{1}{2}(\boldsymbol{x}^2+d\boldsymbol{x}\boldsymbol{a})e_\infty+e_0-\tfrac{1}{2}d\boldsymbol{a}e_0e_\infty-\tfrac{1}{4}d\boldsymbol{x}^2\boldsymbol{a}\,\cancel{e_\infty^2})$$

$$= \boldsymbol{x}+\tfrac{1}{2}(\boldsymbol{x}^2+d(\boldsymbol{x}\boldsymbol{a}+\boldsymbol{a}\boldsymbol{x}))e_\infty+e_0-\tfrac{1}{4}d^2\boldsymbol{a}^2\underbrace{e_\infty e_0 e_\infty}_{-2e_\infty}$$

$$-\tfrac{1}{2}d\boldsymbol{a}(\overbrace{e_0e_\infty+e_\infty e_0}^{-2})-\tfrac{1}{4}d\boldsymbol{a}(\boldsymbol{x}^2+d\boldsymbol{x}\boldsymbol{a})\,\cancel{e_\infty^2}$$

$$= \boldsymbol{x}+d\boldsymbol{a}+\tfrac{1}{2}(\boldsymbol{x}^2+d(\boldsymbol{x}\boldsymbol{a}+\boldsymbol{a}\boldsymbol{x})+d^2\boldsymbol{a}^2)e_\infty+e_0$$

$$= (\boldsymbol{x}+d\boldsymbol{a})+\tfrac{1}{2}(\boldsymbol{x}+d\boldsymbol{a})^2+e_0$$

$$= p(\boldsymbol{x}+d\boldsymbol{a})$$

Translators and Rotors are Unit Versors

▷ for translators, independent of $\boldsymbol{a}$ and d

$$t\overleftarrow{t} = (1-\tfrac{1}{2}d\boldsymbol{a}e_\infty)(1+\tfrac{1}{2}d\boldsymbol{a}e_\infty)$$

$$= 1+\tfrac{1}{2}d(\cancel{\boldsymbol{a}e_\infty-\boldsymbol{a}e_\infty})+\tfrac{1}{4}d^2\boldsymbol{a}^2\,\cancel{e_\infty^2}$$

$$= 1$$

▷ for rotors, independent of α and $\boldsymbol{b}$

$$r\overleftarrow{r} = (\cos\tfrac{1}{2}\alpha-\boldsymbol{b}\sin\tfrac{1}{2}\alpha)(\cos\tfrac{1}{2}\alpha+\boldsymbol{b}\sin\tfrac{1}{2}\alpha)$$

$$= \cos^2\tfrac{1}{2}\alpha+\boldsymbol{b}(\cancel{\cos\tfrac{1}{2}\alpha\sin\tfrac{1}{2}\alpha-\sin\tfrac{1}{2}\alpha\cos\tfrac{1}{2}\alpha})-\boldsymbol{b}^2\sin^2\tfrac{1}{2}\alpha$$

$$= \cos^2\tfrac{1}{2}\alpha+\sin^2\tfrac{1}{2}\alpha = 1$$

Motors ($\mathbb{SE}(3)$): Combined Translator & Rotor

▷ the product of translator t and rotor r is a ***motor***:

$$m = tr = e^{-\frac{1}{2}d\mathbf{a}e_\infty} e^{-\frac{1}{2}\alpha\mathbf{bc}} = (1 - \tfrac{1}{2}d\mathbf{a}e_\infty)(\cos\tfrac{1}{2}\alpha - \mathbf{bc}\sin\tfrac{1}{2}\alpha)$$

$$= \underbrace{\cos\tfrac{1}{2}\alpha}_{\text{scalar}} - \underbrace{(\mathbf{bc}\sin\tfrac{1}{2}\alpha + \tfrac{1}{2}d\cos\tfrac{1}{2}\alpha\mathbf{a}e_\infty)}_{\text{bivector}} + \underbrace{\tfrac{1}{2}d\sin\tfrac{1}{2}\alpha\mathbf{abc}e_\infty}_{\text{quadvector}}$$

▷ the horosphere is closed under the its action

$$mp(\boldsymbol{x})\overleftarrow{m} = trp(\boldsymbol{x})\overleftarrow{r}\overleftarrow{t} = tp(r\boldsymbol{x}\overleftarrow{r})\overleftarrow{t} = p(tr\boldsymbol{x}\overleftarrow{r}\overleftarrow{t})$$

$$= p(m\boldsymbol{x}\overleftarrow{m})$$

▷ and of course motors are unit versors

$$m\overleftarrow{m} = tr\overleftarrow{tr} = t(r\overleftarrow{r})\overleftarrow{t} = t\overleftarrow{t} = 1$$

Appendix D: Screw Transformations

Geometry of the Screw Transformation

$$\boldsymbol{x}' = m\boldsymbol{x}\overleftarrow{m} = tr\boldsymbol{x}\overleftarrow{r}\overleftarrow{t}$$

$$t = 1 - \tfrac{1}{2} d\boldsymbol{a} e_\infty$$

$$r = \cos\tfrac{1}{2}\alpha - \boldsymbol{b}\sin\tfrac{1}{2}\alpha$$

$$\boldsymbol{a}^2 = 1;\ \boldsymbol{b}^2 = -1$$

$$\boldsymbol{a}\cdot\boldsymbol{b} = 0$$

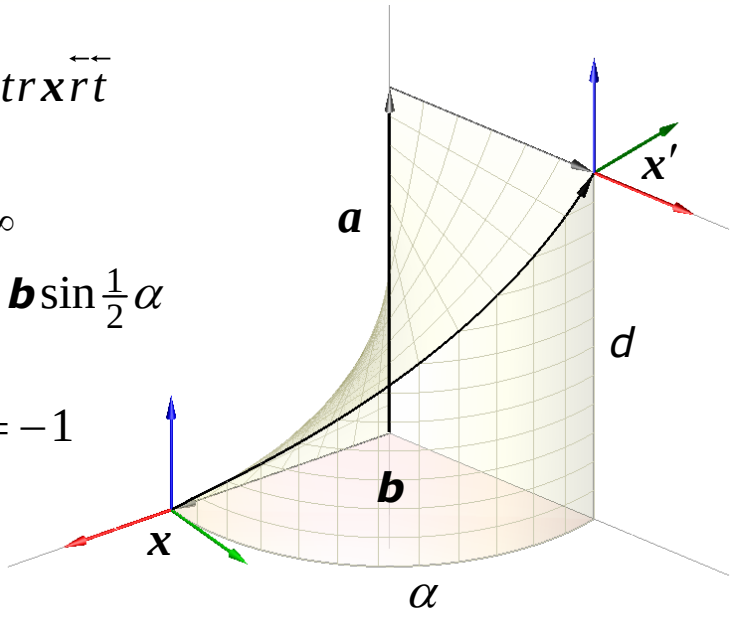

$$\boldsymbol{abc}e_\infty = e_{123\infty}$$

Geometry of the Screw Transformation

$$\boldsymbol{x}' = m\boldsymbol{x}\overleftarrow{m} = tr\boldsymbol{x}\overleftarrow{r}\overleftarrow{t}$$

$$t = 1 - \tfrac{1}{2} d\boldsymbol{a} e_\infty$$

$$r = \cos\tfrac{1}{2}\alpha - \boldsymbol{b}\sin\tfrac{1}{2}\alpha$$

$$\boldsymbol{a}^2 = 1;\ \boldsymbol{b}^2 = -1$$

$$\boldsymbol{a}\cdot\boldsymbol{b} = 0$$

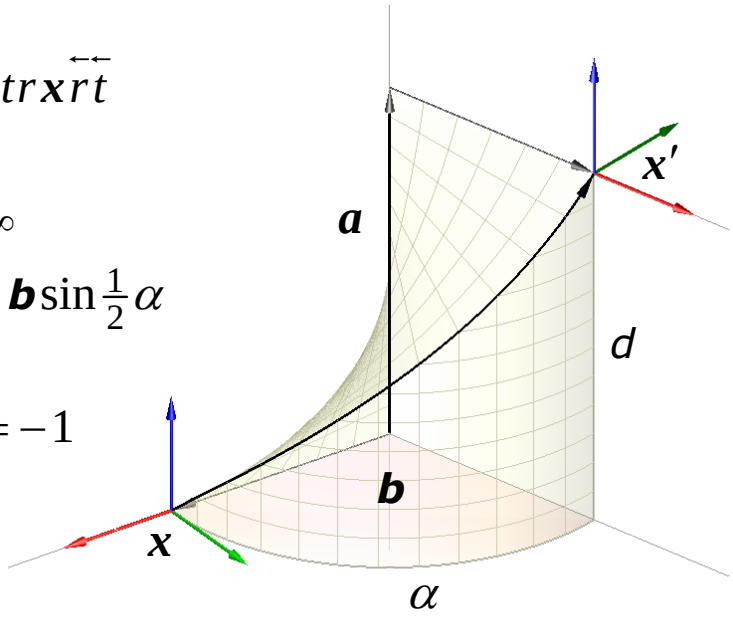

$$\boldsymbol{abc}e_\infty = e_{123\infty}$$

Algebra of the Screw Transformation

▷ we extract the parallel and perpendicular parts

$$\boldsymbol{t} = \boldsymbol{t}\boldsymbol{b}\overleftarrow{\boldsymbol{b}} = (\boldsymbol{t}\cdot\boldsymbol{b})\overleftarrow{\boldsymbol{b}} + (\boldsymbol{t}\wedge\boldsymbol{b})\overleftarrow{\boldsymbol{b}} = \boldsymbol{t}_{\|\boldsymbol{b}} + \boldsymbol{t}_{\perp\boldsymbol{b}} = \boldsymbol{u} + \boldsymbol{w}$$

▷ set $w = \exp(-\frac{1}{2}\boldsymbol{w}e_\infty) = 1 - \frac{1}{2}\boldsymbol{w}e_\infty$, likewise u and v:

$$m = tr = (wu)r = w(ur) = w(vr\overleftarrow{v}) = ws$$

▷ now, $\boldsymbol{u} = \boldsymbol{v} - r\boldsymbol{v}\overleftarrow{r}$ and $\boldsymbol{v}\overleftarrow{r} = r\boldsymbol{v}$, so $\boldsymbol{v} = (1-r^2)^{-1}\boldsymbol{u}$ and

$$s = vr\overleftarrow{v} = v\exp(-\tfrac{1}{2}\theta\boldsymbol{b})\overleftarrow{v} = \exp(-\tfrac{1}{2}\theta v\boldsymbol{b}\overleftarrow{v})$$
$$= \cos\tfrac{1}{2}\theta - v\boldsymbol{b}\overleftarrow{v}\sin\tfrac{1}{2}\theta$$

The Logarithm of a Motor

▷ we can now put the motor in screw form:

$$m = ws = wvr\overleftarrow{v} = \exp(-\tfrac{1}{2}\boldsymbol{w}e_\infty)\exp(-\tfrac{1}{2}\theta v\boldsymbol{b}\overleftarrow{v})$$
$$= (1-\tfrac{1}{2}\boldsymbol{w}e_\infty)(\cos\tfrac{1}{2}\theta - \sin\tfrac{1}{2}\theta v\boldsymbol{b}\overleftarrow{v})$$

▷ in which the tanslation and rotation ***commute***, so

$$\log m = \log(ws) = \log(w) + \log(s)$$
$$= -\tfrac{1}{2}\boldsymbol{w}e_\infty - \tfrac{1}{2}\theta v\boldsymbol{b}\overleftarrow{v}$$

~~Baker-Campbell-Hausdorff Formula~~

▷ translation and rotation generally don't commute, so

$$\log(\exp(-\tfrac{1}{2}\boldsymbol{t}e_\infty)\exp(-\tfrac{1}{2}\theta\boldsymbol{b})) = -\tfrac{1}{2}\boldsymbol{t}e_\infty - \tfrac{1}{2}\theta\boldsymbol{b}$$
$$+\tfrac{1}{2}(\tfrac{1}{2}\boldsymbol{t}e_\infty \times \tfrac{1}{2}\theta\boldsymbol{b})$$
$$+\tfrac{1}{12}((\tfrac{1}{2}\boldsymbol{t}e_\infty \times (\tfrac{1}{2}\boldsymbol{t}e_\infty \times \tfrac{1}{2}\theta\boldsymbol{b})) - (\tfrac{1}{2}\theta\boldsymbol{b} \times (\tfrac{1}{2}\boldsymbol{t}e_\infty \times \tfrac{1}{2}\theta\boldsymbol{b})))$$
$$+\tfrac{1}{24}(((\tfrac{1}{2}\boldsymbol{t}e_\infty \times (\tfrac{1}{2}\boldsymbol{t}e_\infty \times \tfrac{1}{2}\theta\boldsymbol{b})) \times \tfrac{1}{2}\theta\boldsymbol{b}))$$
$$+\ldots$$

where $a \times b = ab - ba$ is the commutator product

Square Magnitude of a Screw Logarithm

▷ finally, we use $v\boldsymbol{b}\bar{v} = \boldsymbol{b}(1 + (1-r^2)^{-1}\boldsymbol{u}e_\infty)$ and $\theta\,\boldsymbol{b}(1-r^2)^{-1}\boldsymbol{u} = (\operatorname{sinc}\tfrac{1}{2}\theta)^{-1}\bar{r}\boldsymbol{u} = \theta\boldsymbol{v}$ to write

$$\log m = -\tfrac{1}{2}\boldsymbol{w}e_\infty - \tfrac{1}{2}\theta\, v\boldsymbol{b}\bar{v}$$
$$= -\tfrac{1}{2}(\boldsymbol{w} + \theta\boldsymbol{v})e_\infty - \tfrac{1}{2}\theta\boldsymbol{b}$$

▷ whereby

$$|\log m|^2 = \tfrac{1}{4}(\boldsymbol{w}^2 + (\boldsymbol{v}^2 + 1)\theta^2)$$

Appendix E: Connections, Geodesics and Dispersion

One-Parameter Subgroups

▷ screw logs are not metric – no triangle inequality

▷ not bi-invariant – $\mathbb{SE}(3)$ has no such bilinear form

  ▷ Killing form is degenerate, Klein form is indefinite

▷ but we can form 1-parameter subgroups

$$\varphi_{1,\boldsymbol{x}}(s) = \exp(s\boldsymbol{x}) = (1 - \tfrac{s}{2}\boldsymbol{t}e_\infty)(\cos\tfrac{s}{2}\alpha - \sin\tfrac{s}{2}\alpha\hat{\boldsymbol{b}})$$

▷ we can always pick a bi-invariant connection such that these 1-parameter subgroups are geodesics

Cartan-Schouten Connections

▷ Cartan connections uniquely determined by $\nabla_x y|_1$

▷ Cartan-Schouten connections have $\nabla_x x|_1 = 0$, so 1-parameter subgroups are geodesics

▷ those of the form $\nabla_x y|_1 = a\, x \times y$ are bi-invariant

	action at 1	curvature	torsion
(+)-connection	$\nabla_x y\|_1 = x \times y$	$R = 0$	$T = +x \times y$
(0)-connection	$\nabla_x y\|_1 = \frac{1}{2} x \times y$	$R = \frac{1}{4}(x \times y) \times z$	$T = 0$
(−)-connection	$\nabla_x y\|_1 = 0$	$R = 0$	$T = -x \times y$

Dispersion and Barycentre as Fixed Point

▷ let dispersion about x_0 of n motors x_k, weights w_k, be

$$\sigma^2(x_0) = \sum_{k=1}^{n} w_k \, |\log(x_0^{-1} x_k)|^2$$

▷ fixed-point algorithm (Pennec & Arsigny, 2013):

initialize $\quad x_{0,0} = 1$

repeat $\quad x_{0,i+1} = x_{0,i} \exp\left(\sum_{k=1}^{n} w_k \log(x_{0,i}^{-1} x_k) \right)$

until $\quad |\log x_{0,i+1}^{-1} x_{0,i}|^2 \le \varepsilon \sigma^2(x_{0,i})$

The Barycentre Nulls the Weighted Sum

▷ suppose we have convergence, so $x_{0,i+1} = x_{0,i} = x_0$

then

$$x_{0,i+1} = x_{0,i} \underbrace{\exp\left(\sum_{k=1}^{n} w_k \log(x_{0,i}^{-1} x_k) \right)}_{=1}$$

or just

$$\boxed{\sum_{k=1}^{n} w_k \log(x_0^{-1} x_k) = 0}$$

Invariance of the Barycentre

▷ left invariance is immediate

$$x_0^{-1}x_k = x_0^{-1}(a^{-1}a)x_k = (ax_0)^{-1}(ax_k)$$

▷ right invariance follows from

$$x_0\left(\sum_{k=1}^{n} w_k \log(x_0^{-1}x_k)\right)x_0^{-1} = \sum_{k=1}^{n} w_k \log(x_k x_0^{-1})$$

$$x_k x_0^{-1} = x_k(aa^{-1})x_0^{-1} = (x_k a)(x_0 a)^{-1}$$

▷ so we also have invariance under inversion

$$(x_0^{-1}x_k)^{-1} = x_k^{-1}x_0 = (x_k^{-1})(x_0^{-1})^{-1}$$